Geochemical and Economic Evaluation of Brine Exchange as a Means of Produced Water Management

By
© 2022
Anthony Pham
B.S., University of Kansas, Lawrence 2020

Submitted to the graduate degree program in Environmental Engineering and the Graduate Faculty of the University of Kansas in partial fulfillment of the requirements for the degree of Master of Science

Chair: Dr. Edward Peltier

Dr. Justin Hutchison

Dr. Reza Barati

Date Defended: May 2nd, 2022

The thesis committee for Anthony Pham certifies that this is the approved version of the following thesis:

Geochemical and Economic Evaluation of Brine Exchange as a Means of Produced Water Management

Chair: Dr. Edward Peltier

Date Approved: May 11th, 2022

Abstract

The extraction of crude oil generates large amounts of wastewater, also referred to as brine or produced water. This water is often high in salinity, heavy metals, and other toxic compounds. Its constituents make conventional treatment difficult and expensive, so a common practice is to inject this water deep underground for long-term storage. While convenient, deep well injection of produced water has been linked to environmental concerns, such as increased water stress and induced seismic activity. Alternative methods to produced water management are critical to alleviating concerns associated with current produced water disposal practices. Produced water brine exchange is one such alternative method that involves exchanging produced water between reservoirs to create a salinity gradient. A lower salinity brine is injected into a high salinity reservoir for use in Low Salinity Waterflooding (LSWF)—a practice that can lead to increased oil recovery. The high salinity brine is injected into the low salinity reservoir for long-term disposal, maintaining reservoir pressure.

This study evaluates brine exchange between the Arbuckle formation (~20,000 mg/L TDS) and Lansing-Kansas City (LKC) formation (~150,000 mg/L TDS). To ensure geochemical compatibility between the injected brine, the in-situ brine, and reservoir rock and to evaluate the economic potential of brine exchange, a series of mixing experiments, geochemical modeling, and economic analysis were conducted. Bulk mixing and coreflooding experiments were conducted to evaluate brine-solid compatibility under both non-transport limited conditions and transport dominated conditions experienced in real-world environments. Experimental results were supplemented with geochemical modeling using PHREEQC with three sets of thermodynamic databases (PHREEQC, PITZER, and MINTEQ) to aid with compatibility

analysis. Additionally, a techno-economic assessment was conducted to gauge economic viability of potential brine exchange projects.

Results from the mixing experiments showed the risk of calcium carbonate scale formation is present in brine-brine-rock systems with low salinities (high ratio of Arbuckle:LKC brines) but only to a minor degree. None of the three databases used for geochemical modeling could accurately capture all trends in aqueous cation concentrations due to inherent limitations in each approach. Further study to identify discrepancies between model approaches and experimental results is warranted. Lastly, simulation modeling revealed that the economic viability of conducting brine exchange is highly correlated with the distance between wells and the energy cost of brine transportation. Conditions needed for economically viable operations have been identified, and the boundary between viable and unviable conditions have been found to be resilient to changes to material costs. The results gathered identify scenarios where brine exchange could be feasible and the key parameters needed to assess the risk of geochemical incompatibility.

Acknowledgements

I would like to acknowledge and thank my advisor, Dr. Edward Peltier, as well as Dr. Justin Hutchison and Dr. Reza Barati for all the guidance they have provided throughout the course of my studies. I would also like to thank Dr. Joel Tetteh for the countless hours of assistance he has provided me during my laboratory work, Berexco for the industry knowledge and expertise they shared with us, and both the Kansas Water Resources Institute and National Science Foundation (EPSCoR Grant #1632892) for providing us with the means to conduct this research.

Finally, I would like to extend special thanks to Maya Hubbs, a dear friend who has been a constant pillar of support throughout the most challenging, monotonous, and frustrating moments of my studies. I cannot begin to image what my experience would have been like without your presence.

Contents

1 Introduction

The process of oil extraction is often accompanied by the coextraction of wastewater. This byproduct, referred to as produced water (PW) or brine, represents the largest waste stream of oil and gas operations as the ratio of produced water to oil can range from 1:1 to 100:1[1,2]. The exact constituents of this water vary greatly depending on the geological formation it originated from, but management of this waste is difficult due to elevated levels of one (or often multiple) of the following: salinity, residual oil, organic components, heavy metals, production chemicals, and naturally occurring radioactive material[1,3,4].

Rather than treat produced water to a degree suitable for environmental release, producers typically turn to disposal or reuse to handle their waste. Disposal involves injecting brine deep underground, where it can be stored indefinitely. While simple and economical, it has been linked to induced seismic activity[5] and other environmental concerns such as water stress in drier regions of the world. Reusing produced water for other oil extraction purposes is preferred but may not always be possible due to the large quantity of brine generated.

One of the most prevalent forms of reuse is to reinject the water back into the original formation. This practice—known as water flooding, secondary recovery, or enhanced oil recovery—has the benefit of increasing the productive life of a reservoir by 1) maintaining operating pressures by replacing extracted fluids and 2) displacing hydrocarbons from rocks and mobilizing them towards the extraction wells[6,7]. While water of any composition can be used for waterflooding, increased oil recovery can be observed if the injected water contains a lower salinity than the connate water[8]. This practice is referred to as Low Salinity Waterflooding (LSWF) and leads to a dilemma where well operators must decide to either facilitate waste disposal by reinjecting produced water back into a reservoir or optimize oil recovery by

importing and injecting low salinity water and finding alternative disposal means for the original brine.

The mechanism leading to increased oil recovery during LSWF is not fully understood for carbonate reservoirs. While there is no consensus, most published works link improved oil recovery to wettability alterations of the reservoir rock surfaces[9]. The mechanisms behind wettability alterations include the following proposals depending on the rock and brine composition: mineral dissolution[10,11], multicomponent ionic enchange[12,13], expansion of the electrical double layer[14], and electrostatic bond linkage[15,16]. The term "low salinity" in LSWF is a misnomer as numerous lab and field experiments have shown the overall salinity level of injection water has little to no correlation on improved oil recovery. In their review of multiple waterflooding experiments, both Snosy et al.[17] and Tetteh et al.[18] concluded no significant trend exists between the overall brine salinity value and increased oil recovery. Rather, a combination of the ion composition and concentration of key ions (specifically Ca^{2+}, Mg^{2+}, Na^{+}, and SO_4^{2-}) have a greater impact on recovery. It could be assumed high salinity water could be used for injection as long as the concentration of these specific ionic species are low enough, but this subject requires additional study. Here, the term "low salinity brine" is used in reference to the low concentration of key ionic species rather than the overall salinity of the water.

Due to its abundance and relative homogeneity compared to formation water, sea water has been the preferred source of injection water for coastal operations. However, for landlocked regions, LSWF can be conducted using freshwater resources (such as shallow aquifers or rivers) or dilutions of formation water using freshwater[19]. This results in two major environmental concerns. First, the consumption and eventual injection of freshwater resources can increase water stress, especially in regions where freshwater supplies are already strained. Second, the

excess produced water will most likely be disposed of through deep well injection via Class II injection wells, and this practice has been linked to induced seismic activity[5]. While this concern has been alleviated to a degree through the passage of state legislation limiting the maximum pressure gradient of wells[20–22], there are still concerns about the overall capacity of these formations to accommodate produced water disposal when oil production is high. Thus, the ideal scenario still involves limiting reliance of this practice or outright eliminating it.

Brine exchange offers a potential solution to both concerns without diminishing the benefits of LSWF. During brine exchange, the produced water from one oil operation is transported to another and used as the injection water for LSWF. Additionally, the produced water from the second reservoir can be transferred back to the first and reinjected—mainly for the purpose of pressure maintenance with the added benefit of being an alternative disposal method (**Figure** 1). As long as a salinity gradient exists between the two reservoirs, brine exchange can be conducted.

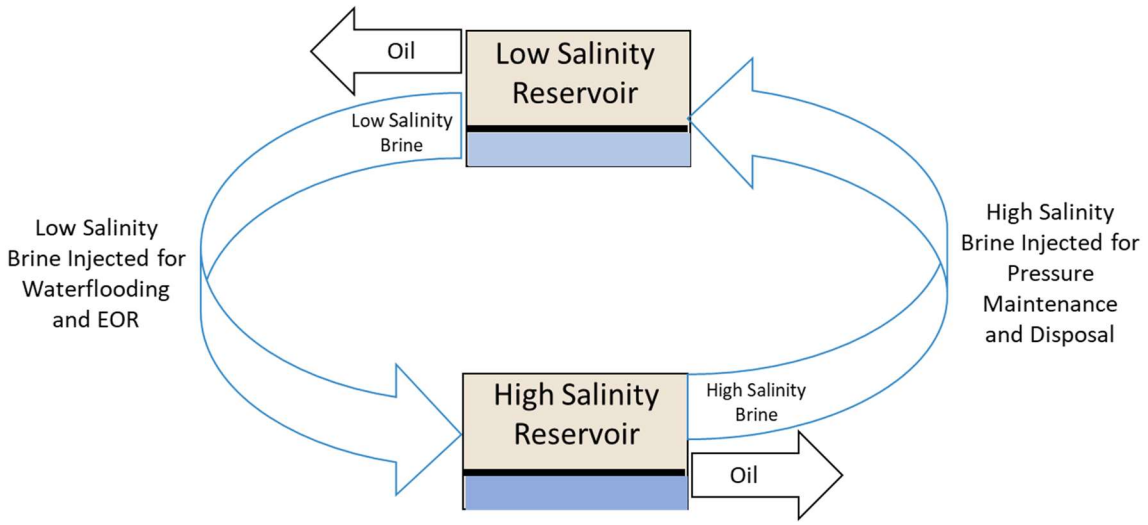

Figure 1 Proposed sequence of brine exchange between two oil reservoirs

Unfortunately, attitudes towards brine exchange can be best described as apprehensive due to potential operational issues. One of the most prominent concerns, and the focus of this

paper, is brine incompatibility— the potential for precipitation reactions to occur as the result of chemical reactions or oversaturation. Deposition of solids (scale formation) onto equipment or within the rock surfaces may lead to operational issues such as decreased recovery, equipment corrosion, and increased strain on injectors[23].

The potential impacts of fluid incompatibility have been known for decades[24], with salts of Ca^{2+}, Ba^{2+}, Sr^{2+}, SO_4^{2-}, and CO_3^{2-} being the species of greatest concern[25]. Despite this, modern literature regarding LSWF is dominated by research investigating the mechanisms responsible for its effects on oil recovery. Studies that examine scale formation tend to focus on its inhibition through the ad-hoc addition of scale inhibitors rather than the factors responsible for it[26–29]. Additionally, nearly all these studies are conducted using seawater, diluted connate water, or synthetic brines made to replicate these fluids as the source of the injection water. Virtually no research exists that uses produced water from a separate reservoir as a source of injection water for waterflooding.

The purpose of this study is to address this gap in knowledge by evaluating the geochemical compatibility of brine exchange between two Kansas reservoirs. Produced water from the Arbuckle geologic formation (~20,000 mg/L TDS) was combined with produced water from the Lansing-Kansas City (LKC) formation (~150,000 mg/L TDS) in bulk mixing and coreflooding experiments to evaluate fluid compatibility and scale formation potential. Changes in cation composition were measured through inductively coupled plasma–optical emission spectrometry (ICP-OES) to indicate the presence of reactions between carbonate solids from the LKC reservoir and dissolved salts. Experimental data from both experiments were then compared to simulation results to gauge the utility of common geochemical models at predicting the viability of brine exchange. Additionally, the economic feasibility of conducting the exchange was

examined by constructing a techno-economic assessment model. The uncertainty of the economic model was evaluated using Monte Carlo simulation. This study demonstrates compatibility between the Arbuckle and LKC in liquid-liquid mixtures with only minor, yet manageable, incompatibility in Liquid-Liquid-Solid systems where the ratio of Arbuckle to LKC brines is high. Geochemical simulation results were found to have inherent limitations, which limited accuracy; and the economic analysis revealed parameters needed for profitable operations. The results of this study reveal the potential of large-scale brine exchange to reduce large quantities of water disposed during day-to-day operations.

2 Methods and Materials

2.1 Produced Water

Produced water samples were obtained from two active oil fields within Barton County, KS. Ionic compositions were determined through ICP–OES (Optima 2000 DV instrument, PerkinElmer) and Ion Chromatography (IC) (Dionex Integrion HPIC with Dioinex IonPac AS18 column) (**Table** 1). Samples were filtered using 0.45 μm PVDF vacuum filters prior to analysis and experimentation. The sum of ionic constituents was calculated to determine Total Dissolved Solids (TDS).

Table 1 Ionic composition (mg/L) of PW samples determined through ICP-OES and IC. Concentrations Below Detection Limit (B.D.L.) are shaded in grey. Ionic Strength (I.S.) and TDS are found in the bottom row

		Arbuckle	LKC
Cations	**Ba**	B.D. L.	B.D.L.
	K	120 ± 10	213 ± 44
	Fe	B.D. L.	B.D.L.
	Mn	B.D.L.	B.D.L.
	Mg	325 ± 12	2366 ± 108
	Al	B.D.L.	B.D.L.
	Sr	57 ± 2	578 ± 41
	Li	6 ± 0.1	14 ± 0.5
	Ca	943 ± 24	6133 ± 111
	Na	6702 ± 59	52093 ± 587
Anions	**Cl^-**	12075 ± 338	99605 ± 1328
	NO_2^-	B.D.L.	46 ± 12
	SO_4^{2-}	1391 ± 13	864 ± 12
	Br^-	50 ± 16	328 ± 17
	NO_3^-	3 ± 1	12 ± 7
	I.S. (M)	0.426 ± 0.026	3.078 ± 0.044
	TDS (ppm)	21672 ± 475	162252 ± 2268

2.2 Rock

Limestone samples were obtained from the LKC geologic formation in the Central Kansas Uplift region within an active reservoir located in Haskell County, KS. Crushed samples were analyzed through X-Ray Diffraction (XRD) (Bruker PROTEUM diffraction system at ambient temperature with monochromated CuKα radiation (λ = 1.54178 Å)), and the mineral composition is shown in the following table.

Table 2 Composition of limestone determined through XRD (% wt/wt)

	Calcite	Dolomite	Quartz
Lansing Kansas City (LKC) Carbonate	84.9	11.7	3.4

2.3 Bulk Mixing Experiments

Bulk mixing experiments were conducted to observe interactions between the brines and limestone. Liquid-Liquid (L-L) interactions between brines were evaluated by mixing Arbuckle and LKC brines in the following volumetric ratios (A:LKC): 10:90, 50:50, and 90:10. Samples were divided into 1.75 mL samples and placed in a shaker table maintained at 53°C. Samples

were removed at set intervals (ranging from 1 – 21 days) and filtered using 0.45 μm PTFE syringe filters. pH measurements of samples were recorded (Thermo Fischer ROSS Micro Combination pH Electrode) before being diluted and acidified with concentrated nitric acid (2% v/v) for analysis via ICP-OES.

Liquid-Liquid-Solid (L-L-S) interactions were evaluated in a similar manner, but ground LKC limestone (53 μm – 75 μm in size) was added to each mixture in a ratio of 1 g limestone:20 mL mixed brine prior to long term storage. To minimize the effects of atmospheric CO_2, sample tubes were sealed with Teflon tape. Additionally, mixing ratios of 0:100 and 100:0 were also utilized to observe interactions between the limestone and unmixed brine.

2.4 Geochemical Simulation

Geochemical interactions between the brines and limestone were modeled within PHREEQC—software specializing in geochemical and physical processes developed by the United States Geological Survey[30]. The simulation was coded to reflect the conditions of the bulk mixing experiments. PHREEQC has the capability to utilize a variety of thermodynamic databases to calculate equilibrium behavior without requiring any changes to the initial code. The following databases were utilized in this study: PHREEQC, PITZER, and MINTEQ. In addition to utilizing different equilibrium constants and different salts of possible chemical species, the models vary in their approach to activity corrections at high salinity conditions. The PHREEQC and MINTEQ databases utilize a combination of WATEQ and Davies equations, while the PITZER database relies on the Pitzer correlations[31]. The goal of the simulation was to evaluate the behavior of mixed brine samples after extended contact with LKC limestone through the examination of equilibrium concentration alongside saturation indexes of potential mineral

species formed and then compare this to experimental data. A description of the major components of the simulation and comparison of the models can be found in Appendix B.

2.5 Coreflooding Experiments

Coreflooding experiments were conducted using an apparatus identical to the one described by Tetteh et al.[32] (**Figure** 2). Limestone cores obtained from the LKC formation were utilized and stored in synthetic high salinity brine (**Table** 3) prior to flooding. A total of three coreflooding experiments were conducted with the main variable being alterations to the brine sequence and timeframe (**Figure** 3). Sequence 1 was conducted to establish baseline behavior of the brine-rock system, Sequence 2 investigated the influence of crude oil, and Sequence 3 was conducted to ensure the short flooding times of the previous tests did not obscure any major phenomena. Additionally, Sequence 3 involved flooding with a synthetic low salinity brine (**Table** 3) to observe the interaction between the Arbuckle brine and an even lower salinity brine. For each sequence, brine flowrate was set to 1 mL/min, chamber temperature was set to 53°C, and the effluent was collected in 1.5 mL intervals.

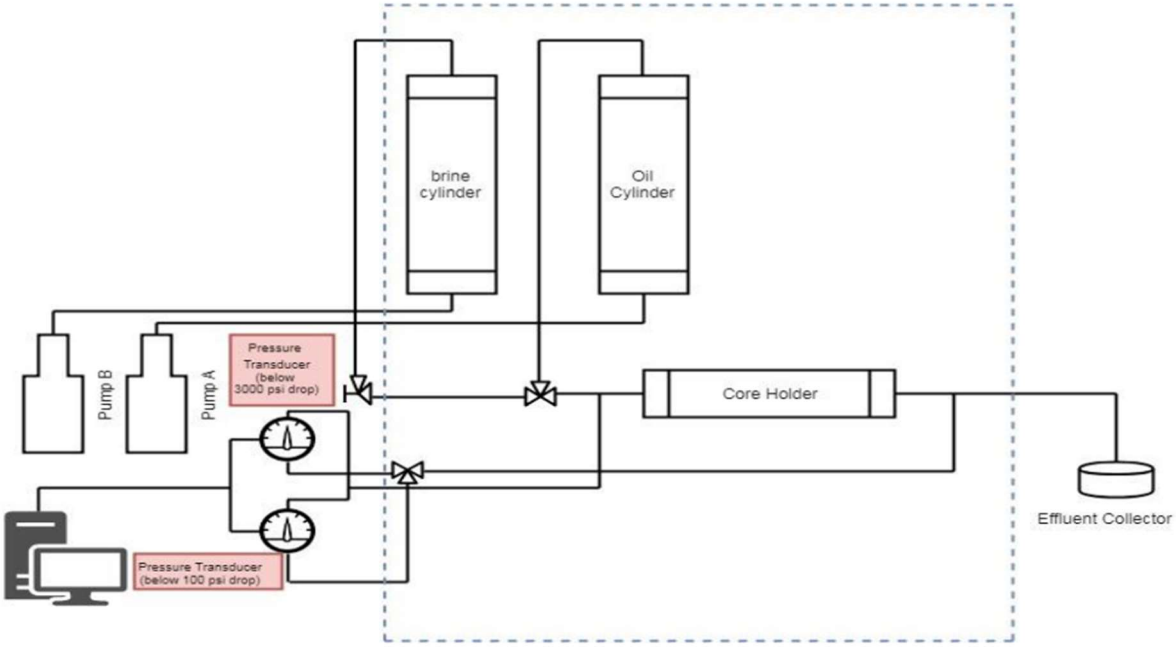

Figure 2 Coreflooding setup utilized for this experiment[32]

Cores for each sequence, approximately 1.5 inches in diameter and 3 inches in length, were obtained from the LKC reservoir. Before flooding, each core was cleaned using a Dean-Stark setup with toluene and methanol in a 1:1 volumetric ratio for 30 days to remove all crude oil present. Cores were then dried in an 80 ºC oven to evaporate the residual solvent. The cores were saturated with a high salinity synthetic brine (**Table** 3) by applying a vacuum and were then stored in the same brine until they were utilized. For the core used in Sequence 2, crude oil was pumped through the core after brine saturation followed by an aging step for 40 days at a temperature between 80 ºC and 90 ºC. Physical properties of the cores are shown in **Table** 4.

The coreflooding effluent was collected continuously in 1.5 mL increments with a system flowrate of 1 mL/min. pH of each sample was measured before filtration with a 0.45 μm PTFE syringe filter. Filtered effluent was diluted, acidified, and analyzed via ICP-OES.

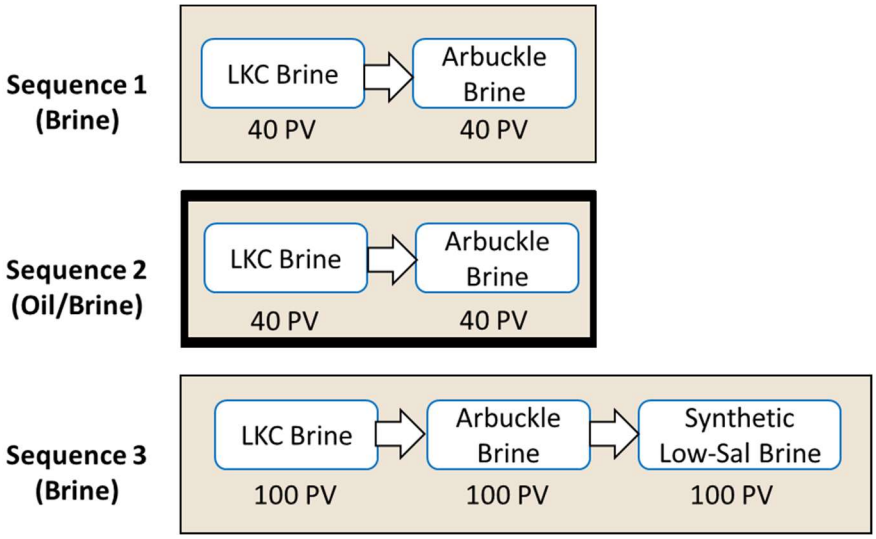

Figure 3 Coreflooding brine injection sequences; Sequences 1 and 2 utilized injection intervals of 40 PV, Sequence 3 utilized 100 PV intervals, and Sequence 2 was conducted in the presence of crude oil

Table 3 Ionic composition of synthetic brine (mg/L)

	Ca^{2+}	Mg^{2+}	Na^{+}	K^{+}	Cl^{-}	SO_4^{2-}	I.S. (M)	TDS (ppm)
Low Salinity	134	34	588	6	1,249	0	0.04	2,011
High Salinity	11,000	2,800	48,000	500	101,913	260	3.27	164,473

Table 4 Physical Properties of Core Samples

Sequence	**1**	**2**	**3**
Permeability (mD)	24.40	134.78	20.42
Pore Volume (cm^3)	6.38	5.60	8.53
Bulk Volume (cm^3)	23.22	23.28	33.86
Porosity	0.27	0.24	0.25

2.6 Economic Analysis via Techno-Economic Assessment and Monte Carlo Simulation

While brine exchange benefits in the form of increased oil recovery and reduced brine disposal volumes, it can only be implemented if the benefits (mainly the revenue increase from improved oil recovery) can outweigh the costs (infrastructure investment and energy costs from transportation). As real-world construction data is sparse due to the novelty of the process, the

economic viability of a hypothetical brine exchange operation was determined through techno-economic assessment, and the uncertainty was evaluated using Monte Carlo analysis.

The economic model consists of the following key components: infrastructure costs, operational costs, savings from reduced disposal needs, and increased income from improved oil recovery. The first component of the simulation was accounted for by incorporating the WaterCOSTE model developed by researchers at the University of Arizona[33]. This model was developed to predict the construction costs of a potable water pipeline through open land. The model accounts for both material and labor costs (installation and excavation). The original model was modified to incorporate sensitivity analysis and fit within the Monte Carlo framework. Variables not provided within the WaterCOSTE model were obtained from other sources, mainly the RSMeans 2020 handbook[34] or other articles/government databases.

Operational costs and disposal savings were incorporated by adding additional equations onto the end of the WaterCOSTE model. Operational costs consist of energy costs needed to transport brine between two reservoirs. This was accounted for by calculating the frictional losses through the pipeline as well as the energy needed to overcome them. This was then converted to electricity costs. Disposal savings were incorporated by multiplying the volume of the produced water by typical brine disposal costs per barrel (between 0.10 – 0.14 $/barrel within Kansas)[35].

The following are major key assumptions made when constructing the model to calculate infrastructure cost:

- All pipes are installed in open, flat terrain with negligible disturbances (i.e., no utility lines, roads, groundwater, right of way, etc.)

- Pipes are installed in rippable material, which can be removed via excavator (i.e., no bedrock or other difficult material)
- Pipelines are primarily straight with negligible bends, fittings, and valves
- Pipes are constructed out of PVC due to corrosion risk
- 10-year lifespan of the project with negligible maintenance cost

The following were key assumptions made regarding enhanced oil recovery scenario of the model:

- 22.2 barrels of injection water is needed for every barrel of oil extracted
    - This value was based on the average Produced Water:Oil ratio for the state of Kansas[36] and a volumetric balance assumption between extracted and injected liquids
- Enhanced Oil Recovery (EOR) of crude oil varies between 4% - 12%
    - This was incorporated into the model by increasing daily output of oil wells by 4% - 12%

To aid with comparison, a second model was constructed using alternative cost estimates for material and labor from an industry contact[35]. This method greatly simplifies the infrastructure costs by assuming construction will take place via a specialized third-party contractor rather than being handled in-house. The following values were implemented in this version of the model:

- Trenching is $0.75/ft regardless of pipe diameter
- Pipe diameters other than 3” or 4” are not used
    - 3” pipe costs $3.70/ft and 4” pipe costs $4.65/ft

Due to recent global events, the impact of variable material costs has become of greater concern. To determine the sensitivity of a brine exchange project to variable material costs, the

economic simulations were rerun multiple times with the base pipe material cost values all being multiplied by a fixed amount (-25% and +25%). Outputs are shown in **Figure** 9, which can be found in Section 3.3 Techno-Economic Assessment and Monte Carlo Results, and were compared to the base case to determine sensitivity.

The series of equations comprising the cost estimates of infrastructure, operations, disposal savings, and increased oil income were coded in MATLAB. The Monte Carlo, sensitivity analysis, and Spearman Rank correlation calculations were also handled by the same software. A full outline of the code and a list of inputs and assumptions can be found in Appendix C and E.

3 Results

3.1 Bulk Mixing Experiments

3.1.1 Brine-Brine Mixtures

Concentrations of Ca, Mg, and Sr along with pH measurements of brine-brine samples are shown in **Figure** 4. Concentration values showed no major variations over time indicating liquid-liquid compatibility as a decrease in concentration would have been observed had precipitation occurred. pH measurements showed slight variations during the initial days, but this was likely due to exchange with the atmosphere. This rise at the beginning of the experiment suggests the system was undersaturated with respect to CO_2. This was mitigated in future experiments by sealing sample vials with Teflon tape.

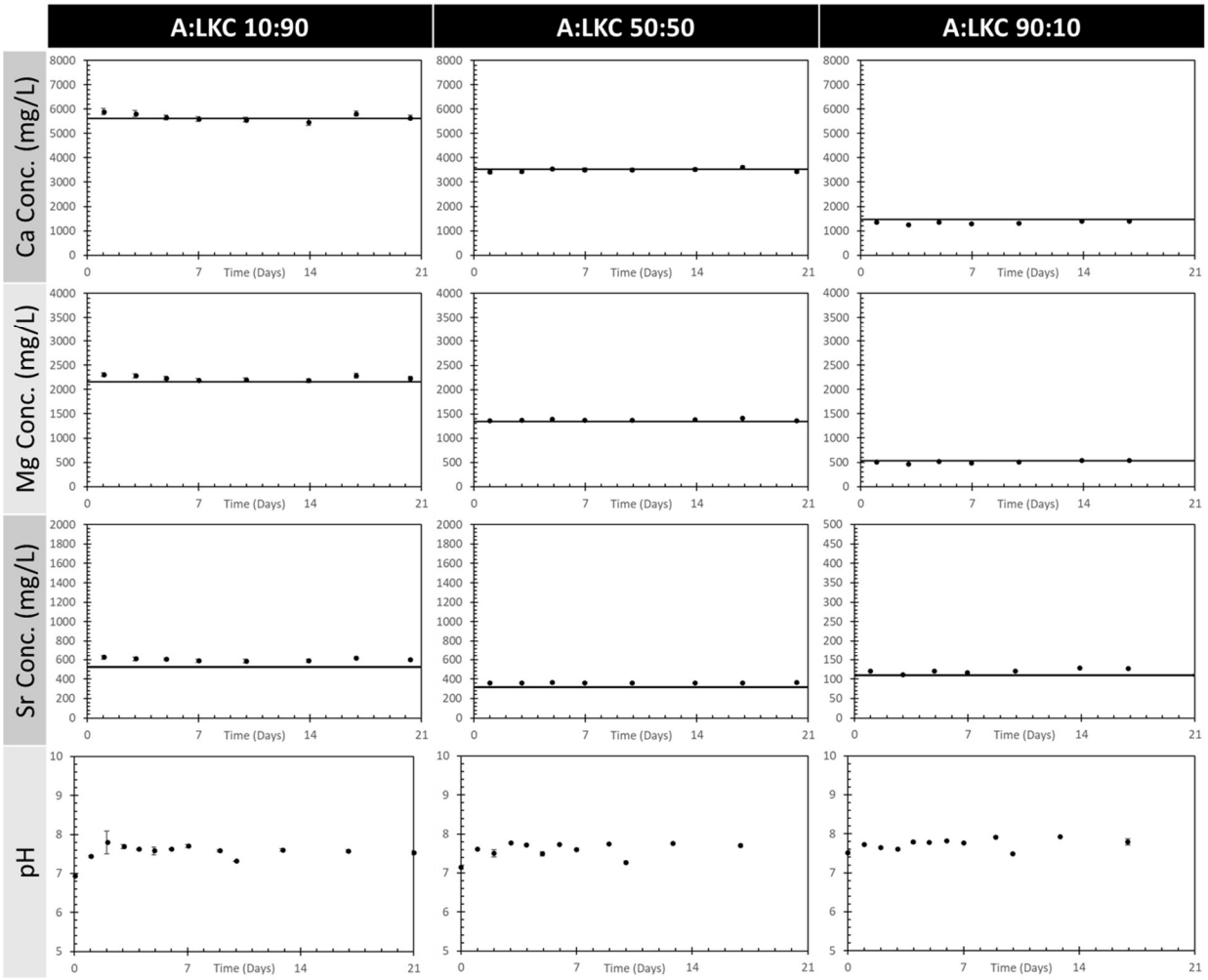

Figure 4 Cation and pH measurements of 10:90, 50:50, and 90:10 L-L bulk mixing samples; initial values (solid black line) plotted alongside experimented data; ±σ error bars plotted but not visible. Expanded figures can be found in Appendix A

3.1.2 Brine-Brine-Solid Mixtures

Experimental data of Ca and Mg measurements (**Figure** 5) show a net increase in concentration of both Ca and Mg for A:LKC S 10:90 and 50:50 mixing ratios. The 90:10 sample displayed a net decrease in concentration for Ca and no significant change for Mg. The change in concentrations of these cations can be attributed to the dissolution/precipitation of either calcite or dolomite. As decreases in ion concentration serve as signs of incompatibility, the A:LKC 90:10 sample warrants concern. Mechanisms responsible for this behavior and their significance are discussed in latter sections.

Sr measurements all show a net increase in concentration, but this is most likely due to the detection limits of the instrument as there was no source of Sr in the mixtures. The high salt content of the samples required dilutions on the scale of 500x and 1000x to produce samples within tolerable salinity. As a result, cations with comparatively low concentrations (i.e., Sr) become difficult to measure accurately.

Geochemical simulation results are plotted alongside experimental data. Mean Absolute Percent Error (MAPE) was calculated to evaluate the fit of each model to the experimental data (**Table** 5 and **Table** 6). Low MAPE values (≤ 5.0%) indicate a good fit in the case of PHREEQC predictions or no significant change when looking at differences relative to initial conditions.

Based on the MAPE values of the geochemical model predictions, each of the three databases had more trouble with Mg than Ca. The PHREEQC database showed limitations at high salinity conditions. The PITZER struggled with mixed brines across the entire salinity range. MINTEQ showed the reverse trend and had large errors at low salinity conditions. This behavior can be attributed to inherent limitations of the databases and are discussed in later sections. Sr error should not be accepted at face value as they are impacted by detection limits of the ICP-OES.

Samples containing unmixed Arbuckle and LKC brines and limestone were prepared and analyzed to serve as baseline conditions. The LKC and limestone mixture was expected to show no significant change in ionic concentration as the brine would have equilibrated with the rock before it was extracted from the reservoir. MAPE values confirm this as the error compared to initial conditions was 3.1% (seen in **Table** 5 below).

Concentrations within the Arbuckle and limestone samples show signs of dissolution occurring. MAPE values for Ca and Mg from initial conditions were 4.7% and 6.1%, respectively. Explanations of this phenomenon are described in latter sections.

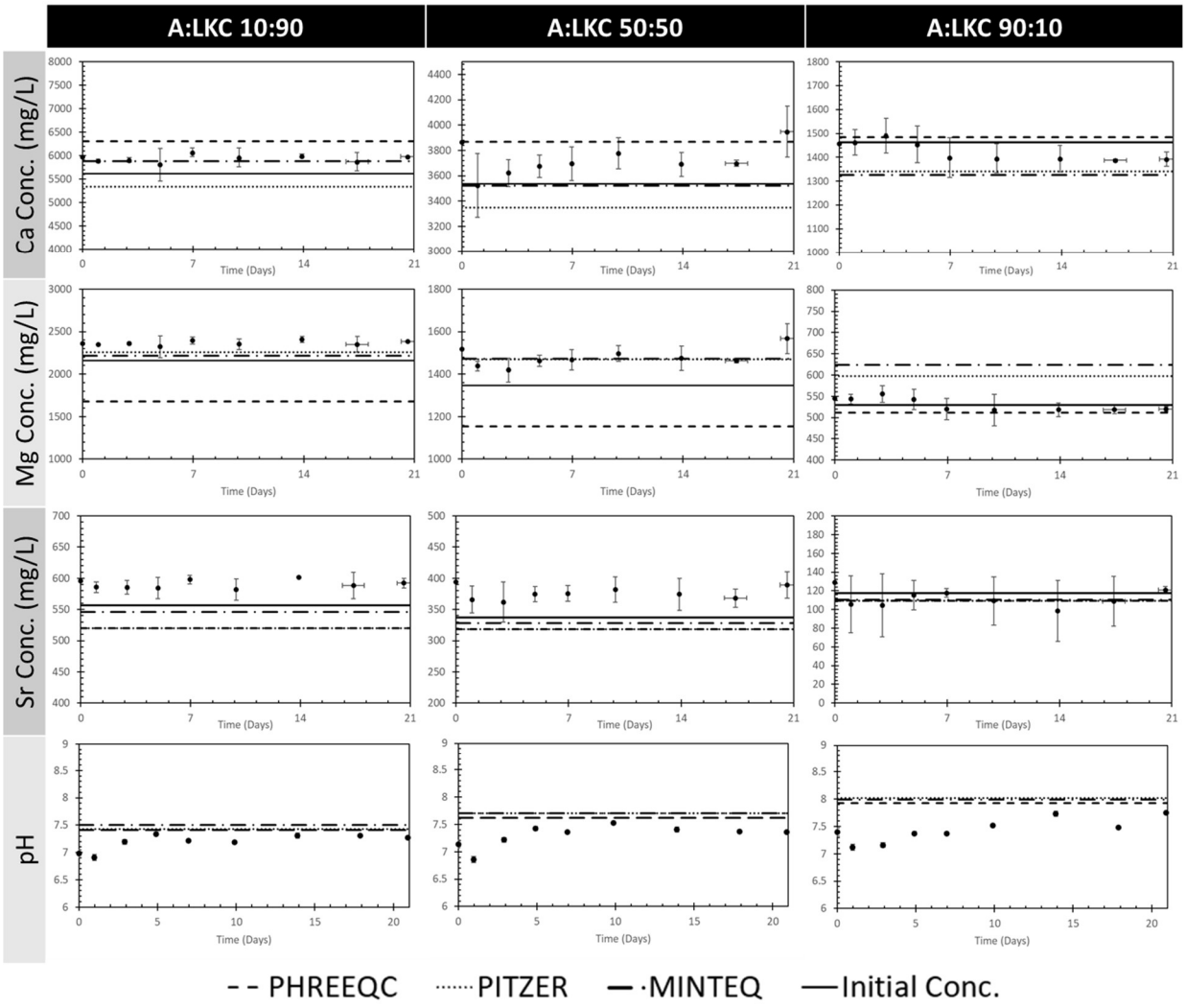

Figure 5 Cation and pH measurements of 10:90, 50:50, and 90:10 L-L-S bulk mixing samples; initial values (solid black line) plotted alongside experimented data and PHREEQC equilibrium predictions; ±σ error bars plotted but not visible for all points; note the offset y-axis

Table 5 MAPE of Liquid-Liquid-Solid PHREEQC Predictions

	PHREEQC				PITZER[a]				MINTEQ			
	Ca	**Mg**	**Sr**	**pH**	**Ca**	**Mg**	**Sr**	**pH**	**Ca**	**Mg**	**Sr**	**pH**
A:LKC 0:100	13.53	25.04	2.66	3.55	4.19	2.64	2.65	3.08	6.61	1.88	6.96	4.9
A:LKC 10:90	6.17	29.08	11.96	3.06	10.04	48.35	11.96	3.02	1.27	6.23	7.43	4.37
A:LKC 50:50	4.5	21.96	15.2	4.59	9.97	45.94	15.19	5.75	5.32	2.06	12.6	5.73
A:LKC 90:10	4.31	3.57	6.3	6.11	5.84	38.55	6.31	7.53	6.97	17.5	6.49	7.06
A:LKC 100:0	7.15	3.13	6.05	6.39	14.28	9.25	6.05	7.67	17.07	15.83	5.49	7.3

[a] Simulations were conducted using an older version of the database file (ver. 3.6.2). Newer versions utilize updated constants for calcite but produce results with less accuracy. See Section 10 Appendix D: PITZER Database for more detail.

Table 6 MAPE of Liquid-Liquid-Solid Initial Conditions

	Initial Conditions		
	Ca	**Mg**	**Sr**
A:LKC 0:100	4.59	3.12	6.96
A:LKC 10:90	5.51	8.55	11.07
A:LKC 50:50	4.93	8.94	15.67
A:LKC 90:10	3.06	2.51	6.26
A:LKC 100:0	4.69	6.05	5.49

3.1.3 Brine-Solid Mixtures

To establish baseline behaviors, unmixed Arbuckle and LKC brines (**Figure** 6) were combined with limestone solids (ratios of 0:100 and 100:0). LKC + Solid samples display minor signs of precipitation for all elements analyzed, indicating oversaturation. The inverse behavior was seen in the Arbuckle and solid mixture and suggests the brine is undersaturated for these elements. Model outputs were inconsistent, with each database underpredicting one cation while overpredicting the other. pH in both sets of samples increased sharply on Day 5 and plateaued after this period. This may have been caused by a loose seal in the sample vials, but the possibility of a slow reaction cannot be excluded.

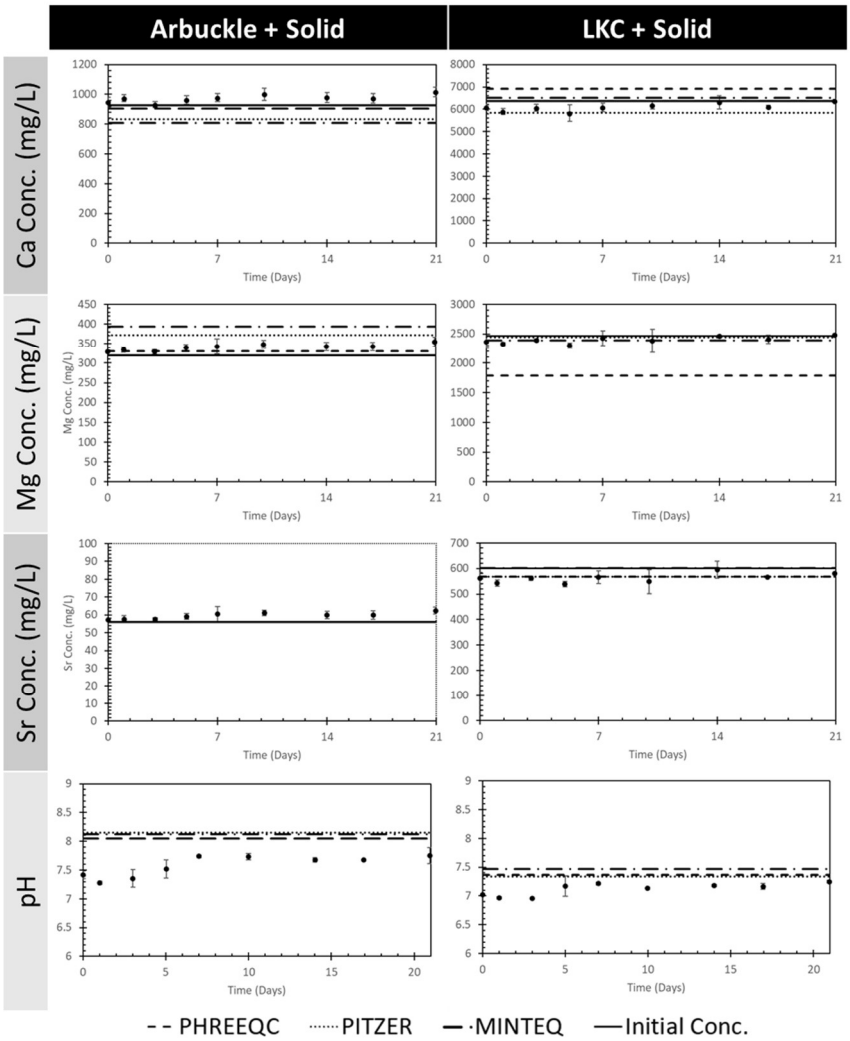

Figure 6 Cation and pH measurements of A:LKC 100:0 and 0:100 bulk mixing samples; initial values plotted alongside experimented data and PHREEQC equilibrium predictions; ±σ error bars plotted but not visible for all points

3.2 Corefloodling Results

Ca and Mg concentrations of coreflooding effluents were plotted against Pore Volume (PV) and pressure (**Figure** 7). Results across all three sequences show that effluent concentrations quickly shift to match the concentration of the flooding water, with the transition being completed within 6 PV.

Pressure data is included alongside concentration data and display typical trends common for these types of experiments. Sequence 1 displays a gradual increase in pressure over the course of the flooding. There are multiple possible mechanisms which could be responsible for

this behavior. The cores were obtained from reservoir rock, so high heterogeneity could have prevented the system from reaching steady state. Additionally, the flow of brine through the core may have resulted in fines migration, the phenomenon where loose particles are dislodged from the rock surface causing pore blockage downstream and increasing pressure. While it is possible precipitation reactions may have occurred and impeded flow, the results of the bulk mixing experiments and cation measurements during the coreflooding experiments indicate no strong signs of these reactions occurring to any significant degree.

Sequence 2 starts with a sudden decrease but quickly levels off, and this trend represents the ideal behavior for coreflooding experiments. While all cores came from the same formation, the use of reservoir samples means heterogeneity is high, and two cores located in close proximity to one another can have very different properties. Here, the higher permeability of the core used in Sequence 2 (**Table** 4) likely had an impact on the behaviors seen during the flooding.

Sequence 3 is noticeably different than Sequence 1 despite being similar in setup and execution. Sudden drops and spikes coincide with points where brine pumps were stopped and refiled, which occurred more often due to the increased timespan of the flooding. Had the pumps been refiled more quickly or not stopped at all, it is likely the trend would have more closely resembled Sequence 1. The pressure data here should not be relied upon heavily as the interference caused by the pump refilling period reduces confidence in the data.

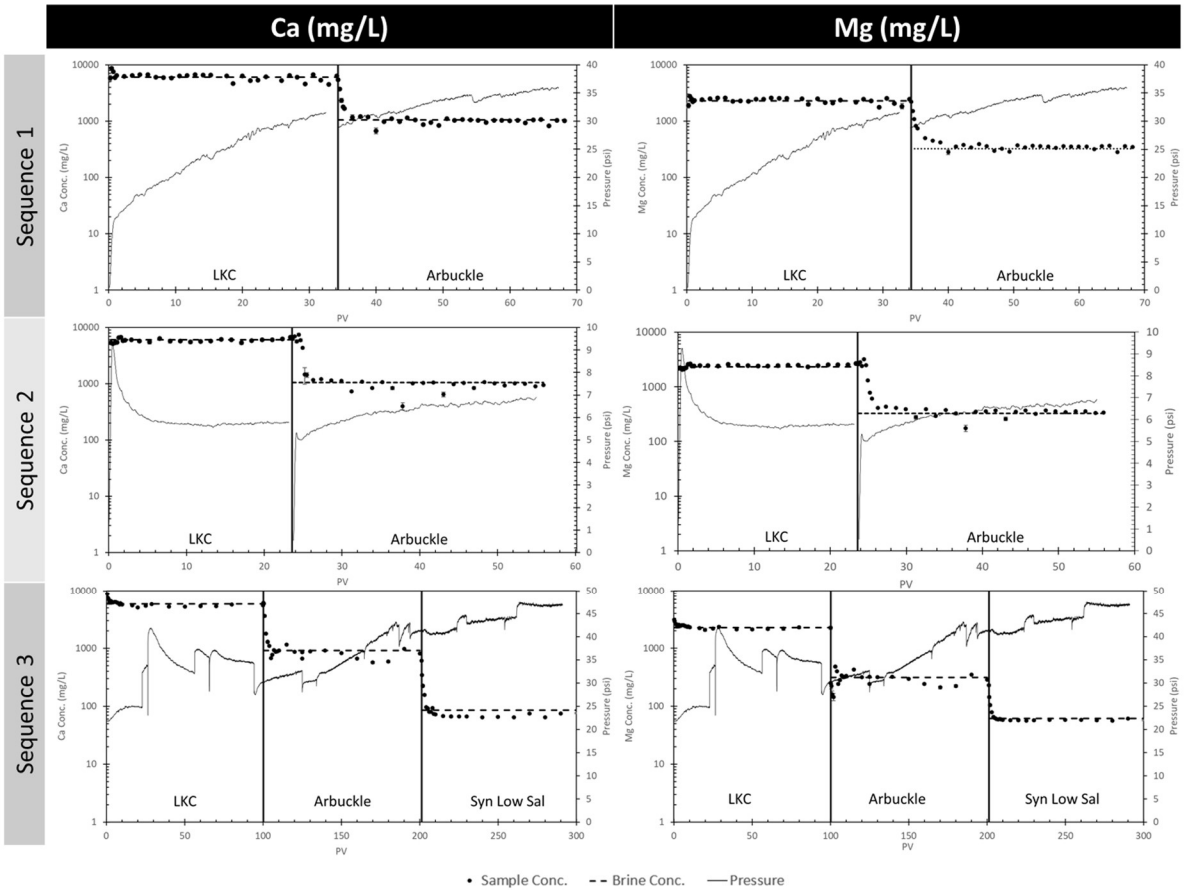

Figure 7 Ca and Mg concentrations of coreflooding samples (left axis) plotted alongside pressure (right axis)

3.3 Techno-Economic Assessment and Monte Carlo Results

The daily net benefit/cost in terms of dollars per day of potential brine exchange projects as a function of both distance and brine flowrate are shown in **Figure** 8. The simulation was run twice: once using data from literature and again using cost estimates from an industry contact. Approximate breakeven lines are plotted alongside model outputs. Additionally, Spearman Rank Correlation calculations were performed on each variable and can be seen in Appendix C: WaterCOSTE Model Input and Output.

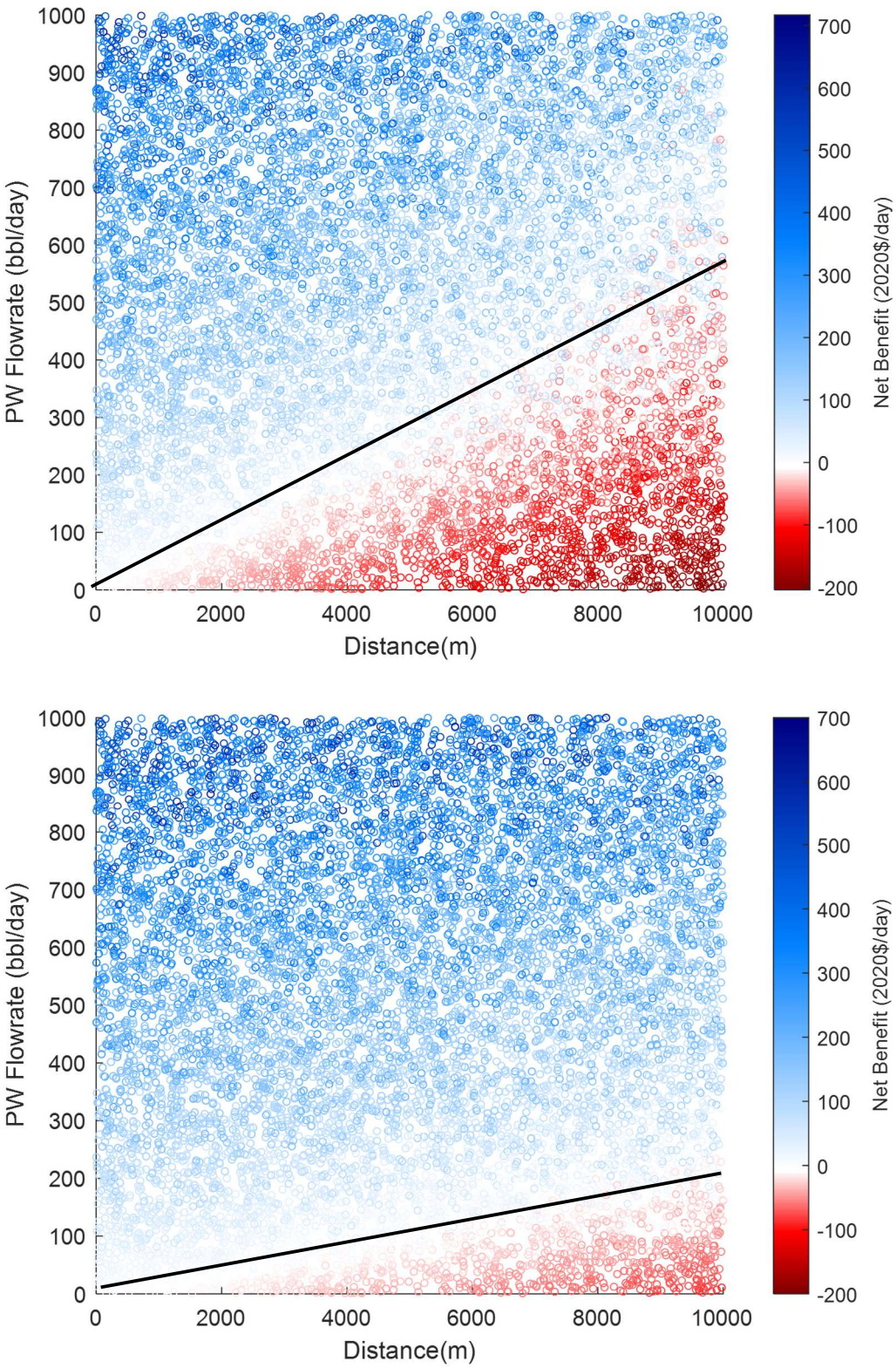

Figure 8 Economic simulation results utilizing the WaterCOSTE model (top) and cost estimates from an industry contact (bottom). Breakeven line plotted alongside datapoints

Sensitivity analysis performed by varying base pipe material costs is shown in **Figure** 9 below. The graphs based on the Water COSTE model are nearly indistinguishable from each other and their base case scenario, which indicates increasing or decreasing the costs of material has a minimal effect on the overall economic viability of the project. The only impact this modification has compared to the base case is the boundary between viability and unviability is less sharp, but the size and position of the regions themselves remain unchanged. Overall, a change in material cost will be a major concern only if the project was operating near the breakeven point. Projects located far into the viable/unviable regions will not suddenly shift due to these changes.

The sets of graphs utilizing industry estimates do have a noticeable shift corresponding to material price changes. As expected, a decrease in material price results in a greater profitable operating range and vice versa for an increase in material price. As with the previous sets of graphs, the boundary between feasibility and infeasibility becomes less sharp, but only when prices increase. A table depicting the changes in average and median values of Net Benefit between simulation runs is shown below.

Table 7 Mean and median net benefit values obtained from individual economic analysis simulations

	Model	**Mean Net Benefit Value (2020$/day)**	**Median Net Benefit Value (2020$/day)**
Base Scenario	WaterCOSTE	106.93	91.92
	Industry Estimate	180.00	167.66
-25% Material Cost	WaterCOSTE	107.51	92.43
	Industry Estimate	188.31	176.28
+25% Material Cost	WaterCOSTE	106.35	91.31
	Industry Estimate	155.38	143.27

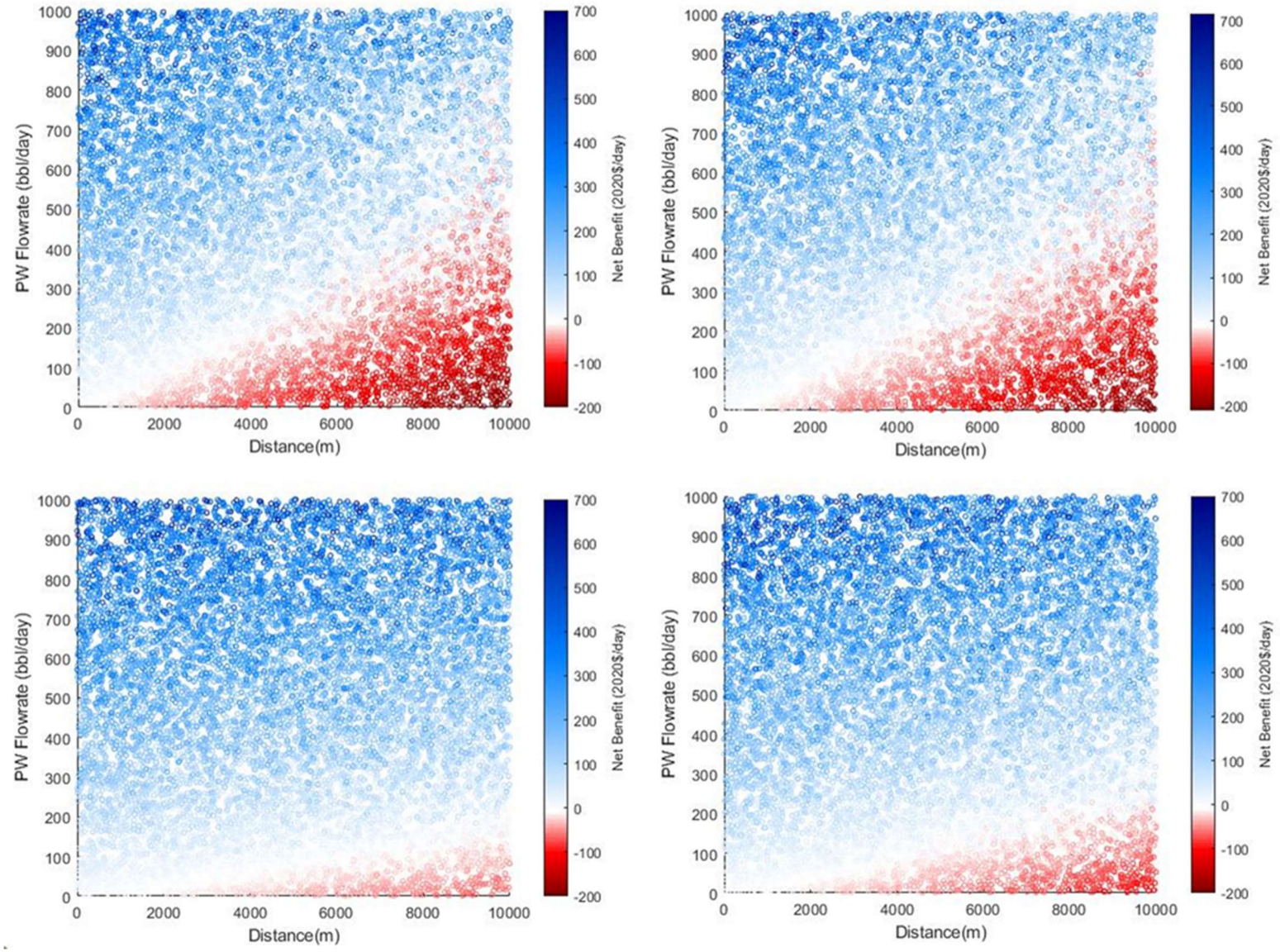

Figure 9 Sensitivity Analysis of Material Cost. WaterCOSTE based output with -25% (top left) and +25% (top right) change in pipe cost shown alongside industry contact-based estimates with -25% (bottom left) and +25% (bottom right) price change

4 Discussions

4.1 Geochemical Compatibility of Arbuckle and LKC Brines

The experiments conducted in this study show a trend of geochemical compatibility between the Arbuckle and LKC brines, however some of the results indicate there are areas where incompatibility may be a concern (**Figure** 5). Conditions where incompatibility may be present, the mechanisms responsible for dissolution/precipitation, and geochemical behavior under the influence of flow conditions are discussed in the following sections.

4.1.1 Compatibility between Arbuckle and LKC brines in L-L Systems

Figure 4 indicates the cation composition in mixed brine samples did not display major deviations from initial conditions throughout the course of the experiment, indicating the absence of any chemical reaction. The main factor behind this is the lack of Ba in either of the water samples. Ba and SO_4 ions are a large concern within the oil industry as they readily react with one another to form $BaSO_4$ ($pK_{sp} = 9.97$)[37] and lead to scaling. Decades have been spent trying to characterize its formation and mitigate it[26,38], but it continues to be a problem for operators to this day. If potential injection water contains Ba in any appreciable concentration while the connate has SO_4 (or vice versa), brine-brine incompatibility should be anticipated.

4.1.2 Compatibility of Brines in L-L-S Systems

The data presented in **Figure** 5 suggests that at a specific mixing ratio of Arbuckle and LKC brine, the equilibrium of the mixture shifts from favoring the dissolved mineral species to their solid form. This leads to the following questions: 1) what mechanism is responsible for these reactions and 2) how do mixing ratios affect it.

The behavior of carbonate species during low salinity water injection has been characterized in previous studies. Tale et al.[39] and Esene et al.[40] both investigated the bulk dissolution and precipitation of carbonate minerals in their studies regarding wettability

alterations. Tale et al. coupled bulk dissolution experiments with surface reactivity models and observed how the use of synthetic low salinity brine (TDS = 36,109 ppm; Ionic Strength = 0.64 M) resulted in the precipitation of calcite (~0.8 mmol/L) and dissolution of dolomite (~0.5 mmol/L) with dilutions of this brine decreasing the magnitude of this behavior. Esene et al. developed a reactive transport model to simulate injected brine behavior in the presence of sulfate and noticed similar behaviors. The degree of precipitation/dissolution of calcite and dolomite, respectively, varied with sulfate content and distance from the injection source, but it was less than those seen in Tale et al. and this study. This is likely due to the higher salinity brine used (TDS = 245,980 ppm) and different limestone composition (50/50 volumetric ratio of calcite and dolomite).

Both Tale et al. and Esene et al. attributed this precipitation of calcite and dissolution of dolomite to the amount of carbonate available within the system. The mineral species react according to the following schemes:

Table 8 Limestone dissolution mechanisms

$\text{Calcite} + H^+ \leftrightarrow Ca^{2+} + HCO_3^-$	[$pK_{sp} = 8.46$][37]	Eqn 1
$\text{Dolomite} + 2H^+ \leftrightarrow Ca^{2+} + Mg^{2+} + 2HCO_3^-$	[$pK_{sp} = 11$][37]	Eqn 2

Prior to the bulk mixing experiments, the produced water was exposed to the atmosphere during transport and storage long enough to reach equilibrium with the atmosphere, and the atmospheric CO_2 dissolved into the brine and formed HCO_3^-. After the two brines were mixed and sealed, the equilibrium of the mineral species shifted with the direction being dictated by the HCO_3^- saturation of the mixture.

The quantity of HCO_3^- present within each brine is dictated by the solubility of CO_2. The "salting out" of CO_2 is a phenomenon in which the solubility of the gas decreases as the salinity

of a solution increases due to the increased polarity between liquid molecules. This is a possible mechanism responsible for the trends observed. This decrease is difficult to measure as it is highly dependent upon the specific ions present as well as the quantity of gaseous CO_2 present. Liu et al.[41] attempted to quantify this decrease and found solubility decreased by approximately 4% as the concentration of NaCl increased from 1,000 ppm to 15,000 ppm at a partial pressure of 2 MPa (**Figure** 10). The trend of the data suggests this disparity will increase as the partial pressure is decreased.

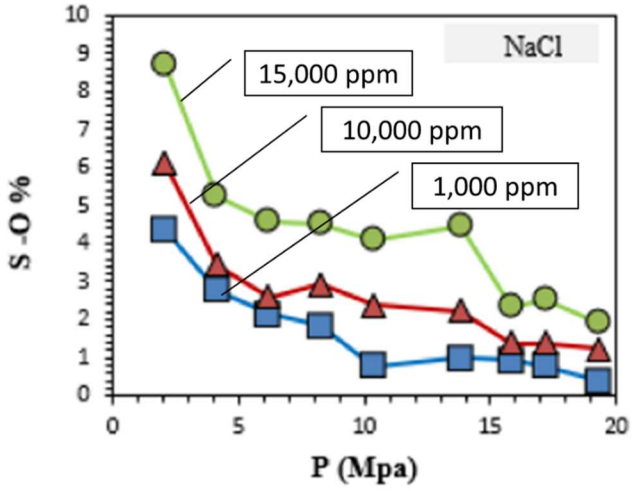

Figure 10 Salting Out Effect of NaCl on CO_2. Percent difference of solubility in DI water and saline solution plotted against partial pressure. Adapted from Liu et al., 2021

When the ratio of Arbuckle to LKC brine was low, the system was undersaturated with respect to HCO_3^- due to the low solubility of CO_2 in the LKC brine, so dissolution of mineral species occurred to restore equilibrium. In mixtures where Arbuckle brine was present in a greater quantity, HCO_3^- was oversaturated as CO_2 is more soluble in Arbuckle brine than mixed brine, and precipitation of calcite occurred to restore equilibrium. However, this created a deficit in Ca, so dolomite began dissolving in response, resulting in a slight increase in Mg. This creates a delicate situation for operators as injecting low salinity water in carbonate reservoirs increases the risk for scale formation, yet low salinity water has been shown to improve oil recovery[8,17,42].

The behavior seen here will occur even if the initial brine samples are at equilibrium with the atmosphere as the relationship between salinity and CO_2 solubility is nonlinear (**Figure** 10).

4.1.3 Compatibility in L-S Systems

Limestone was combined with Arbuckle and LKC brines to evaluate behavior in the absence of mixing. The composition of the LKC brine after the addition of solids was expected to remain constant as the brine should have reached equilibrium with the limestone before it was extracted. Results support this claim as the ion composition showed minor variance. The small deviation can be attributed to dilution and analytical limitations of the ICP-OES.

The mixture of Arbuckle brine and limestone shows signs of mineral dissolution (**Figure** 6) which is interesting since this would be a reversal of the trend observed in the previous mixtures. While there are mechanisms that could explain the dissolution of calcite material (mainly the increase in calcite solubility due to increased gypsum presence[43]), the conditions for this to happen (high SO_4^- concentrations to facilitate gypsum formation) were not met in these experiments. It is likely that the behavior observed in this mixture was due to the Arbuckle brine not being at complete equilibrium with the atmosphere as previously thought or errors attributed to analyzing low ion concentrations.

The results gathered here do not fully support nor disprove the compatibility of Arbuckle and LKC brines. On one hand, analysis of the carbonate equilibrium mechanism and predictions among geochemical simulations depict signs of precipitation and incompatibility between brines, most notably at low salinity conditions. On the other, experimental data shows a clear sign of mineral dissolution, indicating compatibility. Fortunately, this inconclusiveness is irrelevant in a field application of brine exchange. Even the most severe cases of calcium carbonate scale

buildup can be treated easily and cheaply with an HCl flush of the impacted region, and nothing in the results indicates scale formation will be a major concern even if it does occur.

4.1.4 Fluid Flow Effects on Brine Compatibility

Based on the results of the three individual experiments (**Figure** 7), displacement of the connate brine by the injected brine is the dominant transport mechanism during waterflooding rather than mixing. Within all floodings, the injected brine displaces the previous brine quickly (within 6 PV). This occurred regardless of the presence of crude oil (Sequence 2) or the salinity difference between the two brines (Sequence 3). While it can be assumed some mixing between brines occurs at the liquid interface, the interaction between the injection brine and the surrounding rock is more important in the context of scale formation, especially within the area surrounding the injection well. As such, more weight should be given to the compatibility of A:LKC 100:0 and 90:10 mixtures of the previous experiment.

The results seen here agree with the findings of other studies focused on the mathematics and modeling of brine behavior during waterflooding. Sorbie and Mackay[44,45] noted how injected brines tend to displace connate brine rather than mix within homogeneous rocks or systems which can be accurately described with 1-dimensional flow. They, as well as Attar and Muggeridge[46], also observed how vertical and lateral heterogeneity in the surrounding rock can lead to increased brine mixing due to complex flow patterns. In systems where brine-brine compatibility is a concern, Sorbie and Mackay noted how this results in additional care being needed to protect the wellbore region where most precipitation is likely to occur. Heterogeneity may be beneficial for the Arbuckle and LKC system as greater mixing shifts the equilibrium in favor of dissolution (i.e., reduces scaling concerns) (**Figure** 5). Additionally, studies investigating the wettability alteration mechanisms have found the release of Ca ions into

solution may contribute to increased oil recovery, but further studies are needed to better quantify this effect[10,47,48]. It should be noted both Sorbie and Mackay and Attar and Muggeridge focused on systems with brine-brine incompatibility and did not investigate the geochemical interactions with the surrounding rock. As such, the implications on solid-brine incompatibility on long term flow behavior warrants further study.

4.2 Accuracy of Geochemical Model Predictions

As seen in **Figure** 5 and **Table** 5, none of the three thermodynamic databases evaluated in this study could accurately predict geochemical behavior across all mixing ratios. Since modeling will be the primary method of determining initial viability for future brine exchange projects, it is important to understand the constraints of these models as they are all commonly used within the industry. Limitations of thermodynamic databases within PHREEQC have been the subjects of previous studies[31,49], and it has been shown each database evaluated here possesses at least one shortcoming which affects the model predictions.

4.2.1 PHREEQC Database Evaluation

PHREEQC predictions consistently overestimated Ca concentrations and underestimated Mg with Mg deviations being more severe. A possible explanation for this can be attributed to the database's inability to handle high ionic strength environments. The PHREEQC database relies on a combination of WATEQ and Davies equations for activity correction[31]. However, the accuracy of these equations begins to decrease above 1.0 M I.S. and 0.5 M I.S., respectively. Horbrand et al. validated the database against experimental data and found positive deviations began to occur above 1.0 molal NaCl[49]. These findings are consistent with the results of this experiment as the accuracy of Ca predictions became greater as salinity of mixed samples decreased (**Table** 5).

Mg was more difficult to model as these compounds are impacted by temperature limitations in addition to salinity. Lu et al. found solubility predictions for dolomite (the only source of Mg in this study) were only accurate up to 25 ºC, which is less than half of the temperature used in this study. This coupled with the difficulty of predicting Ca behavior, led to the inaccuracy of the model. Interestingly, the Mg predictions for the A:LKC 90:10 mixture was more accurate than others, which suggests limitations are minimized at lower salinity and lower Ca conditions.

4.2.2 PITZER Database Evaluation

Unlike the PHREEQC database, the PITZER can accommodate higher salinity conditions (up to 6 M I.S.) due to its use of the Pitzer equations for activity corrections. However, model outputs deviated from measured values by the greatest degree, highlighting a critical shortcoming not found in the other databases. Horbrand et al. attributed under predictions of calcite solubility to PITZER's lack of calcium complexes (specifically $CaHCO_3^+$), which is found in other databases. Complexes are soluble but un-ionized species, which means their constituents do not play a role in all equilibrium calculations. As they do not exist within PITZER, the model cannot account for the loss of Ca^{2+} and CO_3^{2-} ions due to their formation, and solubility is underpredicted. Additionally, Horbrand et al. also noted accuracy of the database decreased in a salinity window of 1 – 2 M NaCl but fit experimental data above and below this range. While no further investigation was conducted, it is possible Ca complexes could be at fault as their formation has been shown to be impacted by ionic strength[50].

The PITZER database has undergone notable revisions in the past few years. Starting with Version 3.7.0, constants associated with calcite were updated to reflect more accurate values. However, our modeled results with the updated database yielded a worse fit with the

experimental data, with models predicting heavy dissolution of calcite for all brine mixtures. As database updates were recent, no literature is available for comparison. See Appendix B for more detail.

4.2.3 MINTEQ Database Evaluation

The MINTEQ database was designed to model reactions within surface waters and uses similar activity correction methods to the PHREEQC database. It still relies on both the Davies and WATEQ equations but has a greater reliance on the Davies and has a lower salinity tolerance as a result (up to 0.4 M NaCl)[31], resulting in the upper salinity limits for this model being slightly out of the range used in these experiments (**Table** 1). However, these models are consistently higher for Ca concentrations and lower for Mg, indicating some underlying discrepancy within the datafile. While MINTEQ and PHREEQC do possess slightly different thermodynamic and equilibrium constants for calcite and dolomite, the main difference lies within their approach to fugacity calculations. PHREEQC relies on the Peng-Robinson approach while MINTEQ utilizes the Ideal Gas Law, which breaks down at high salinity conditions[31]. As MINTEQ was overestimating the solubility of CO_2 (and by extension HCO_3^-), the result was an underprediction of calcite solubility compared to PHREEQC.

Unexpectedly, the MINTEQ predictions produced a closer match to Ca measurements at higher salinity conditions despite errors of the Ideal Gas Law being minimized at lower salinity conditions. Based on limitations of this database, it would be expected for accuracy to be higher when salinity is low. This may be an indication that errors caused by the Ideal Gas Law and those caused by activity corrections are occurring in opposite directions and canceling each other out at high salinity conditions.

While inaccurate on their own, the MINTEQ and PHREEQC predictions show promise at establishing a direction for cation concentration changes under a limited set of conditions. If these limitations could be better defined, the models would still prove useful in determining whether precipitation will occur at all and if concerns of incompatibility are warranted.

4.2.4 Utility of Geochemical Simulations

While none of the three databases evaluated could match experimental data across all samples, this does not mean modeling is useless with regards to predicting geochemical compatibility of brine samples. For real-world scenarios, the most important piece of information to obtain is the direction of ionic concentration change relative to initial conditions (i.e. whether concentration shifts upwards due to dissolution or downwards due to precipitation). Determining the magnitude of this change is secondary as operators are more interested in knowing whether precipitation will occur rather than how much solid will be formed. While modifying the modeling approaches to a degree where they can predict equilibrium concentrations accurately will likely require extensive work, modifying them to the point where they can reliably predict the direction of concentration change or identify the range of conditions where their accuracies are acceptable may be more feasible and will still prove valuable in real-world applications.

4.3 Economic Analysis

The output of the techno-economic assessment and the Monte Carlo simulation reveals the Pareto frontier for potential brine exchange operations. The viable conditions predicted utilizing the WaterCOSTE model are more constrained compared to the model utilizing industry cost estimates. This is likely due to differences in their approach to pipe installation costs. The WaterCOSTE model assumes a company has trained employees available but will need to rent construction equipment. In the oil and gas industry, it is common to hire a third party to handle

every aspect of pipeline construction. While outsourcing labor typically incurs additional costs compared to in-house labor, the efficiency and expertise of the third-party assumed in this scenario are enough to drive down the final cost.

Spearman Rank Coefficients were calculated for each variable used in the economic model (**Table** 13). As expected, variables that represent additional cost possessed negative correlations with the Net Benefit of the project. In contrast, those representing income or cost savings had positive correlations with Net Benefit. Flowrate has a strong positive correlation with the Net Benefit as it was assumed the relationship between produced water to increased oil recovery was linear. Real case scenarios would provide a more nuanced relationship and likely shift the correlation to the negative region had they been implemented in the model.

The sensitivity analysis results shown in **Figure** 9 indicate a ±25% shift in pipe material cost has a minor effect on the overall economic viability of the project. Looking at the WaterCOSTE based models, fluctuations in material price produced no major changes. The location of the Pareto frontier remains constant between simulations (**Figure** 9) and the shifts to the mean and median net benefit values were minimal (**Table** 7). This is likely due to the complexity and degree of manipulation of variables within the model, which obscured the impact a single variable had on the final calculations. While it can be said the profitable regions became more profitable and the non-profitable regions less so, the boundary between these regions did not change, meaning overall project feasibility is also left unchanged. Concern is only warranted if the project was operating near the breakeven line, which has become less sharp and less distinct with these changes.

Applying the same adjustments to material prices in the model based on industry estimates resulted in noticeable changes. Lower prices resulted in a greater range of profitability and

higher prices resulted in the opposite. The reason why these sets of figures behaved differently than the previous is likely due to the simpler approach taken by this method. Since there are fewer variables, and each are manipulated to a lesser degree, changes to the values are more noticeable in the model output.

5 Conclusions and Future Areas of Research

Operational viability of a potential brine exchange operation was evaluated by determining the geochemical compatibility of low salinity Arbuckle brine (injection water) and high salinity LKC brine (in-situ water). Ionic concentration measurements of mixed samples indicated brine-brine mixtures are compatible with one another across all mixing ratios—mainly attributed to the lack of Ba ions in the samples. Brine mixtures combined with LKC limestone were compatible at high salinity mixtures (low ratio of Arbuckle to LKC brines) but displayed signs of incompatibility as salinity decreased (high ratio of Arbuckle to LKC brines) due to hypothesized changes in CO_2 solubility and the resulting shift in equilibrium. Mixtures of Arbuckle brine and LKC limestone show signs of mineral dissolution, which would indicate a sudden reversal in dissolution/precipitation trends seen in the observed mixtures. However, this most likely indicates equilibrium had not been reached between Arbuckle brine and CO_2 prior to experimentation rather than another underlying mechanism. While incompatibility was predicted at low salinity conditions, MAPE calculations indicate scale formation will only be minor (if it occurs at all) and not enough to warrant concern if a pilot operation were to be initiated.

Experimental data were compared to PHREEQC equilibrium models using the PHREEQC, PITZER, and MINTEQ thermodynamic databases to determine simulation reliability at field conditions. No model was able to consistently match experimental data due to inherent limitations of each database. The PHREEQC and MINTEQ suffer from low ionic strength

tolerance with the latter also suffering from constraints of using the Ideal Gas Law for fugacity calculations. While the PITZER can handle a broader salinity range, the equilibrium and thermodynamic constants for several Ca species are either inadequate or outright missing. While no database can match data across all conditions, each model possesses a window where predictions match experimental results closely. This study suggests the window of applicability is dependent upon ionic strength, but further study is needed to rule out the impact of ionic composition. Even in situations where no single model can provide a close match, multiple models can be combined to establish the upper/lower bounds for concentration or a range of potential values.

Techno-economic assessment and Monte Carlo analysis provided an initial estimate for the range of conditions needed for economically viable operations. It is expected distance and energy costs represent two significant cost factors, while income from enhanced oil recovery and disposal savings represent significant forms of benefit. When comparing estimates using the WaterCOSTE approach and the guidelines obtained from industry, the WaterCOSTE produced more conservative costs and a narrowed range of viable operating conditions. This is likely due to the inability to account for bulk savings and the efficiency increase of hiring a third-party to handle procurement and installation.

While the results of the study are promising, additional research could be conducted to increase the confidence and depth of the conclusions reached. Similar mixing experiments should be conducted with larger samples volumes to mitigate atmospheric exchange during the aging step. Additionally, the reliability of the thermodynamic databases can be increased by better understanding the limitation of each approach. This study varied the ionic strength of mixed brine samples, but the influence of specific ions or combinations of these ions should be

investigated further. Limestone samples of varying mineral composition should also be examined to evaluate any potential impacts on model accuracy.

6 References

(1) Neff, J.; Lee, K.; DeBlois, E. M. Produced Water: Overview of Composition, Fates, and Effects. In *Produced Water: Environmental Risks and Advances in Mitigation Technologies*; Lee, K., Neff, J., Eds.; Springer: New York, NY, 2011; pp 3–54. https://doi.org/10.1007/978-1-4614-0046-2_1.

(2) EPA. *Summary of Input on Oil and Gas Extraction Wastewater Management Practices Under the Clean Water Act*; EPA-821-S19-001; 2020; p 38.

(3) Guerra, K.; Drewes, J. Produced Water in the Western United States: Geographical Distribution, Occurrence, and Composition. *Environ. Eng. Sci. - Env. ENG SCI* **2008**, *25*, 239–246. https://doi.org/10.1089/ees.2007.0026.

(4) Veil, J. A.; Puder, M. G.; Elcock, D. *A White Paper Describing Produced Water from Production of Crude Oil, Natural Gas, and Coal Bed Methane.*; ANL/EA/RP-112631; Argonne National Lab., IL (US), 2004. https://doi.org/10.2172/821666.

(5) Ellsworth, W. L. Injection-Induced Earthquakes. *Science* **2013**, *341* (6142). https://doi.org/10.1126/science.1225942.

(6) Vishnyakov, V.; Suleimanov, B.; Salmanov, A.; Zeynalov, E. 7 - Oil Recovery Stages and Methods. In *Primer on Enhanced Oil Recovery*; Vishnyakov, V., Suleimanov, B., Salmanov, A., Zeynalov, E., Eds.; Gulf Professional Publishing, 2020; pp 53–63. https://doi.org/10.1016/B978-0-12-817632-0.00007-4.

(7) Veil, J. *U.S. Produced Water Volumes and Management Practices in 2017*; Groundwater Reserach & Education Foundation, 2020.

(8) Sheng, J. J. Critical Review of Low-Salinity Waterflooding. *J. Pet. Sci. Eng.* **2014**, *120*, 216–224. https://doi.org/10.1016/j.petrol.2014.05.026.

(9) Derkani, M. H.; Fletcher, A. J.; Abdallah, W.; Sauerer, B.; Anderson, J.; Zhang, Z. J. Low Salinity Waterflooding in Carbonate Reservoirs: Review of Interfacial Mechanisms. *Colloids Interfaces* **2018**, *2* (2), 20. https://doi.org/10.3390/colloids2020020.

(10) Hiorth, A.; Cathles, L. M.; Madland, M. V. The Impact of Pore Water Chemistry on Carbonate Surface Charge and Oil Wettability. *Transp. Porous Media* **2010**, *85* (1), 1–21. https://doi.org/10.1007/s11242-010-9543-6.

(11) Hiorth, A.; Cathles, L.; Kolnes, J.; Vikane, O.; Lohne, A.; Madland, M. Chemical Modelling of Wettability Change in Carbonate Rocks. In *10th Wettability Conference, Abu Dhabi, UAE*; 2008; pp 1–9.

(12) Ligthelm, D. J.; Gronsveld, J.; Hofman, J.; Brussee, N.; Marcelis, F.; van der Linde, H. Novel Waterflooding Strategy by Manipulation of Injection Brine Composition. In *EUROPEC/EAGE conference and exhibition*; OnePetro, 2009.

(13) Lager, A.; Webb, K.; Black, C. Impact of Brine Chemistry on Oil Recovery. In *IOR 2007-14th European symposium on improved oil recovery*; European Association of Geoscientists & Engineers, 2007; p cp-24.

(14) Winsauer, W. O.; McCardell, W. M. Ionic Double-Layer Conductivity in Reservoir Rock. *J. Pet. Technol.* **1953**, *5* (05), 129–134.

(15) Mahani, H.; Keya, A. L.; Berg, S.; Nasralla, R. Electrokinetics of Carbonate/Brine Interface in Low-Salinity Waterflooding: Effect of Brine Salinity, Composition, Rock Type, and PH on ?-Potential and a Surface-Complexation Model. *SPE J.* **2016**, *22* (01), 53–68. https://doi.org/10.2118/181745-PA.

(16) Brady, P. V.; Krumhansl, J. L.; Mariner, P. E. Surface Complexation Modeling for Improved Oil Recovery; OnePetro, 2012. https://doi.org/10.2118/153744-MS.

(17) Snosy, M. F.; Abu El Ela, M.; El-Banbi, A.; Sayyouh, H. Comprehensive Investigation of Low Salinity Waterflooding in Carbonate Reservoirs. *J. Pet. Explor. Prod. Technol.* **2021**. https://doi.org/10.1007/s13202-021-01330-y.

(18) Tetteh, J. T.; Brady, P. V.; Barati Ghahfarokhi, R. Review of Low Salinity Waterflooding in Carbonate Rocks: Mechanisms, Investigation Techniques, and Future Directions. *Adv. Colloid Interface Sci.* **2020**, *284*, 102253. https://doi.org/10.1016/j.cis.2020.102253.

(19) Bertero, L.; Chierici, G. L.; Gottardi, G.; Mesini, E.; Mormino, G. Chemical Equilibrium Models: Their Use in Simulating the Injection of Incompatible Waters. *SPE Reserv. Eng.* **1988**, *3* (01), 288–294. https://doi.org/10.2118/14126-PA.

(20) *Kansas Administrative Code Agency 28 - DEPARTMENT OF HEALTH AND ENVIRONMENT*; Vol. 28-45b–1.

(21) *Oklahoma Administrative Code Title 252 - Department of Environmental Quality*; Vol. 252:652-9–1.

(22) *Title 267 - NEBRASKA OIL AND GAS CONSERVATION COMMISSION*; Vol. 267-4–006.

(23) Abouie, A.; Korrani, A. K.; Shirdel, M.; Sepehrnoori, K. Comprehensive Modeling of Scale Deposition by Use of a Coupled Geochemical and Compositional Wellbore Simulator. *SPE J.* **2017**, *22* (04), 1225–1241. https://doi.org/10.2118/185942-PA.

(24) Patton, C. C. Water Quality Control and Its Importance in Waterflooding Operations. *J. Pet. Technol.* **1988**, *40* (09), 1123–1126. https://doi.org/10.2118/18459-PA.

(25) Moghadasi, J.; Jamialahmadi, M.; Müller-Steinhagen, H.; Sharif, A.; Ghalambor, A.; Izadpanah, M. R.; Motaie, E. Scale Formation in Iranian Oil Reservoir and Production Equipment During Water Injection; OnePetro, 2003. https://doi.org/10.2118/80406-MS.

(26) Vetter, O. J.; Kandarpa, V.; Harouaka, A. Prediction of Scale Problems Due to Injection of Incompatible Waters. *J. Pet. Technol.* **1982**, *34* (02), 273–284. https://doi.org/10.2118/7794-PA.

(27) Khormali, A.; Sharifov, A. R.; Torba, D. I. Increasing Efficiency of Calcium Sulfate Scale Prevention Using a New Mixture of Phosphonate Scale Inhibitors during Waterflooding. *J. Pet. Sci. Eng.* **2018**, *164*, 245–258. https://doi.org/10.1016/j.petrol.2018.01.055.

(28) Ko, S.; Wang, X.; Zhao, Y.; Dai, C.; Lu, Y.-T.; Deng, G.; Paudyal, S.; Mateen, S.; Kan, A. T.; Tomson, M. B. Prevention of Mineral Scale Deposition Using Dispersants and Inhibitors; OnePetro, 2020. https://doi.org/10.2118/200670-MS.

(29) Mohammadi, M.; Riahi, S. Experimental Investigation of Water Incompatibility and Rock/Fluid and Fluid/Fluid Interactions in the Absence and Presence of Scale Inhibitors. *SPE J.* **2020**, *25* (05), 2615–2631. https://doi.org/10.2118/201117-PA.

(30) Parkhurst, D. L.; Appelo, C. A. J. *Description of Input and Examples for PHREEQC Version 3: A Computer Program for Speciation, Batch-Reaction, One-Dimensional Transport, and Inverse Geochemical Calculations*; Techniques and Methods; USGS Numbered Series 6-A43; U.S. Geological Survey: Reston, VA, 2013; Vol. 6-A43, p 519. https://doi.org/10.3133/tm6A43.

(31) Lu, P.; Zhang, G.; Apps, J.; Zhu, C. Comparison of Thermodynamic Data Files for PHREEQC. *Earth-Sci. Rev.* **2022**, *225*, 103888. https://doi.org/10.1016/j.earscirev.2021.103888.

(32) Tetteh, J. T.; Veisi, M.; Brady, P. V.; Barati Ghahfarokhi, R. Surface Reactivity Analysis of the Crude Oil–Brine–Limestone Interface for a Comprehensive Understanding of the Low-Salinity Waterflooding Mechanism. *Energy Fuels* **2020**, *34* (3), 2739–2756. https://doi.org/10.1021/acs.energyfuels.9b03664.

(33) Chee, R.; Lansey, K.; Chee, E. Estimation of Water Pipe Installation Construction Costs. *J. Pipeline Syst. Eng. Pract.* **2018**, *9* (3), 04018008. https://doi.org/10.1061/(ASCE)PS.1949-1204.0000323.

(34) Hale, D.; R.S. Means Company. *Heavy Construction Costs with RSMeans Data.*; 2019.

(35) Wreath, D. RE: Questions about Economics of Waterfloods and Disposal, 2022.

(36) Clark, C. E.; Veil, J. A. *Produced Water Volumes and Management Practices in the United States.*; Argonne National Lab.(ANL), Argonne, IL (United States), 2009.

(37) SOLUBILITY AND EQUILIBRIUM CONSTANT. In *Lange's Handbook of Chemistry*; Speight, J. G., Ed.; McGraw-Hill Education: New York, 2017.

(38) Weintritt, D. J.; Cowan, J. C. Unique Characteristics of Barium Sulfate Scale Deposition. *J. Pet. Technol.* **1967**, *19* (10), 1381–1394. https://doi.org/10.2118/1523-PA.

(39) Tale, F.; Kalantariasl, A.; Shabani, A.; Abbasi, S.; Zohoorian, A. H.; Khamehchi, E. Experimental and Simulation Study of Low Salinity Brine Interactions with Carbonate Rocks. *J. Pet. Sci. Eng.* **2020**, *184*, 106497. https://doi.org/10.1016/j.petrol.2019.106497.

(40) Esene, C.; Onalo, D.; Zendehboudi, S.; James, L.; Aborig, A.; Butt, S. Modeling Investigation of Low Salinity Water Injection in Sandstones and Carbonates: Effect of Na+ and SO42−. *Fuel* **2018**, *232*, 362–373. https://doi.org/10.1016/j.fuel.2018.05.161.

(41) Liu, B.; Mahmood, B. S.; Mohammadian, E.; Khaksar Manshad, A.; Rosli, N. R.; Ostadhassan, M. Measurement of Solubility of CO2 in NaCl, CaCl2, MgCl2 and MgCl2 + CaCl2 Brines at Temperatures from 298 to 373 K and Pressures up to 20 MPa Using the Potentiometric Titration Method. *Energies* **2021**, *14* (21). https://doi.org/10.3390/en14217222.

(42) Al-Shalabi, E. W.; Sepehrnoori, K. A Comprehensive Review of Low Salinity/Engineered Water Injections and Their Applications in Sandstone and Carbonate Rocks. *J. Pet. Sci. Eng.* **2016**, *139*, 137–161. https://doi.org/10.1016/j.petrol.2015.11.027.

(43) Sheikholeslami, R. Mixed Salts—Scaling Limits and Propensity. *Desalination* **2003**, *154* (2), 117–127. https://doi.org/10.1016/S0011-9164(03)80012-7.

(44) Sorbie, K. S.; Mackay, E. J. Mixing of Injected, Connate and Aquifer Brines in Waterflooding and Its Relevance to Oilfield Scaling. *J. Pet. Sci. Eng.* **2000**, *27* (1), 85–106. https://doi.org/10.1016/S0920-4105(00)00050-4.

(45) Mackay, E. J.; Sorbie, K. S. Brine Mixing in Waterflooded Reservoirs and the Implications for Scale Prevention; OnePetro, 2000. https://doi.org/10.2118/60193-MS.

(46) Attar, A.; Muggeridge, A. H. Evaluation of Mixing in Low Salinity Waterflooding; OnePetro, 2016. https://doi.org/10.2118/179803-MS.

(47) Hiorth, A.; Cathles, L.; Kolnes, J.; Vikane, O.; Lohne, A.; Korsnes, R.; Madland, M. V. A CHEMICAL MODEL FOR THE SEAWATER-CO 2 - CARBONATE SYSTEM – AQUEOUS AND SURFACE CHEMISTRY; 2008.

(48) Chandrasekhar, S.; Sharma, H.; Mohanty, K. K. Dependence of Wettability on Brine Composition in High Temperature Carbonate Rocks. *Fuel* **2018**, *225*, 573–587. https://doi.org/10.1016/j.fuel.2018.03.176.

(49) Hörbrand, T.; Baumann, T.; Moog, H. C. Validation of Hydrogeochemical Databases for Problems in Deep Geothermal Energy. *Geotherm. Energy* **2018**, *6* (1), 20. https://doi.org/10.1186/s40517-018-0106-3.

(50) Larson, T.; Sollo, F. W.; McGurk, F. *COMPLEXES AFFECTING THE SOLUBILITY OF CALCIUM CARBONATE IN WATER*; 68; University of Illinois at Urbana-Champaign, 1973.

(51) CAT (Caterpillar, Inc.). *Caterpillar Performance Handbook*; 2016.

(52) Sağlam, B.; Bettemir, Ö. H. Estimation of Duration of Earthwork with Backhoe Excavator by Monte Carlo Simulation. *J. Constr. Eng. Manag. Innov.* **2018**, *1*, 85–94. https://doi.org/10.31462/jcemi.2018.01085094.

(53) EIA. *Electricity data browser - Average retail price of electricity*. https://www.eia.gov/electricity/data/browser/#/topic/7?agg=0,1&geo=vvvvvvvvvvvvo&endsec=vg&linechart=ELEC.PRICE.US-ALL.A&columnchart=ELEC.PRICE.US-ALL.A&map=ELEC.PRICE.US-ALL.A&freq=A&ctype=linechart&ltype=pin&rtype=s&maptype=0&rse=0&pin= (accessed 2021-07-19).

(54) Loh, H. P.; Loyns, J.; White, C. W. *Process Equipment Cost Estimation, Final Report*; DOE/NETL-2002/1169; DOE, 2002; p 78.

(55) EIA. *Kansas Crude Oil First Purchase Price (Dollars per Barrel)*. https://www.eia.gov/dnav/pet/hist/LeafHandler.ashx?n=PET&s=F002020__3&f=A (accessed 2021-11-30).

(56) Budiman, M. *Latin Hypercube Sampling*. Latin Hypercube Sampling. https://www.mathworks.com/matlabcentral/fileexchange/4352-latin-hypercube-sampling (accessed 2022-04-08).

(57) R, T. *roundtowardvec*. roundtowardevec. https://www.mathworks.com/matlabcentral/fileexchange/37674-roundtowardvec (accessed 2022-04-08).

(58) Childress, N. *bluewhitered*. bluewithered. https://www.mathworks.com/matlabcentral/fileexchange/4058-bluewhitered (accessed 2022-04-08).

7 Appendix A: Expanded Experimental Results

The following figures depict enlarged graphs of bulk mixing experiment results. Data shown here is identical to those seen in **Figure** 4 and **Figure** 5.

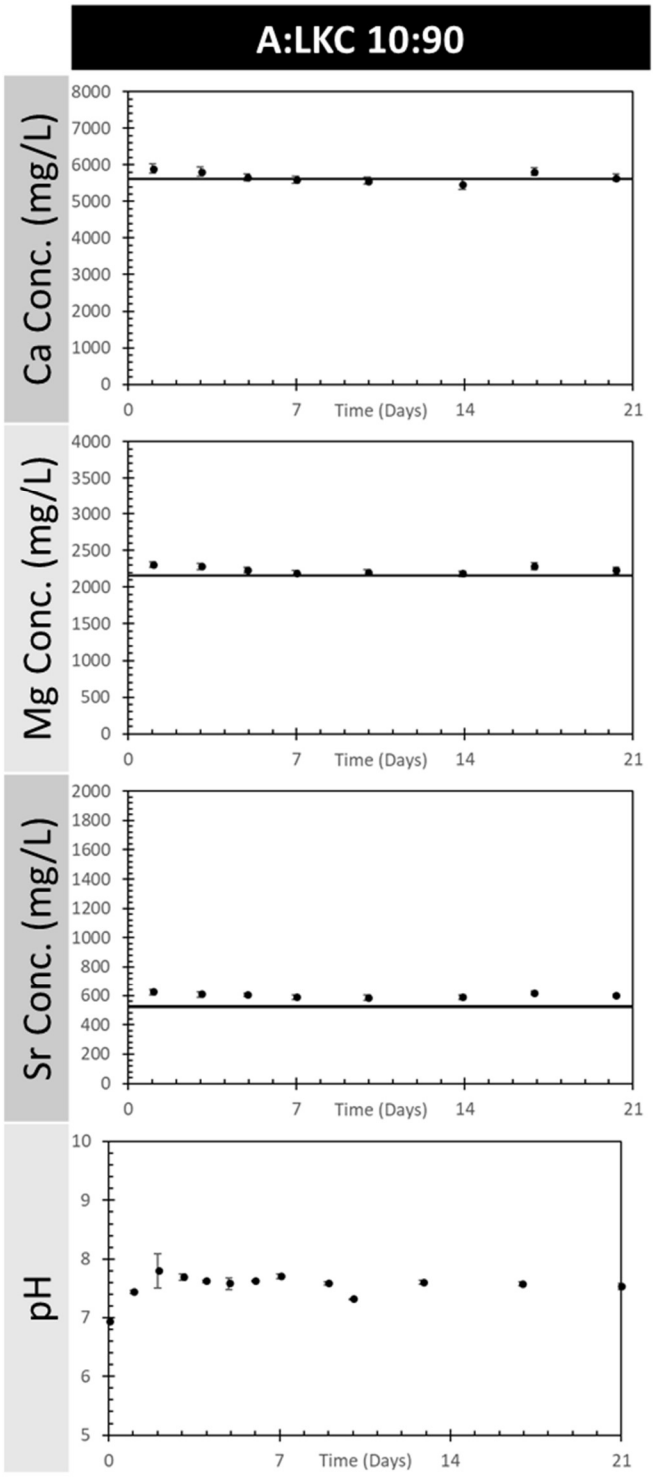

Figure 11 Cation and pH measurements of 10:90 L-L bulk mixing samples; initial values (solid black line) plotted alongside experimented data; ±σ error bars plotted but negligible in some cases

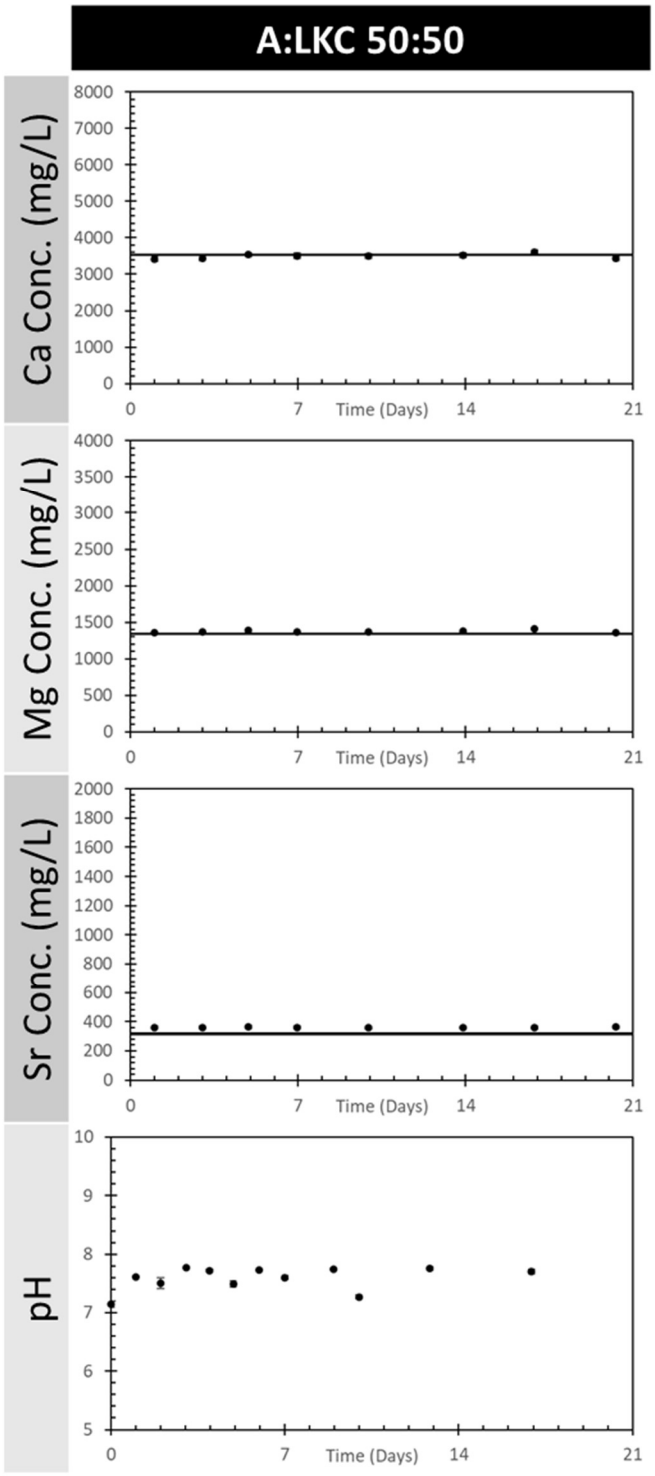

Figure 12 Cation and pH measurements of 50:50 L-L bulk mixing samples; initial values (solid black line) plotted alongside experimented data; ±σ error bars plotted but negligible in some cases

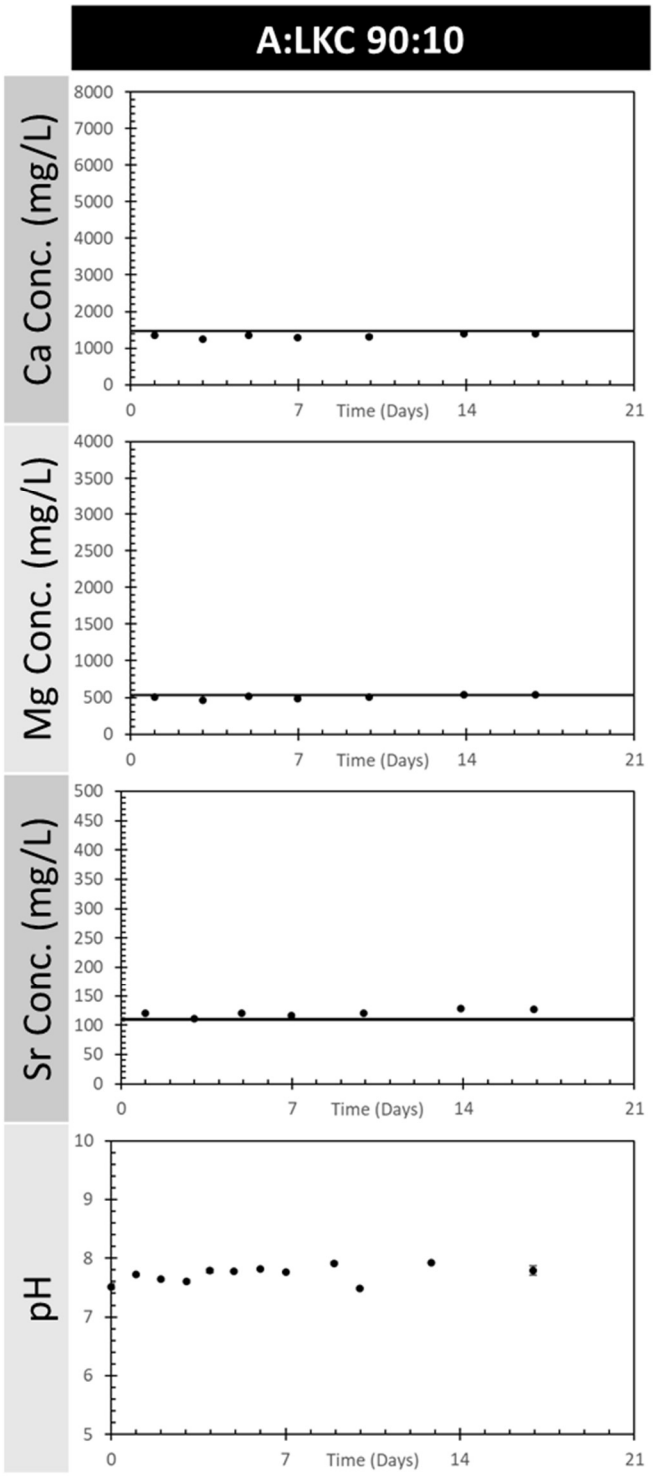

Figure 13 Cation and pH measurements of 90:10 L-L bulk mixing samples; initial values (solid black line) plotted alongside experimented data; ±σ error bars plotted but negligible in some cases

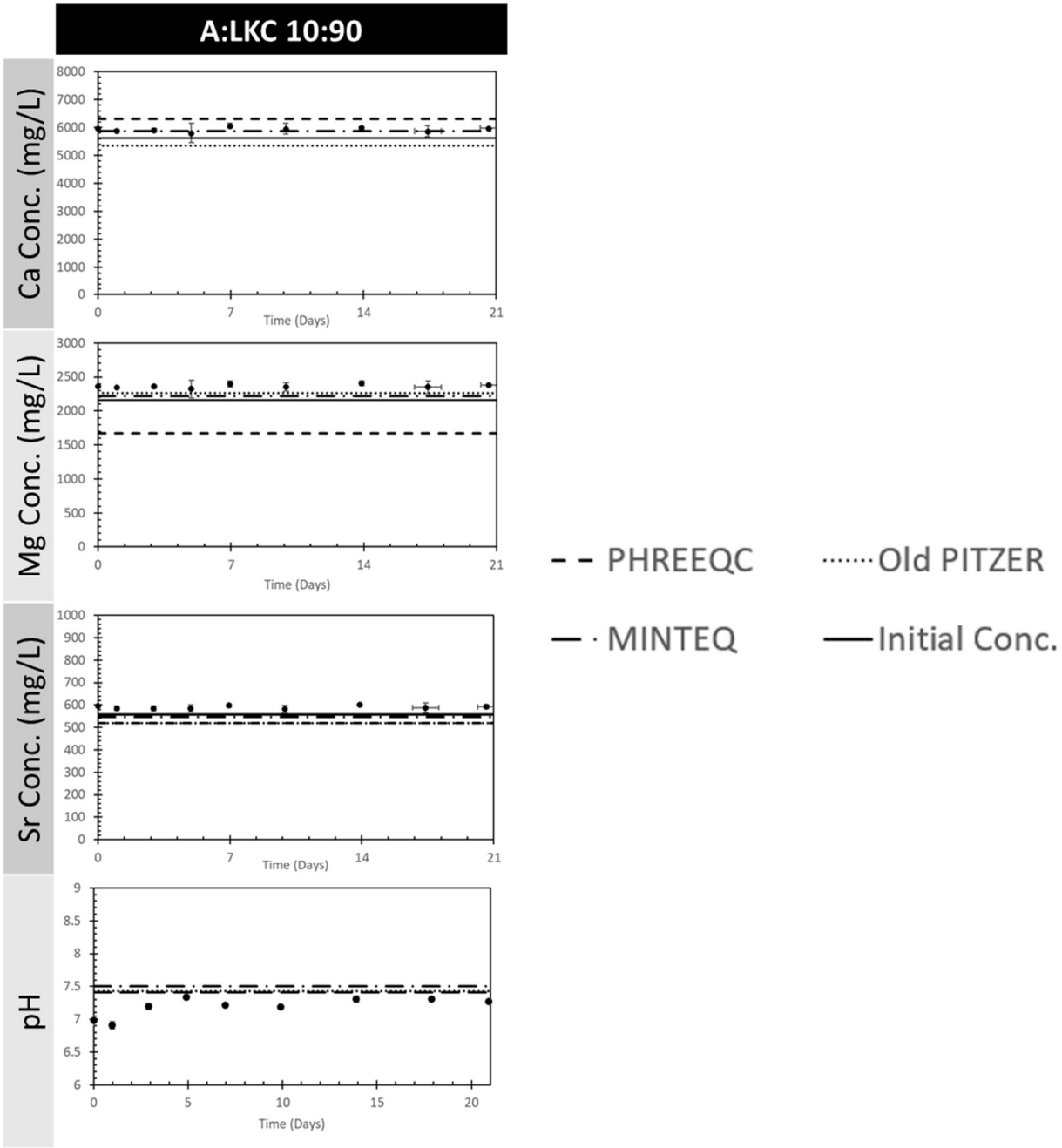

Figure 14 Cation and pH measurements of 10:90 L-L-S bulk mixing samples; initial values (solid black line) plotted alongside experimented data and PHREEQC equilibrium predictions; ±σ error bars plotted but negligible in some cases

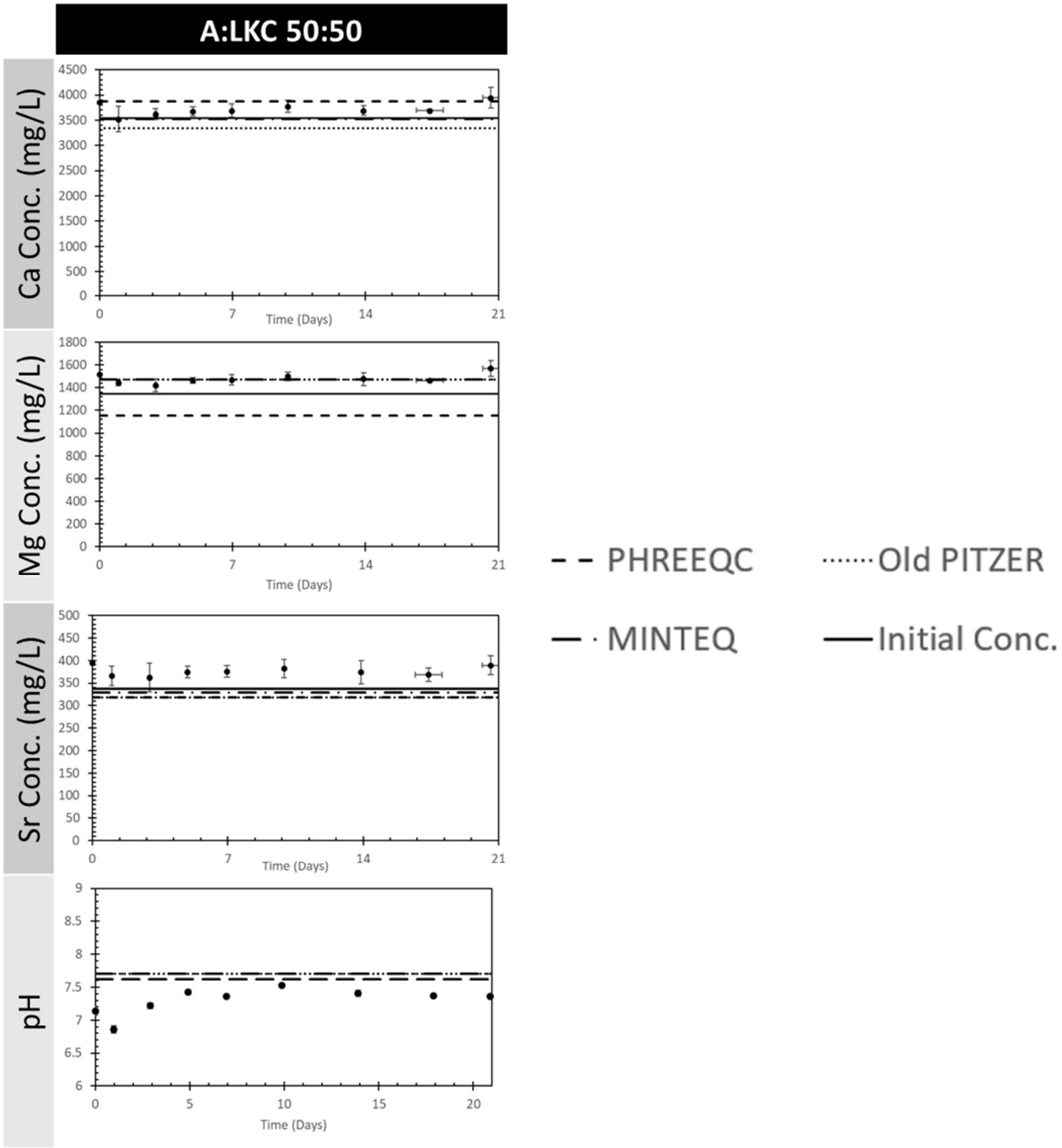

Figure 15 Cation and pH measurements of 50:50 L-L-S bulk mixing samples; initial values (solid black line) plotted alongside experimented data and PHREEQC equilibrium predictions; ±σ error bars plotted but negligible in some cases

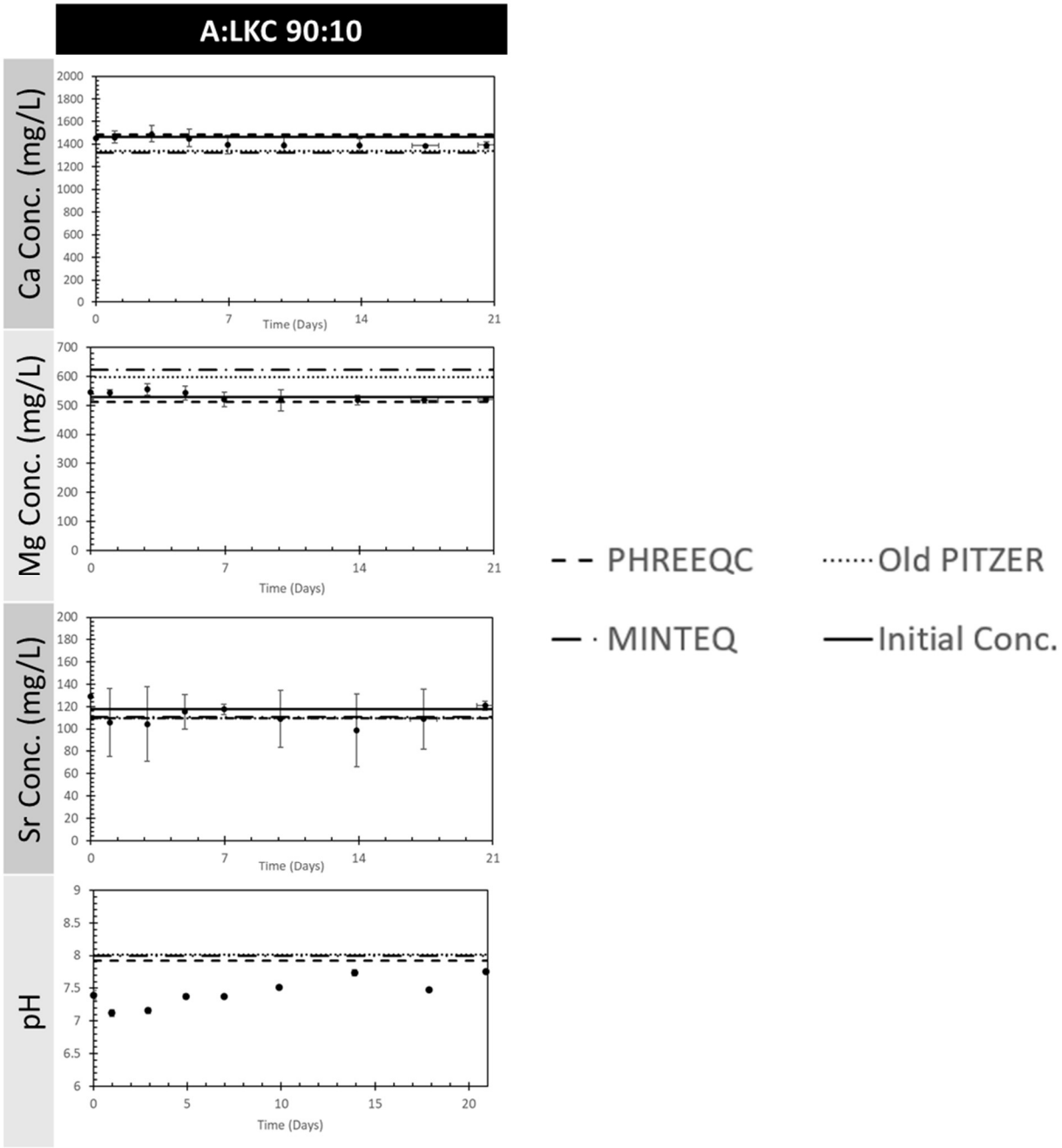

Figure 16 Cation and pH measurements of 90:10 L-L-S bulk mixing samples; initial values (solid black line) plotted alongside experimented data and PHREEQC equilibrium predictions; ±σ error bars plotted but negligible in some cases

8 Appendix B: Geochemical Modeling

The following figure outlines the code sequence of the PHREEQC geochemical model.

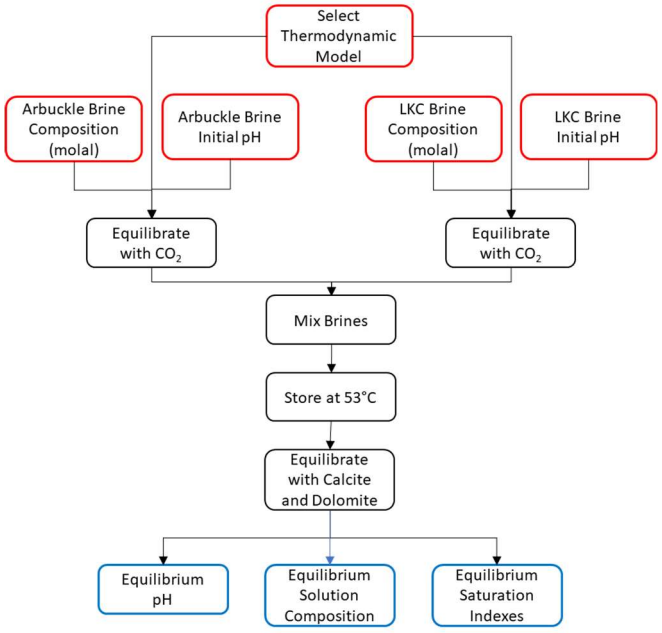

Figure 17 PHREEQC model flowchart; Red outlines indicate inputs and blue indicate outputs

The following tables contain saturation index calculation values of the PHREEQC models. Values between -1 and 1 were highlighted to show emphasis.

Table 9 PHREEQC Saturation Index values using PHREEQC database

		A:LKC S 0:100			A:LKC S 10:90			A:LKC S 30:70			A:LKC S 50:50			A:LKC S 70:30			A:LKC S 90:10			A:LKC S 100:0		
Phase	Formula	SI**	log IAP	log K (326 K, 1 atm)	SI**	log IAP	log K (326 K, 1 atm)	SI**	log IAP	log K (326 K, 1 atm)	SI**	log IAP	log K (326 K, 1 atm)	SI**	log IAP	log K (326 K, 1 atm)	SI**	log IAP	log K (326 K, 1 atm)	SI**	log IAP	log K (326 K, 1 atm)
Anhydrite	CaSO4	-0.69	-5.3	-4.61	-0.68	-5.3	-4.61	-0.71	-5.32	-4.61	-0.73	-5.35	-4.61	-0.76	-5.37	-4.61	-0.79	-5.41	-4.61	-0.81	-5.42	-4.61
Aragonite	CaCO3	-0.13	-8.69	-8.56	-0.13	-8.69	-8.56	-0.13	-8.69	-8.56	-0.13	-8.69	-8.56	-0.13	-8.69	-8.56	-0.13	-8.69	-8.56	-0.13	-8.69	-8.56
Calcite	CaCO3	0	-8.69	-8.69	0	-8.69	-8.69	0	-8.69	-8.69	0	-8.69	-8.69	0	-8.69	-8.69	0	-8.69	-8.69	0	-8.69	-8.69
Celestite	SrSO4	-0.03	-6.85	-6.82	-0.04	-6.86	-6.82	-0.03	-6.85	-6.82	-0.03	-6.85	-6.82	-0.05	-6.87	-6.82	-0.1	-6.93	-6.82	-0.19	-7.01	-6.82
CH4(g)	CH4	-21.4	-24.37	-2.97	-22.5	-25.51	-2.97	-22.2	-25.18	-2.97	-23.1	-26.1	-2.97	-23	-25.92	-2.97	-24.5	-27.45	-2.97	-25.3	-28.29	-2.97
CO2(g)	CO2	-4.19	-5.93	-1.73	-4.18	-5.91	-1.73	-4.22	-5.96	-1.73	-4.27	-6	-1.73	-4.33	-6.06	-1.73	-4.42	-6.16	-1.73	-4.49	-6.22	-1.73
Dolomite	CaMg(CO3)2	0	-17.68	-17.68	0	-17.68	-17.68	0	-17.68	-17.68	0	-17.68	-17.68	0	-17.68	-17.68	0	-17.68	-17.68	0	-17.68	-17.68
Gypsum	CaSO4:H2O	-0.75	-5.38	-4.63	-0.76	-5.38	-4.63	-0.76	-5.39	-4.63	-0.77	-5.39	-4.63	-0.78	-5.41	-4.63	-0.8	-5.42	-4.63	-0.8	-5.43	-4.63
H2(g)	H2	-9.95	-13.09	-3.14	-10.2	-13.38	-3.14	-10.1	-13.28	-3.14	-10.4	-13.49	-3.14	-10.3	-13.43	-3.14	-10.7	-13.78	-3.14	-10.8	-13.97	-3.14
H2O(g)	H2O	-0.89	-0.04	0.85	-0.9	-0.04	0.85	-0.88	-0.03	0.85	-0.88	-0.02	0.85	-0.87	-0.02	0.85	-0.86	-0.01	0.85	-0.86	0	0.85
H2S(g)	H2S	-20.4	-28.31	-7.94	-21.5	-29.43	-7.94	-21.2	-29.15	-7.94	-22.2	-30.09	-7.94	-22	-29.96	-7.94	-23.6	-31.52	-7.94	-24.4	-32.38	-7.94
Halite	NaCl	-1.11	0.48	1.59	-1.01	0.58	1.59	-1.33	0.26	1.59	-1.6	-0.01	1.59	-1.95	-0.36	1.59	-2.49	-0.9	1.59	-2.96	-1.37	1.59
O2(g)	O2	-55	-58.03	-3.04	-54.4	-57.45	-3.04	-54.6	-57.63	-3.04	-54.1	-57.18	-3.04	-54.3	-57.29	-3.04	-53.5	-56.57	-3.04	-53.1	-56.18	-3.04
Strontianite	SrCO3	-0.85	-10.24	-9.39	-0.86	-10.25	-9.39	-0.82	-10.22	-9.39	-0.8	-10.2	-9.39	-0.79	-10.19	-9.39	-0.82	-10.21	-9.39	-0.89	-10.28	-9.39
Sulfur	S	-16.1	-11.82	4.28	-16.9	-12.65	4.28	-16.8	-12.46	4.28	-17.5	-13.2	4.28	-17.4	-13.12	4.28	-18.6	-14.33	4.28	-19.3	-15	4.28
Sylvite	KCl	-3.37	-2.34	1.03	-3.31	-2.28	1.03	-3.51	-2.48	1.03	-3.67	-2.64	1.03	-3.87	-2.84	1.03	-4.15	-3.13	1.03	-4.39	-3.36	1.03

Table 10 PHREEQC Saturation Index values using PITZER database

		A:LKC S 0:100			A:LKC S 10:90			A:LKC S 30:70			A:LKC S 50:50			A:LKC S 70:30			A:LKC S 90:10			A:LKC S 100:0		
Phase	Formula	SI**	log IAP	log K (326 K, 1 atm)	SI**	log IAP	log K (326 K, 1 atm)	SI**	log IAP	log K (326 K, 1 atm)	SI**	log IAP	log K (326 K, 1 atm)	SI**	log IAP	log K (326 K, 1 atm)	SI**	log IAP	log K (326 K, 1 atm)	SI**	log IAP	log K (326 K, 1 atm)
Anhydrite	CaSO4	-0.75	-5.39	-4.64	-0.77	-5.41	-4.64	-0.8	-5.44	-4.64	-0.83	-5.47	-4.64	-0.85	-5.49	-4.64	-0.86	-5.5	-4.64	-0.86	-5.5	-4.64
Aragonite	CaCO3	-0.34	-8.79	-8.45	-0.34	-8.79	-8.45	-0.34	-8.79	-8.45	-0.34	-8.79	-8.45	-0.34	-8.79	-8.45	-0.34	-8.79	-8.45	-0.34	-8.79	-8.45
Arcanite	K2SO4	-7.49	-9.1	-1.61	-7.47	-9.08	-1.61	-7.42	-9.03	-1.61	-7.36	-8.97	-1.61	-7.27	-8.88	-1.61	-7.11	-8.72	-1.61	-6.95	-8.56	-1.61
Artinite	Mg2CO3(OH)2:3H2O	-3.22	14.48	17.7	-3.14	14.56	17.7	-3	14.71	17.7	-2.86	14.84	17.7	-2.74	14.97	17.7	-2.62	15.09	17.7	-2.55	15.15	17.7
Bischofite	MgCl2:6H2O	-5.29	-1.04	4.25	-5.44	-1.19	4.25	-5.76	-1.52	4.25	-6.15	-1.9	4.25	-6.63	-2.39	4.25	-7.36	-3.11	4.25	-7.98	-3.73	4.25
Bloedite	Na2Mg(SO4)2:4H2O	-6.91	-9.25	-2.35	-6.94	-9.29	-2.35	-7.04	-9.38	-2.35	-7.16	-9.5	-2.35	-7.33	-9.67	-2.35	-7.61	-9.96	-2.35	-7.9	-10.25	-2.35
Brucite	Mg(OH)2	-2.45	-13.03	-10.57	-2.39	-12.97	-10.57	-2.27	-12.85	-10.57	-2.16	-12.74	-10.57	-2.06	-12.64	-10.57	-1.97	-12.54	-10.57	-1.91	-12.49	-10.57
Burkeite	Na6CO3(SO4)2	-13.32	-14.09	-0.77	-13.43	-14.2	-0.77	-13.69	-14.46	-0.77	-14.05	-14.82	-0.77	-14.57	-15.34	-0.77	-15.48	-16.25	-0.77	-16.38	-17.16	-0.77
Calcite	CaCO3	0	-8.79	-8.79	0	-8.79	-8.79	0	-8.79	-8.79	0	-8.79	-8.79	0	-8.79	-8.79	0	-8.79	-8.79	0	-8.79	-8.79
Carnallite	KMgCl3:6H2O	-7.67	-3.22	4.44	-7.88	-3.44	4.44	-8.36	-3.92	4.44	-8.92	-4.47	4.44	-9.62	-5.17	4.44	-10.64	-6.2	4.44	-11.5	-7.06	4.44
Celestite	SrSO4	0.01	-6.81	-6.82	0	-6.82	-6.82	-0.03	-6.85	-6.82	-0.05	-6.87	-6.82	-0.07	-6.89	-6.82	-0.11	-6.94	-6.82	-0.19	-7.01	-6.82
CO2(g)	CO2	-4.1	-5.83	-1.73	-4.15	-5.89	-1.73	-4.26	-6	-1.73	-4.37	-6.1	-1.73	-4.46	-6.19	-1.73	-4.54	-6.28	-1.73	-4.59	-6.33	-1.73
Dolomite	CaMg(CO3)2	0	-17.68	-17.68	0	-17.68	-17.68	0	-17.68	-17.68	0	-17.68	-17.68	0	-17.68	-17.68	0	-17.68	-17.68	0	-17.68	-17.68
Epsomite	MgSO4:7H2O	-4.15	-5.83	-1.68	-4.13	-5.81	-1.68	-4.1	-5.78	-1.68	-4.06	-5.74	-1.68	-4.03	-5.71	-1.68	-3.99	-5.66	-1.68	-3.96	-5.64	-1.68
Gaylussite	CaNa2(CO3)2:5H2O	-6.56	-15.98	-9.42	-6.56	-15.98	-9.42	-6.58	-16	-9.42	-6.64	-16.06	-9.42	-6.75	-16.18	-9.42	-7.01	-16.43	-9.42	-7.3	-16.72	-9.42
Glaserite	NaK3(SO4)2	-12.01	-15.44	-3.43	-12	-15.42	-3.43	-11.97	-15.4	-3.43	-11.94	-15.37	-3.43	-11.89	-15.32	-3.43	-11.81	-15.23	-3.43	-11.73	-15.16	-3.43
Glauberite	Na2Ca(SO4)2	-3.25	-8.96	-5.71	-3.31	-9.02	-5.71	-3.44	-9.15	-5.71	-3.6	-9.3	-5.71	-3.8	-9.5	-5.71	-4.12	-9.82	-5.71	-4.42	-10.12	-5.71
Goergeyite	K2Ca5(SO4)6H2O	-7.46	-36.11	-28.66	-7.51	-36.17	-28.66	-7.61	-36.27	-28.66	-7.68	-36.34	-28.66	-7.69	-36.35	-28.66	-7.58	-36.23	-28.66	-7.42	-36.07	-28.66
Gypsum	CaSO4:2H2O	-0.81	-5.49	-4.67	-0.82	-5.49	-4.67	-0.83	-5.51	-4.67	-0.84	-5.52	-4.67	-0.85	-5.52	-4.67	-0.84	-5.52	-4.67	-0.84	-5.51	-4.67
H2O(g)	H2O	-0.9	-0.05	0.85	-0.89	-0.04	0.85	-0.89	-0.03	0.85	-0.88	-0.02	0.85	-0.87	-0.02	0.85	-0.86	-0.01	0.85	-0.86	0	0.85
Halite	NaCl	-1.03	0.59	1.62	-1.13	0.49	1.62	-1.36	0.26	1.62	-1.63	-0.01	1.62	-1.97	-0.36	1.62	-2.51	-0.89	1.62	-2.98	-1.36	1.62
Hexahydrite	MgSO4:6H2O	-4.14	-5.78	-1.65	-4.12	-5.77	-1.65	-4.1	-5.74	-1.65	-4.07	-5.72	-1.65	-4.04	-5.69	-1.65	-4.01	-5.66	-1.65	-3.99	-5.63	-1.65
Huntite	CaMg3(CO3)4	-2.2	5.24	7.44	-2.2	5.24	7.44	-2.2	5.24	7.44	-2.2	5.24	7.44	-2.2	5.24	7.44	-2.2	5.24	7.44	-2.2	5.24	7.44
Kainite	KMgClSO4:3H2O	-7.63	-7.82	-0.19	-7.7	-7.89	-0.19	-7.85	-8.04	-0.19	-8.03	-8.22	-0.19	-8.24	-8.43	-0.19	-8.53	-8.72	-0.19	-8.76	-8.95	-0.19
Kalicinite	KHCO3	-7.47	-17.41	-9.94	-7.48	-17.42	-9.94	-7.49	-17.43	-9.94	-7.49	-17.43	-9.94	-7.47	-17.41	-9.94	-7.43	-17.37	-9.94	-7.38	-17.32	-9.94
Kieserite	MgSO4:H2O	-4.71	-5.54	-0.84	-4.72	-5.56	-0.84	-4.74	-5.58	-0.84	-4.76	-5.6	-0.84	-4.78	-5.61	-0.84	-4.78	-5.61	-0.84	-4.77	-5.61	-0.84
Labile_S	Na4Ca(SO4)3:2H2O	-6.95	-12.62	-5.67	-7.04	-12.71	-5.67	-7.25	-12.92	-5.67	-7.51	-13.19	-5.67	-7.88	-13.55	-5.67	-8.49	-14.16	-5.67	-9.09	-14.76	-5.67
Leonhardite	MgSO4:4H2O	-4.8	-5.69	-0.89	-4.8	-5.68	-0.89	-4.79	-5.68	-0.89	-4.78	-5.67	-0.89	-4.77	-5.66	-0.89	-4.75	-5.64	-0.89	-4.74	-5.62	-0.89
Leonite	K2Mg(SO4)2:4H2O	-10.81	-14.79	-3.98	-10.78	-14.76	-3.98	-10.73	-14.71	-3.98	-10.66	-14.64	-3.98	-10.56	-14.53	-3.98	-10.38	-14.36	-3.98	-10.21	-14.19	-3.98
Magnesite	MgCO3	-0.96	-8.89	-7.93	-0.96	-8.89	-7.93	-0.96	-8.89	-7.93	-0.96	-8.89	-7.93	-0.96	-8.89	-7.93	-0.96	-8.89	-7.93	-0.96	-8.89	-7.93
MgCl2_2H2O	MgCl2:2H2O	-13.28	-0.85	12.43	-13.44	-1.02	12.43	-13.81	-1.38	12.43	-14.23	-1.8	12.43	-14.75	-2.32	12.43	-15.51	-3.08	12.43	-16.14	-3.71	12.43
MgCl2_4H2O	MgCl2:4H2O	-7.36	-0.95	6.41	-7.52	-1.1	6.41	-7.86	-1.45	6.41	-8.27	-1.85	6.41	-8.77	-2.36	6.41	-9.51	-3.1	6.41	-10.13	-3.72	6.41
Mirabilite	Na2SO4:10H2O	-3.76	-4.04	-0.29	-3.75	-4.03	-0.29	-3.75	-4.04	-0.29	-3.79	-4.08	-0.29	-3.89	-4.17	-0.29	-4.12	-4.4	-0.29	-4.38	-4.67	-0.29
Misenite	K8H6(SO4)7	-82.4	-93.21	-10.81	-82.52	-93.32	-10.81	-82.71	-93.52	-10.81	-82.82	-93.63	-10.81	-82.78	-93.58	-10.81	-82.41	-93.22	-10.81	-81.94	-92.74	-10.81
Nahcolite	NaHCO3	-3.9	-14.64	-10.74	-3.94	-14.68	-10.74	-4.02	-14.77	-10.74	-4.12	-14.86	-10.74	-4.24	-14.98	-10.74	-4.43	-15.17	-10.74	-4.6	-15.35	-10.74
Natron	Na2CO3:10H2O	-6.61	-7.44	-0.82	-6.59	-7.41	-0.82	-6.56	-7.38	-0.82	-6.57	-7.39	-0.82	-6.64	-7.47	-0.82	-6.86	-7.69	-0.82	-7.13	-7.96	-0.82
Nesquehonite	MgCO3:3H2O	-3.87	-9.03	-5.17	-3.85	-9.02	-5.17	-3.82	-8.99	-5.17	-3.8	-8.96	-5.17	-3.77	-8.94	-5.17	-3.75	-8.92	-5.17	-3.74	-8.9	-5.17
Pentahydrite	MgSO4:5H2O	-4.45	-5.73	-1.28	-4.44	-5.73	-1.28	-4.43	-5.71	-1.28	-4.41	-5.69	-1.28	-4.39	-5.67	-1.28	-4.36	-5.65	-1.28	-4.34	-5.63	-1.28
Pirssonite	Na2Ca(CO3)2:2H2O	-6.61	-15.84	-9.23	-6.62	-15.86	-9.23	-6.67	-15.9	-9.23	-6.75	-15.99	-9.23	-6.89	-16.13	-9.23	-7.17	-16.41	-9.23	-7.47	-16.7	-9.23
Polyhalite	K2MgCa2(SO4)4:2H2O	-11.74	-25.48	-13.74	-11.75	-25.5	-13.74	-11.78	-25.52	-13.74	-11.78	-25.53	-13.74	-11.74	-25.48	-13.74	-11.6	-25.34	-13.74	-11.44	-25.18	-13.74
Portlandite	Ca(OH)2	-7.74	-12.93	-5.19	-7.67	-12.86	-5.19	-7.55	-12.74	-5.19	-7.44	-12.63	-5.19	-7.34	-12.53	-5.19	-7.25	-12.44	-5.19	-7.19	-12.38	-5.19
Schoenite	K2Mg(SO4)2:6H2O	-10.56	-14.88	-4.33	-10.52	-14.85	-4.33	-10.44	-14.77	-4.33	-10.36	-14.68	-4.33	-10.24	-14.57	-4.33	-10.04	-14.37	-4.33	-9.87	-14.2	-4.33
Sylvite	KCl	-3.32	-2.18	1.14	-3.39	-2.25	1.14	-3.54	-2.4	1.14	-3.71	-2.57	1.14	-3.92	-2.79	1.14	-4.22	-3.09	1.14	-4.47	-3.33	1.14
Syngenite	K2Ca(SO4)2:H2O	-7.62	-14.54	-6.92	-7.61	-14.53	-6.92	-7.58	-14.5	-6.92	-7.54	-14.46	-6.92	-7.46	-14.38	-6.92	-7.31	-14.23	-6.92	-7.15	-14.07	-6.92
Thenardite	Na2SO4	-3.13	-3.57	-0.44	-3.17	-3.61	-0.44	-3.27	-3.71	-0.44	-3.4	-3.83	-0.44	-3.58	-4.01	-0.44	-3.88	-4.32	-0.44	-4.19	-4.62	-0.44
Trona	Na3H(CO3)2:2H2O	-10.32	-21.7	-11.38	-10.37	-21.75	-11.38	-10.5	-21.88	-11.38	-10.68	-22.06	-11.38	-10.94	-22.32	-11.38	-11.41	-22.79	-11.38	-11.88	-23.26	-11.38

Table 11 PHREEQC Saturation Index values using MINTEQ database

		A:LKC S 0:100			A:LKC S 10:90			A:LKC S 30:70			A:LKC S 50:50			A:LKC S 70:30			A:LKC S 90:10			A:LKC S 100:0		
Phase	Formula	SI**	log IAP	log K (326 K, 1 atm)	SI**	log IAP	log K (326 K, 1 atm)	SI**	log IAP	log K (326 K, 1 atm)	SI**	log IAP	log K (326 K, 1 atm)	SI**	log IAP	log K (326 K, 1 atm)	SI**	log IAP	log K (326 K, 1 atm)	SI**	log IAP	log K (326 K, 1 atm)
Anhydrite	CaSO4	-0.43	-5.3	-4.87	-0.44	-5.31	-4.87	-0.47	-5.34	-4.87	-0.5	-5.38	-4.87	-0.55	-5.42	-4.87	-0.59	-5.47	-4.87	-0.61	-5.49	-4.87
Aragonite	CaCO3	-0.17	-8.73	-8.56	-0.17	-8.73	-8.56	-0.17	-8.73	-8.56	-0.17	-8.73	-8.56	-0.17	-8.73	-8.56	-0.17	-8.73	-8.56	-0.17	-8.73	-8.56
Artinite	MgCO3:Mg(OH)2:3H2O	-3.02	4.77	7.79	-3	4.79	7.79	-2.95	4.84	7.79	-2.89	4.9	7.79	-2.82	4.97	7.79	-2.73	5.06	7.79	-2.66	5.13	7.79
Brucite	Mg(OH)2	-1.47	13.69	15.17	-1.47	13.7	15.17	-1.44	13.72	15.17	-1.41	13.76	15.17	-1.36	13.81	15.17	-1.29	13.88	15.17	-1.23	13.93	15.17
Calcite	CaCO3	0	-8.73	-8.73	0	-8.73	-8.73	0	-8.73	-8.73	0	-8.73	-8.73	0	-8.73	-8.73	0	-8.73	-8.73	0	-8.73	-8.73
Celestite	SrSO4	-0.84	-7.33	-6.49	-0.8	-7.29	-6.49	-0.72	-7.22	-6.49	-0.66	-7.15	-6.49	-0.6	-7.09	-6.49	-0.57	-7.06	-6.49	-0.6	-7.09	-6.49
CH4(g)	CH4	-116.88	-153.14	-36.26	-26.96	-63.22	-36.26	-111.93	-148.2	-36.26	-28.45	-64.71	-36.26	-28.24	-64.5	-36.26	-27.98	-64.24	-36.26	-29.63	-65.89	-36.26
CO2(g)	CO2	-4.4	-22.52	-18.13	-4.4	-22.53	-18.13	-4.42	-22.54	-18.13	-4.44	-22.57	-18.13	-4.48	-22.61	-18.13	-4.55	-22.67	-18.13	-4.6	-22.73	-18.13
Dolomite	CaMg(CO3)2	0	-17.52	-17.52	0	-17.52	-17.52	0	-17.52	-17.52	0	-17.52	-17.52	0	-17.52	-17.52	0	-17.52	-17.52	0	-17.52	-17.52
Epsomite	MgSO4:7H2O	-3.7	-5.66	-1.96	-3.68	-5.65	-1.96	-3.66	-5.62	-1.96	-3.64	-5.6	-1.96	-3.62	-5.59	-1.96	-3.62	-5.58	-1.96	-3.61	-5.58	-1.96
Gypsum	CaSO4:2H2O	-0.79	-5.39	-4.59	-0.8	-5.39	-4.59	-0.81	-5.41	-4.59	-0.83	-5.43	-4.59	-0.86	-5.45	-4.59	-0.89	-5.48	-4.59	-0.9	-5.5	-4.59
Halite	NaCl	-1.13	0.51	1.64	-1.23	0.41	1.64	-1.44	0.2	1.64	-1.7	-0.06	1.64	-2.04	-0.4	1.64	-2.57	-0.93	1.64	-3.03	-1.39	1.64
Huntite	CaMg3(CO3)4	-3.51	-35.1	-31.59	-3.51	-35.1	-31.59	-3.51	-35.1	-31.59	-3.51	-35.1	-31.59	-3.51	-35.1	-31.59	-3.51	-35.1	-31.59	-3.51	-35.1	-31.59
Hydromagnesite	Mg5(CO3)4(OH)2:4H2O	-9.58	-21.63	-12.05	-9.56	-21.61	-12.05	-9.5	-21.55	-12.05	-9.44	-21.49	-12.05	-9.36	-21.41	-12.05	-9.26	-21.31	-12.05	-9.19	-21.24	-12.05
Lime	CaO	-16.1	13.79	29.89	-16.09	13.79	29.89	-16.08	13.81	29.89	-16.05	13.84	29.89	-16.01	13.88	29.89	-15.94	13.94	29.89	-15.89	13.99	29.89
Magnesite	MgCO3	-0.37	-8.79	-8.42	-0.37	-8.79	-8.42	-0.37	-8.79	-8.42	-0.37	-8.79	-8.42	-0.37	-8.79	-8.42	-0.37	-8.79	-8.42	-0.37	-8.79	-8.42
Mirabilite	Na2SO4:10H2O	-4.05	-3.97	0.08	-4.06	-3.98	0.08	-4.09	-4.01	0.08	-4.16	-4.08	0.08	-4.28	-4.2	0.08	-4.54	-4.46	0.08	-4.82	-4.74	0.08
Natron	Na2CO3:10H2O	-7.09	-7.41	-0.32	-7.08	-7.4	-0.32	-7.08	-7.4	-0.32	-7.11	-7.43	-0.32	-7.2	-7.52	-0.32	-7.41	-7.73	-0.32	-7.66	-7.98	-0.32
Nesquehonite	MgCO3:3H2O	-2.93	-8.92	-5.99	-2.92	-8.91	-5.99	-2.9	-8.88	-5.99	-2.87	-8.86	-5.99	-2.85	-8.84	-5.99	-2.83	-8.81	-5.99	-2.82	-8.8	-5.99
O2(g)	O2	-9.43	65.27	74.7	-54.39	20.31	74.7	-11.9	62.79	74.7	-53.65	21.04	74.7	-53.77	20.93	74.7	-53.92	20.77	74.7	-53.12	21.58	74.7
Periclase	MgO	-5.5	13.74	19.24	-5.5	13.74	19.24	-5.48	13.76	19.24	-5.45	13.78	19.24	-5.41	13.82	19.24	-5.35	13.89	19.24	-5.3	13.94	19.24
Portlandite	Ca(OH)2	-7	13.75	20.74	-6.99	13.75	20.74	-6.97	13.78	20.74	-6.93	13.81	20.74	-6.88	13.86	20.74	-6.81	13.93	20.74	-6.76	13.99	20.74
Strontianite	SrCO3	-1.47	-10.76	-9.29	-1.42	-10.71	-9.29	-1.32	-10.61	-9.29	-1.21	-10.51	-9.29	-1.11	-10.41	-9.29	-1.04	-10.33	-9.29	-1.05	-10.34	-9.29
Sulfur	S	-84.74	-87.11	-2.37	-17.32	-19.69	-2.37	-81.09	-83.47	-2.37	-18.53	-20.91	-2.37	-18.44	-20.81	-2.37	-18.32	-20.69	-2.37	-19.6	-21.97	-2.37
Thenardite	Na2SO4	-3.32	-3.54	-0.21	-3.37	-3.58	-0.21	-3.48	-3.69	-0.21	-3.62	-3.84	-0.21	-3.83	-4.04	-0.21	-4.16	-4.38	-0.21	-4.47	-4.69	-0.21
Thermonatrite	Na2CO3:H2O	-6.96	-7.01	-0.05	-6.99	-7.04	-0.05	-7.06	-7.12	-0.05	-7.17	-7.22	-0.05	-7.32	-7.37	-0.05	-7.6	-7.65	-0.05	-7.89	-7.94	-0.05

9 Appendix C: WaterCOSTE Model Input and Output

The following table contains the variables utilized in the techno-economic simulation as well as their associated values. Unless stated otherwise, variables containing a range of values were assumed to have a uniform distribution. Variables without a provided value were derived from other variables.

Table 12 Economic simulation variable names and values

Code Name	Variable Name	Units	Value	Notes
A_t	Trench Cross Sectional Area	mm^2		Figure 4 Chee et al., 2018
BHP	Brake Horsepower	hp		
C_electricity	Electricity Cost	$/kwh		EIA,2020; Empirical distribution
C_construction_pipe	Total Pipe Construction Cost	$		Eqn 29 Chee et al., 2018
C_demob_exc	Excavator Demobilization Cost	$		RSMeans 2020 Line 01 54 36.50
C_demob_load	Loader Demobilization Cost	$		RSMeans 2020 Line 01 54 36.50
C_demob_tanker	Water Truck Demobilization Cost	$		Table S5 Chee et al, 2018
C_disp_pipe	PW Disposal Cost via Pipe	$/bbl	0.12 ± 10%	Based on industry correspondence
C_disposal	Daily Disposal Cost	$/day		
C_emb_r	Total Cost of Embedment Material	$	0	Assume native material
C_EOR	Income from EOR	$/day		
C_equip	Total Equipment Cost	$		Eqn 35 Chee et al., 2018
C_equip_booster	Cost of Booster Pumps	$/pump		Loh et al., 2002
C_equip_exc	Total Excavator Rental Cost	$		Table S6 Chee et al., 2018
C_equip_load	Total Loader Rental Cost	$		RSMeans 2020 Line 01 54 33 4610-4870
C_equip_tanker	Total Water Truck Rental Cost	$		Table S5 Chee et al, 2018
C_exc_unit	Excavation Cost	$/BCY		RSMeans 2020 31 23 16.13
C_lab	Total Labor Cost	$		Eqn 33 Chee et al., 2018
C_lab_load	Total Loader Labor Cost	$		RSMeans 2020 Medium Equipment Operator
C_lab_pipe	Total Pipe Installation Labor Cost	$		RSMeans 2020 Crew B-20
C_lab_tanker	Total Water Truck Labor Cost	$		RSMeans 2020 Truck Driver (Heavy)

C_lb	Bucket Capacity of Loader	m^3/hr	2.29 - 6.88	Table S7 Chee et al., 2018
C_mob_exc	Excavator Mobilization Cost	$		RSMeans 2020 Line 01 54 36.50
C_mob_load	Loader Mobilization Cost	$		RSMeans 2020 Line 01 54 36.50
C_mob_tanker	Water Truck Mobilization Cost	$		Table S5 Chee et al, 2018
C_oil_bbl	Crude Oil Price	$/bbl		EIA,2021; Empiracle distribution
C_pipe	Total Pipe Material Cost	$		RSMeans 2020 Line 33 14 13.25
C_pumping_day	Daily Pumping Cost	$/day		
C_wat	Total Cost of Construction Water	$		
D_1	Embedment Material Density	kg/m^3		Table S8 Chee et al., 2018
D_b	Bedding Thickness Below Pipe	mm	50.8 ± 10%	Based on professional correspondence
D_c	Bedding Thickness Above Pipe	mm	914.4 ± 10%	Based on professional correspondence
D_e	Embedment Cover Depth	mm	12825.4 ± 10%	Based on professional correspondence
D_ep	Distance from Embedment Pile to Trench	m		Eqn 15 Chee et al., 2018
D_id_in	Pipe Inner Diameter Inch (Rounded Up)	in	1.61 - 11.94	Exact value derived from flow calculations
D_id_in_calc	Theoretical Pipe Diameter	in		
D_id_mm	Pipe Inner Diameter mm (Rounded Up)	mm		
D_Name_in	Pipe Name		1.5 - 12	Sch 40 Pipe specification
D_od_in	Pipe Outer Diameter Inch (Rounded Up)	in	1.91 - 12.75	Exact value derived from flow calculations
D_od_mm	Pipe Outer Diameter mm (Rounded Up)	mm		
d_P_100ft	Head Loss per 100 ft	ft H2O/100 ft		Darcy-Weisbach Equation
d_P_100m	Head Loss per 100 m	ft H2O/100 m		Darcy-Weisbach Equation
d_P_total_ft_H2O	Total Head Loss	ft H2O		
D_sp	Distance Between Spoil Pile and Trench	m		Eqn 15 Chee et al., 2018
D_t	Trench Depth	mm		Eqn 1 Chee et al., 2018
D_w	Distance from Water Source to Job Site	m	5 - 10	Assumed

Dist_mob	Equipment Mobilization Distance	mi	10 - 100	Assumed
E_pump	Pump Energy Requirement	kW		
Eff_motor	Motor Efficiency		0.6 - 0.9	Loh et al., 2002
Eff_pump	Pump Efficiency		0.6 - 0.82	Loh et al., 2002
f_c	Excavator Bucket Fill Factor			CAT, 2016
f_friction	friction factor			Equation 3-2 from AWWA M23 Manual
Loader_wt	Loader Weight	US ton		CAT, 2016
N_bp	Number of Booster Pumps			Assume booster pump needed after 20% pressure drop
N_ep	Number of Embedment Piles			Eqn 14 Chee et al., 2018
N_sp	Number of Spoil Piles			Eqn 14 Chee et al., 2018
N_tanker	Number of Water Trucks Required			Eqn 24 Chee et al., 2018
Net_benefit	Net Benefit of Brine Exchange	$/day		
Oil_EOR	Enhanced Oil Recovery Quantity	bbl/day		Assumed 22.2 barrels of water needed per barrel of oil extracted
P	Percentage of Native Material Needing Processing		0 - 0.2	Assumed
P_back	Backfill Placement Rate	m^3/hr		Eqn 16 Chee et al., 2018
P_emb	Embedment Material Placement Rate	m^3/hr		Eqn 19 Chee et al., 2018
P_exc	Excavator Production Rate	m^3/hr		Eqn 9 Chee et al., 2018
P_o	Maximum Pipe Pressure	psi	79 - 198	ASTM D2466-06 Specification
P_pro	Native Material Processing Rate	m^3/hr		Eqn 18 Chee et al., 2018
P_sc	Native Material Screening Rate	m^3/hr		Eqn 18 Chee et al., 2018
P_sp	Spoil Pile Collection Rate	m^3/hr		Eqn 16 Chee et al., 2018
P_tanker	Water Truck Production Rate per Truck	L/day		Eqn 25 Chee et al., 2018
Percent_EOR	Percent Increased Oil Recovery per Well		0.04 -0.12	Wang et al, 2020
Pipe_ID_Nom_in	Schedule 40 Pipe Inner Diameter	in	1.61 - 11.94	Exact value derived from flow calculations
Pipe_Name_Nom_in	Schedule 4- Pipe Name		1.5 in - 12 in	Exact value derived from flow calculations
Pipe_OD_Nom_in	Schedule 40 Pipe Outer Diameter	in		
Q_oilwell_daily	Daily Crude Oil Production per Well	bbl/day	0.5 - 10	Based on industry correspondence
Q_start	PW Flow Rate	bbl/day	1 - 1000	Model Input

R_exc	Trenching Rate	m/day	57 - 229	Eqn 8 Chee et al., 2018
R_pipe	Pipe Installation Rate	ft/day		RSMeans 2020 Line 33 14 13.25
Re	Reynold's Numer			
S	Percentage of Native Material Needing Screening		0 - 0.2	Assumed
S_l	Embedment Material Shrink Factor		0.8	Table S8 Chee et al, 2018
S_wt	Water Truck Speed	km/hr	64.37	Assumed value
SG_Arbuckle	Specific Gravity of Arbuckle Brine		1.015	Measured Value
t_d	Loder Dumping Time	s	5	Table S7 Chee et al, 2018
T_day	Workday Length	hr	8	Assume standard workday
t_ei	Travel Time of Empty Loader to from Spoil Pile to Trench			Table S7 Cheet et al, 2018
t_es	Loader Travel Time to Trench from Spoil Pile	s		Table S7 Chee et al, 2018
T_hr	Productivity Min Per Hour	min/hr	40 -50	Assumed values
t_i	Excavator Cycle Time	s	18	Saglam and Bettemir, 2018
T_job	Total Length of Job	day		Eqn 34 Chee et al., 2018
t_l	Loader Loading Time	s	9	Table S7 Chee et al, 2018
t_li	Travel Time of Loaded Loader to Spoil Pile	s		Table S7 Cheet et al, 2018
T_load	Total Loader Task Time	hr		Eqn 22 Chee et al., 2018
t_ls	Loader Travel Time to Spoil Pile from Trench to Spoil Pile	s		Table S7 Chee et al, 2018
t_tanker_cycle	Water Truck Cycle Time	s		Eqn 27 Chee et al., 2018
t_tanker_dump	Water Truck Dumping Time	min	5 -20	Assumed
t_tanker_e	Tanker Time Empty Tanker	s		Eqn 28 Chee et al., 2018
t_tanker_l	Travel Time of Loader Tanker	s		Eqn 28 Chee et al., 2018
t_tanker_load	Water Truck Loading Time	min	5 -20	Assumed
V_bed	Bedding Material Volume	m^3 material/ m pipe		Eqn S1 Chee et al., 2018
V_c	Cover Material Volume	m^3 material/ m pipe		Eqn S8 and S9 Chee et al., 2018
V_emb	Embedment Material Volume	m^3 material/ m pipe		Eqn 11 Chee et al., 2018
V_emb_d	Embedment Material Placement Rate	m^3/day		Eqn 12 Chee et al., 2018
V_ep	Embedment Pile Volume	m^3	38.48 ± 10%	Assume max height of 3 and 1.5H:1V

V_exc	Trench volume	m^3		Eqn 4 Chee et al., 2018
V_exc_d	Daily Bank Excavated Material	m^3/day		Eqn 5 Chee et al. 2018
v_fluid_max_ft	Fluid Pipe Velocity (ft)	ft/s	5	Based on typical design parameters
v_fluid_pipe_m	Fluid Pipe Velocity (m)	m/s		
V_h	Haunching Material Volume	m^3 material/ m pipe		Eqn S2 Chee et al., 2018
V_ib	Initial Backfill Material Volume	m^3 material/ m pipe		Eqn S3 Chee et al., 2018
V_m_w	Excavator Bucket Capacity	m^3		Table S11 Chee et al., 2018
V_sp	Spoil Pile Volume	m^3	38.48 ± 10%	Assume max height of 3 and 1.5H:1V
V_wat	Volume of Water for backfill and Embedment	m^3		Eqn 23 Chee et al., 2018
V_wat_d	Volume of Construction Water Needed	L/day		Eqn 26 Chee et al., 2018
V_wt	Water Truck Capacity	L	12870	Assume largest truck size used
W_b	Excavator Bucket Width	mm	457.2 - 1981.2	Table S11 Chee et al., 2018
w_d	Water Content Deficit of Backfill and Embedment Material		0 - 0.05	Assumed
W_emb	Embedment Material Weight	metric ton		Table S8 Chee et al, 2018
W_t	Final Trench Base Width	mm		Chee et al., 2018
W_tr	Trench Width	mm		Eqn 2,3 Chee et al., 2018
x	Distance	m	1 - 10000	Model Input

The following table contains the ρ and p-values of the Spearman's rank order correlation performed for each of the variables used within the simulation.

Table 13 Spearman Rank Correlation Coefficient values between independent variables and Net Benefit used within the Monte Carlo analysis

Code Name	Variable Name	ρ	p-value
C_disp_pipe	PW Disposal Cost via Pipe	0.08	$p < 0.01$
C_equip_booster	Cost of Booster Pumps	0.31	$p < 0.01$
C_equip_load	Total Loader Rental Cost	-0.41	$p < 0.01$
C_equip_tanker	Total Water Truck Rental Cost	-0.41	$p < 0.01$
C_exc_unit	Excavation Cost	0.01	0.14
C_lab_load	Total Loader Labor Cost	-0.41	$p < 0.01$
C_lab_pipe	Total Pipe Installation Labor Cost	-0.42	$p < 0.01$
C_mob_exc	Excavator Mobilization Cost	$\|\rho\| < 0.01$	0.77
C_pipe	Total Pipe Material Cost	-0.34	$p < 0.01$
C_rental_exc	Excavator Rental Cost	$\|\rho\| < 0.01$	0.96
D_1	Embedment Material Density	0.01	0.29
D_b	Bedding Thickness Below Pipe	$\|\rho\| < 0.01$	0.40
D_c	Bedding Thickness Above Pipe	$\|\rho\| < 0.01$	0.33
D_e	Embedment Cover Depth	$\|\rho\| < 0.01$	0.64
D_w	Distance from Water Source to Job Site	$\|\rho\| < 0.01$	0.87
Dist_mob	Equipment Mobilization Distance	$\|\rho\| < 0.01$	0.90
Eff_motor	Motor Efficiency	$\|\rho\| < 0.01$	0.83
Eff_pump	Pump Efficiency	$\|\rho\| < 0.01$	0.75
f_c	Excavator Bucket Fill Factor	$\|\rho\| < 0.01$	0.51
f_friction	friction factor	-0.78	$p < 0.01$
P	Percentage of Native Material Needing Processing	$\|\rho\| < 0.01$	0.56
Percent_EOR	Percent Increased Oil Recovery per Well	0.18	$p < 0.01$
Q_oilwell_daily	Daily Crude Oil Production per Well	$\|\rho\| < 0.01$	0.71
Q_start	PW Flow Rate	0.81	$p < 0.01$
S	Percentage of Native Material Needing Screening	$\|\rho\| < 0.01$	0.42
S_1	Embedment Material Shrink Factor	$\|\rho\| < 0.01$	0.66
S_wt	Water Truck Speed	-0.02	0.11
t_d	Loder Dumping Time	-0.01	0.25
t_es	Loader Travel Time to Trench from Spoil Pile	0.03	$p < 0.01$
T_hr	Productivity Min Per Hour	0.01	0.20
t_i	Excavator Cycle Time	$\|\rho\| < 0.01$	0.36
t_l	Loader Loading Time	$\|\rho\| < 0.01$	0.60
t_li	Travel Time of Loaded Loader to Spoil Pile	0.01	0.23

t_ls	Loader Travel Time to Spoil Pile from Trench to Spoil Pile	0.03	$p < 0.01$
t_tanker_dump	Water Truck Dumping Time	$\|\rho\| < 0.01$	0.44
t_tanker_load	Water Truck Loading Time	-0.01	0.29
V_ep	Embedment Pile Volume	$\|\rho\| < 0.01$	0.91
V_m_w	Excavator Bucket Capacity	$\|\rho\| < 0.01$	0.49
V_sp	Spoil Pile Volume	0.02	0.05
w_d	Water Content Deficit of Backfill and Embedment Material	$\|\rho\| < 0.01$	0.41
x	Distance	-0.44	$p < 0.01$

10 Appendix D: PITZER Database

The PITZER updated constant values for calcite in version 3.7.0. These values as well as previous ones can be seen in the figures below. Model predictions utilizing the updated file can be seen in **Figure** 20, and MAPE calculations using the new equilibrium points are shown in **Table** 14.

```
Calcite
        CaCO3 = CO3-2 + Ca+2
        log_k         -8.406
        delta_h -2.297 kcal
        -analytic   -237.04  -0.1077  0  102.25  6.79e5 # ref. 3 + data from Ellis, 1959, Plummer and Busenberg, 1982
        -Vm 36.9
```

Figure 18 PITZER database constants for calcite prior to version 3.7.0

```
        CaCO3 = CO3-2 + Ca+2
        log_k         -8.406
        delta_h -2.297 kcal
        -analytic  8.481      -0.032644  -2133 # ref. 3 + data from Ellis, 1959, Plummer and Busenberg, 1982
        -Vm 36.9
```

Figure 19 Current PITZER constants for calcite

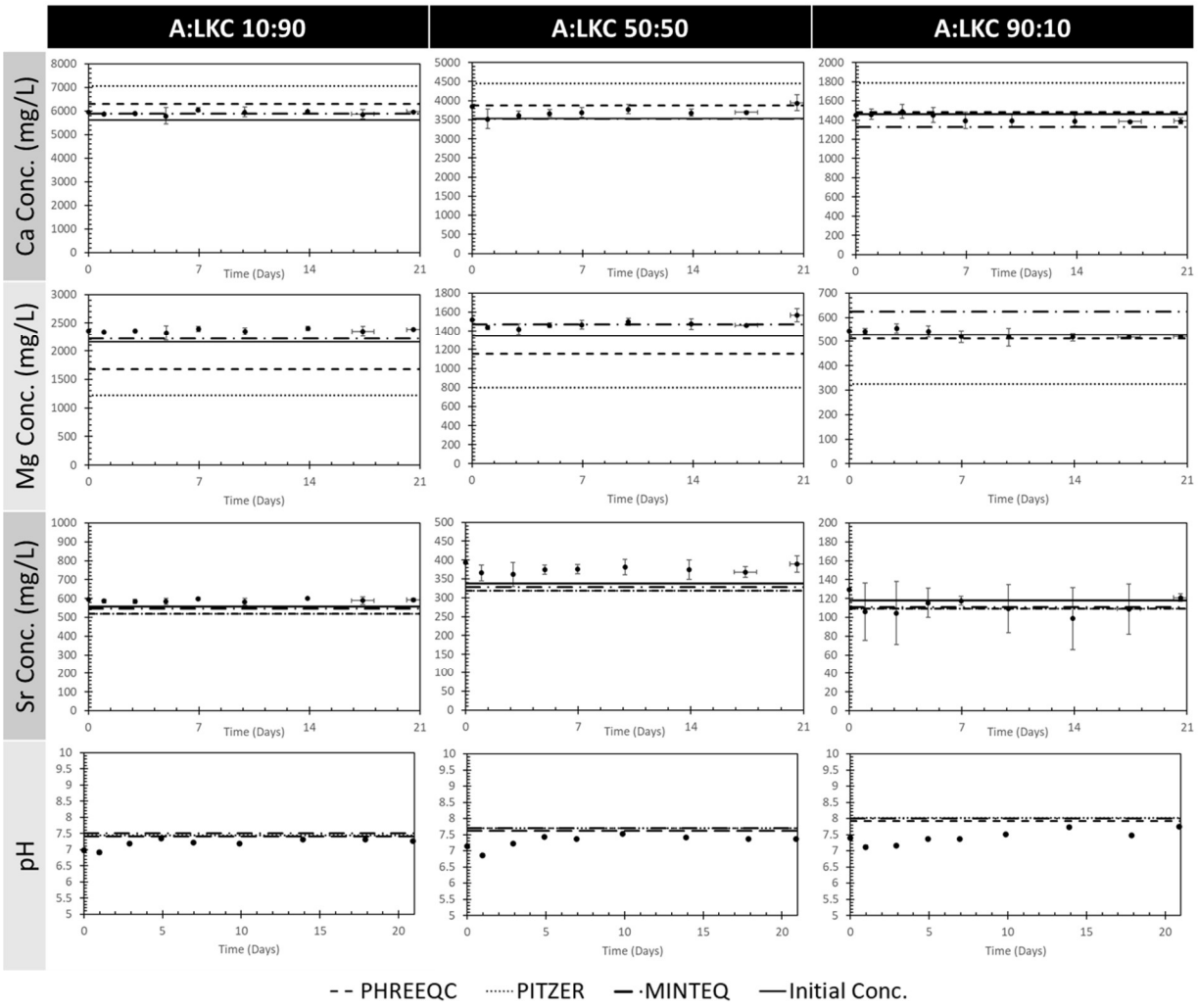

Figure 20 Old PITZER database predictions plotted alongside results of other simulations

Table 14 MAPE values using PHREEQC output with newest PITZER database

	New PITZER			
	Ca	**Mg**	**Sr**	**pH**
A:LKC 10:90	18.80	48.35	11.96	3.35
A:LKC 50:50	19.76	45.94	15.19	5.78
A:LKC 90:10	25.64	38.55	6.30	7.37
A:LKC 100:0	7.67	40.46	6.05	7.50
A:LKC 0:100	3.08	44.88	2.66	3.50

11 Appendix E: Economic Analysis Simulation Code

The following section contains the MATLAB code used to conduct the techno-economic simulation. The code incorporates the WaterCOSTE model to estimate infrastructure cost.

```
%% Input Constants
x = lhsu(1,10000,10000); % distance in meters
   x = round(x);
Q_start = lhsu(1,1000,size(x,1)); % hypothetical starting volumetric flow of PW in barrels/day
%% Labor Constants
 % Hours per Workday
   T_day = 8;
 % Produciton Minutes
   T_hr = lhsu(40,50,size(x,1));
    % Assumes 10 to 20 minutes per hour are spent on actions other than direct work
%% Embedment Constants
 % Embedment Cover Depth (mm); Assume 1 ft
   D_e = lhsu(12*25.4*0.9,12*25.4*1.1,size(x,1));
%% Pipe Size (Inner Diameter)
   D_id_in_calc=zeros(size(x,1),1);
   % Assume max fluid velocity of 5 ft/s before 20% surge factor
   v_fluid_max_ft = 5;
   % Q in units of barrels/day
   % D_p in units of in
   % Diameter is inner diameter
   for i = 1:size(x,1)
      D_id_in_calc(i,1) = sqrt(4*(Q_start(i,1)/24/60/60)*5.615/pi/(v_fluid_max_ft*0.8))*12;
   end
 % Schedule 40 Pipe Size and Pressure
       Pipe_ID_Nom_in = [1.61;2.07;2.47;3.07;3.55;4.03;5.05;6.07;7.98;10.02;11.94];
       Pipe_OD_Nom_in = [1.90;2.38;2.88;3.50;4.00;4.50;5.56;6.63;8.63;10.75;12.75];
       Pipe_Name_Nom_in = [1.5;2;2.5;3;3.5;4;5;6;8;10;12];
       Pipe_Max_Pressure = [198;166;182;158;145.5;133;119.5;106;93;84;79]; % ASTM D2466-06 Specification;
values not listed interpolated
   Pipe_Nom_Array = zeros(size(Pipe_ID_Nom_in,1),2);
   for i =1:size(Pipe_ID_Nom_in,1)
      Pipe_Nom_Array(i,1) = Pipe_ID_Nom_in(i,1);
      Pipe_Nom_Array(i,2) = Pipe_OD_Nom_in(i,1);
      Pipe_Nom_Array(i,3) = Pipe_Name_Nom_in(i,1);
      Pipe_Nom_Array(i,4) = Pipe_Max_Pressure(i,1);
   end
 % Round ID to next closest Nominal Schedule 40 ID
   D_id_in = zeros(size(D_id_in_calc,1),1);
   for i=1:size(x,1)
      if D_id_in_calc(i,1) <= 1.61 % Set min and max inner diameters
         D_id_in(i,1) = 1.61;
      elseif D_id_in_calc(i,1) >= 11.94
         D_id_in(i,1) = 11.94;
      else
         D_id_in(i,1) = roundtowardvec(D_id_in_calc(i,1),Pipe_ID_Nom_in,'ceil');
      end
   end
 % Assign OD and Size Name based on Nominal ID Schedule 40
   D_od_in = zeros(size(x,1),1);
```

```
    D_Name_in = zeros(size(x,1),1);
    row = zeros(size(x,1),1);
    for i =1:size(x,1)
        row(i,1) = find(Pipe_Nom_Array(:,1) == D_id_in(i,1));
        D_od_in(i,1) = Pipe_Nom_Array(row(i,1),2);
        D_Name_in(i,1) = Pipe_Nom_Array(row(i,1),3);
    end
  % Convert Inner/Outer Diameter from in to mm
    D_id_mm=zeros(size(x,1),1);
    D_od_mm=zeros(size(x,1),1);
    for i= 1:size(x,1)
        D_id_mm(i,1)= D_id_in(i,1)*25.4;
        D_od_mm(i,1)= D_od_in(i,1)*25.4;
    end
 %% Trench Excavation
  % Trench Depth
    % D_od_mm Outside Diameter of pipe (mm)
    D_b = lhsu(50.8*0.9,50.8*1.1,size(x,1)); % Bedding thickness below pipe (mm), Assume 2 inches
    D_c = lhsu(914.4*0.9,914.4*1.1,size(x,1)); % Bury Depth over pipe (mm), Assume 3 ft
    D_t = zeros(size(x,1),1);
    for i = 1:size(x)
        D_t(i,1) = D_od_mm(i,1)+D_b(i,1)+D_c(i,1); % Trench depth (mm) (Eqn 1 Chee et al., 2018)
    end
  % Trench Width (assumes all Kansas is covered with Class 4 soil)
   W_tr=zeros(size(x,1),1); % (Eqn 2,3 Chee et al., 2018)
    for i = 1:size(x,1)
        if D_od_mm(i,1) < 1200
            W_tr(i,1)=D_od_mm(i,1)+600;
        else
            W_tr(i,1)=D_od_mm(i,1)+1200;
        end
    end
  % Trench Cross Sectional Area (Assume Kansas is all Type B soil)
   % Units mm^2
   % (Figure 4 Chee et al., 2018)
    A_t=zeros(size(x,1),1);
    for i = 1:size(x,1)
        if D_t(i,1) <= 1219
            A_t(i,1)= W_tr(i,1)*D_t(i,1);
        elseif D_t(i,1) > 1219 && D_t(i,1) <= 6096
            A_t(i,1) = W_tr(i,1)*D_t(i,1)+(D_t(i,1)-1219)^2+(2438*(D_t(i,1)-1219));
        else
            error('Pipe diameter too large');
        end
    end
 %% Pipe Installation Data
  % Installation Rate from (RSMeans 2020 Line 33 14 13.25)
    % Values not explicitly listed were interpolated
   % Pipe Nominal Diameter
    Pipe_Install_Data(:,1) = [1.5;2;2.5;3;3.5;4;5;6;8;10;12];
   % Pipe Install Rates in units of m/day
    Pipe_Install_Data(:,2) = [229;209;152;116;116;116;106;96;80;67;57];
    % Pipe Material Cost per Meter
    Pipe_Install_Data(:,3) = [2.00;2.89;3.87;5.22;7.58;9.94;13.17;16.40;28.22;41.50;58.23];
 %% Trenching Rate R_Pipe
    R_pipe = zeros(size(x,1),1);
```

```
    for i = 1:size(x)
        row(i,1) = find(Pipe_Install_Data(:,1) == D_Name_in(i,1));
        R_pipe(i,1) = Pipe_Install_Data(row(i,1),2);
    end
%% Total Length of Project (days)
 % (Eqn 34 Chee et al., 2018)
    T_job = zeros(size(x,1),1);
    for i = 1:size(x)
        T_job(i,1) = x(i,1)/R_pipe(i,1);
    end
%% Trench Volume
 % (Eqn 4 Chee et al., 2018)
    V_exc=zeros(size(x,1),1);
    for i = 1:size(x,1)
        V_exc(i,1)= A_t(i,1)*x(i,1)/1000000; % Excavated material (m^3)
    end
%% Daily Bank Excavated material (m^3)
 % (Eqn 5 Chee et al. 2018)
    V_exc_d=zeros(size(x,1),1);
    for i = 1:size(x,1)
        V_exc_d(i,1)= A_t(i,1)*R_pipe(i,1)/1000000;
    end
%% Excavator Selection
 % Excevator Bucket Width (Calculates size of excavator bucket in mm)
 % (Table S11 Chee et al., 2018)
 % Assume CAT 315 model used
    W_b=zeros(size(x,1),1);
    for i = 1:size(x,1)
        W_b(i,1)= 152.4*ceil(W_tr(i,1)/152.4); %buckets come in of 6in intervals
    end
    for i = 1:size(x)
        count=0; % Sets maximum and minimum bucket sizes
        while count < size(x)
            count = count +1;
            for i = 1:size(x,1)
                if W_b(i,1) < 457.2
                    W_b(i,1) = 457.2;
                elseif W_b(i,1)> 914.4
                    W_b(i,1) = 914.4;
                else
                    W_b(i,1) = W_b(i,1);
                end
            end
        end
    end
%% Trenching Rate
 % Bucket fill factor assuming soil, boulders and roots
  % (CAT, 2016)[51]
    f_c = lhsu(0.8,1,size(x,1));
 % Bucket Capacity based on Bucket Width
    V_m_w = zeros(size(x,1),1);
        % Assume 1/2 cubic card capacity common (CAT Model 315)
            % Bucket sizes 18in to 36in available)
        % (Table S11 Chee et al., 2018)
    % Uncertainty rante for Bucket Capacity
     V_m_w_uncert = lhsu(0.9,1.1,size(x,1));
```

```
  for i = 1:size(x,1)
     % capcity values are in cubic meters
     if W_b(i,1) == (18+(6*0))*25.4
        V_m_w(i,1) = 0.27*0.7645*V_m_w_uncert(i,1);
     elseif W_b(i,1) == (18+(6*1))*25.4
        V_m_w(i,1) = 0.4*0.7645*V_m_w_uncert(i,1);
     elseif W_b(i,1) == (18+(6*2))*25.4
        V_m_w(i,1) = 0.54*0.7645*V_m_w_uncert(i,1);
     else
        V_m_w(i,1) = 0.69*0.7645*V_m_w_uncert(i,1);
     end
  end
% Cycle Times
 % (Saglam and Bettemir, 2018)[52]
 % Assume all soil is common earth, soft clay, average soil
  t_i = zeros(size(x,1),1);
 % Cycle Time uncertainty range
  t_i_uncert = lhsu(0.9,1.1,size(x,1));
  for i=1:size(x) % Cycle Time in seconds based on bucket capacity in m^3
     if V_m_w(i,1) < 0.76
        t_i(i,1) = 18*t_i_uncert(i,1);
     elseif V_m_w(i,1) > 0.95 && V_m_w(i,1) < 1.72
        t_i(i,1) = 23*t_i_uncert(i,1);
     else
        t_i(i,1) = 30*t_i_uncert(i,1);
     end
  end
% Excavation Production Rate (m^3/hr)
 % (Eqn 9 Chee et al., 2018)
  P_exc = zeros(size(x,1),1);
  for i = 1:size(x)
     P_exc(i,1) = f_c(i,1)*V_m_w(i,1)/t_i(i,1)*T_hr(i,1)*60;
  end
% Trenching Rate (m/day)
 % (Eqn 8 Chee et al., 2018)
  R_exc=zeros(size(x,1),1);
  % Assume 8 hr shifts per day
  for i =1:size(x)
     R_exc(i,1) = P_exc(i,1)*1000000/A_t(i,1)*24;
  end
%% Embedment Calculations
  % Assume Type B Soil
  % Assume Tpye B Soil in Kansas is Class 4 (Soil Stiffness)
% Final Trench Base Width (mm)
 % (Chee et al., 2018)
  W_t = zeros(size(x,1),1);
  for i = 1:size(x)
     if W_tr(i,1) > W_b(i,1)
        W_t(i,1) = W_tr(i,1);
     else
        W_t(i,1) = W_b(i,1);
     end
  end
% Bedding Material Volume (m^3 material /m pipe)
 % (Eqn S1 Chee et al., 2018)
  V_bed = zeros(size(x,1),1);
```

```
  for i =1:size(x)
     V_bed(i,1) = D_t(i,1)*W_t(i,1)*1000/1e9;
  end
% Haunching Material Volume (m^3 material/m pipe)
 % (Eqn S2 Chee et al., 2018)
  V_h = zeros(size(x,1),1);
  for i = 1:size(x)
     V_h(i,1) = (((D_od_mm(i,1)/2)*W_t(i,1))-((pi*(D_od_mm(i,1)^2))/8))*1000/1e9;
  end
% Initial Backfill Material Volume (m^3 material /m pipe)
 % (Eqn S3 Chee et al., 2018)
  V_ib = zeros(size(x,1),1);
  for i =1:size(x)
     if D_t(i,1) <= 1219
        V_ib(i,1) = (((D_od_mm(i,1)/2)*W_t(i,1))-((pi*(D_od_mm(i,1)^2))/8))*1000/1e9;
     elseif D_t(i,1) > 1219 && D_t(i,1) <= 6096 && (D_od_mm(i,1)+D_b(i,1))<=1219
        V_ib(i,1) = (((D_od_mm(i,1)/2)*W_t(i,1))-((pi*(D_od_mm(i,1)^2))/8))*1000/1e9;
     elseif D_t(i,1) > 1219 && D_t(i,1) <= 6096 && (D_od_mm(i,1)+D_b(i,1))> 1219
        V_ib(i,1) = ((((D_od_mm(i,1)/2)*W_t(i,1))- ...
           ((pi*(D_od_mm(i,1)^2))/8)) + ...
           (2*1219*(D_b(i,1)+D_od_mm(i,1)-1219)) + ...
           (2*1.0*(D_b(i,1)+D_od_mm(i,1)-1219)^2))*1000/1e9;
     else
        V_ib(i,1)='Error';
     end
  end
% Cover Material Volume (m^3 material /m pipe)
 % (Eqn S8 and S9 Chee et al., 2018)
     V_c=zeros(size(x,1),1);
     W_1 = zeros(size(x,1),1);
     W_2 = zeros(size(x,1),1);
  for i = 1:size(x)
     if D_t(i,1) <= 1219
        V_c(i,1) = W_t(i,1)*D_e(i,1)*1000/1e9;
     elseif D_t(i,1) <= 6096 && D_t(i,1) > 1219
        if (D_b(i,1) + D_od_mm(i,1) + D_e(i,1)) <= 1219
           V_c(i,1) = W_t(i,1)*D_e(i,1)*1000/1e9;
        elseif (D_b(i,1) + D_od_mm(i,1) + D_e(i,1)) > 1219 && (D_b(i,1) + D_od_mm(i,1)) < 1219
           V_c(i,1) = (D_e(i,1)*W_t(i,1)+ 2*1219*(D_od_mm(i,1)+D_e(i,1)+D_b(i,1)-
1219)+1*((D_od_mm(i,1)+D_e(i,1)+D_b(i,1)-1219)^2))*1000/1e9;
        else
           W_1(i,1) = W_t(i,1)+2*1219+2*1*(D_b(i,1)+D_od_mm(i,1)-1219);
           W_2(i,1) = W_t(i,1)+2*1219+2*1*(D_b(i,1)+D_od_mm(i,1)+D_e-1219);
           V_c(i,1) = (0.5*(W_1(i,1)+W_2(i,1))*D_e)*1000/1e9;
        end
     else
        V_c(i,1) = 'Error';
     end
  end
% Embedment Material Volume (m^3/m)
 % (Eqn 11 Chee et al., 2018)
  V_emb=zeros(size(x,1),1);
  for i = 1:size(x)
     V_emb(i,1) = V_bed(i,1)+V_h(i,1)+V_ib(i,1)+V_c(i,1);
  end
% Embedment Material Volumetric Rate
```

```
% (Eqn 12 Chee et al., 2018)
  V_emb_d=zeros(size(x,1),1);
  for i = 1:size(x)
     V_emb_d(i,1) = V_emb(i,1)*R_pipe(i,1);
  end
% Embedment Material Weight (Native)
 % Assume Density of Type IV (Native) Embedment Material is 1922 kg/m^3 (Table S8 Chee et al, 2018)
  D_1 = lhsu(1922*0.9,1922*1.1,size(x,1));
 % Assume Shrink Factor of Type IV Embedment Material is 0.8 (Table S8 Chee et al, 2018)
  S_1 = lhsu(0.8*0.9,0.8*1.1,size(x,1));
  W_emb = zeros(size(x,1),1);
     for i = 1:size(x)
        W_emb(i,1) = V_emb(i,1)/1000/D_1(i,1)/S_1(i,1)*x(i,1);
     end
%% Spoil Pile Criteria (Native Material)
% Volume of Spoil Pile (m^3)
 % Assume Cone with max height of 3m and 1.5H:1V (horizontal:vertical side slope (m^3)
 % (Chee et al., 2018)
  V_sp = lhsu((1/3)*pi()*(3.5)^2*3*0.9,(1/3)*pi()*(3.5)^2*3*1.1,size(x,1));
% Number of Spoil Piles
% (Eqn 14 Chee et al., 2018)
  N_sp = zeros(size(x,1),1);
  for i = 1:size(x)
     N_sp(i,1) = V_exc_d(i,1)/V_sp(i,1);
  end
% Distance between Spoil Pile and Trench (m)
% (Eqn 15 Chee et al., 2018)
  D_sp = zeros(size(x,1),1);
  for i =1:size(x)
     D_sp(i,1) = N_sp(i,1)/R_pipe(i,1);
  end
%% Loader Travel and Operating Times (Spoil Pile)
% (Table S7 Chee et al, 2018)
% Travel Time of loaded loader to spoil pile
  t_ls = zeros(size(x,1),1);
 % Travel speed Uncertainty
  t_ls_uncert = lhsu(0.9,1.1,size(x,1));
  for i = 1:size(x)
     t_ls(i,1) = D_sp(i,1)/2/(4.47*t_ls_uncert(i,1)); % 4.47 = speed of loaded loader in m/s
  end
% Travel Time of empty loader from spoil pile to trench
  t_es = zeros(size(x,1),1);
  t_es_uncert = lhsu(0.9,1.1,size(x,1));
  for i = 1:size(x)
     t_es(i,1) = D_sp(i,1)/2/(4.92*t_es_uncert(i,1)); % 4.92 = speed of empty loader in m/s
  end
% Dumping and Loading Times (s)
  t_l = lhsu(9*0.9,9*1.1,size(x,1));
  t_d = lhsu(5*0.9,5*1.1,size(x,1));
%% Embedment Pile Criteria (Native Material)
% Volume of Embedment Pile
% Spoil pile is same as embedment pile due to use of native material
  V_ep = lhsu((1/3)*pi()*(3.5)^2*3*0.9,(1/3)*pi()*(3.5)^2*3*1.1,size(x,1));
% Number of Import Piles
  N_ep = zeros(size(x,1),1);
  for i = 1:size(x)
```

```
        N_ep(i,1) = V_emb_d(i,1)/V_ep(i,1);
    end
% Distance between Embedment Pile and Trench (m)
    D_ep = zeros(size(x,1),1);
    for i =1:size(x)
        D_ep(i,1) = N_ep(i,1)/R_pipe(i,1);
    end
%% Loader Travel and Operating Times (Embedment Pile)
% (Table S7 Cheet et al, 2018)
% Travel Time of loaded loader to spoil pile
    t_li = zeros(size(x,1),1);
% Loader Loaded speed uncertainty
    t_li_uncert = lhsu(0.9,1.1,size(x,1));
    for i = 1:size(x)
        t_li(i,1) = D_ep(i,1)/2/(4.47*t_li_uncert(i,1)); % 4.47 = speed of loaded loader in m/s)
    end
% Travel TIme of empty loader from spoil pile to trench
    t_ei = zeros(size(x,1),1);
% Loader Empty speed uncertainty
    t_ei_uncert = lhsu(0.9,1.1,size(x,1));
    for i = 1:size(x)
        t_ei(i,1) = D_ep(i,1)/2/(4.92*t_ei_uncert(i,1)); % 4.92 = speed of empty loader in m/s)
    end
% t_l and t_d assumed to be identical to spoil pile values
%% Front End Loader Selection
% Spoil Pile Collection Rate (m^3/h) and Backfill Placement Rate (m^3/h)
    P_sp = zeros(size(x,1),1);
    P_back = zeros(size(x,1),1);
% Native Embedment Material Screening and Processing
    P_pro = zeros(size(x,1),1);
    P_sc = zeros(size(x,1),1);
 % Percentage of native material which requires Screening and Processing
 % Fix later
    S = lhsu(0,0.2,size(x,1));
    P = lhsu(0,0.2,size(x,1));
% Native Embedment Material Placement Rate
    P_emb = zeros(size(x));
% Bucket Capacity (C_lb) of Loader (m^3)
    % Iterative Calculation
    C_lb = zeros(size(x,1),1); % m^3
    T_load = zeros(size(x,1),1);
    for i = 1:size(x)
        j = 1;
        iter = 1;
       % Determine minimum loader size needed
       % (Table S7 Chee et al, 2018)
        while iter == 1
            if j == 1
                C_lb(i,1) = 2.29;
            elseif j == 2
                C_lb(i,1) = 2.52;
            elseif j == 3
                C_lb(i,1) = 2.91;
            elseif j == 4
                C_lb(i,1) = 3.10;
            elseif j == 5
```

```
            C_lb(i,1) = 3.40;
        elseif j == 6
            C_lb(i,1) = 4.01;
        elseif j == 7
            C_lb(i,1) = 4.78;
        elseif j == 8
            C_lb(i,1) = 5.40;
        elseif j == 9
            C_lb(i,1) = 6.10;
        elseif j == 10
            C_lb(i,1) = 6.88;
        else
            'Error';
            break
        end
      % Spoil Pile Backfill and Collection Rate
       % (Eqn 16 Chee et al., 2018)
        P_back(i,1) = C_lb(i,1)*60*T_hr(i,1)/(t_ls(i,1)+t_es(i,1)+t_l(i,1)+t_d(i,1));
        P_sp(i,1) = P_back(i,1);
      % Processing and Screening Rate of Native Material
       % (Eqn 18 Chee et al., 2018)
        P_pro(i,1) = C_lb(i,1)*60*T_hr(i,1)/(t_l(i,1)+t_d(i,1));
        P_sc(i,1) = P_pro(i,1);
      % Production Rate of Native Embedment Material
       % (Eqn 19 Chee et al., 2018)
        P_emb(i,1) = C_lb(i,1)*60*T_hr(i,1)/(t_li(i,1)+t_es(i,1)+t_l(i,1)+t_d(i,1));
      % Total Time to Accomplish all Tasks (hours)
       % (Eqn 22 Chee et al., 2018)
        T_load(i,1) = (V_exc_d(i,1)/P_sp(i,1)) + (V_emb_d(i,1)/P_emb(i,1)) + (V_exc_d(i,1)/P_sc(i,1))*S(i,1) +
(V_exc_d(i,1)/P_pro(i,1))*P(i,1) + (V_exc_d(i,1)/P_back(i,1));
        if T_load(i,1) > T_day
            j = j+1;
        else
            iter = iter+1;
        end
      end
   end
%% Water Volume Calculations
 % Water Content Deficit of Backfill and Embedment Material (assume 0 - 5%)
   w_d = lhsu(0,0.05,size(x,1));
 % Total Volume of Water (m^3) for Backfill and Embedment
  % (Eqn 23 Chee et al., 2018)
   V_wat = zeros(size(x,1),1);
   for i = 1:size(x)
      V_wat(i,1) = (V_exc(i,1)+V_emb(i,1))*w_d(i,1);
   end
%% Water Truck Calculations
 % Assume Truck Capacity is 12870 L each
   V_wt = 12870;
 % Cycle Time Calculations for Water Truck (min)
  % Distance from Water Source to Job Site (km)
   D_w = lhsu(5,10,size(x,1));
  % Assume Average Speed of Water Truck is 64.37 km/hr
   S_wt = lhsu(64.37*0.9,64.37*1.1,size(x,1));
 % Travel Time for Loaded and Unloaded Tanker (min)
  % (Eqn 28 Chee et al., 2018)
```

```
    t_tanker_l = zeros(size(x,1),1);
    t_tanker_e = zeros(size(x,1),1);
    for i = 1:size(x)
        t_tanker_l(i,1) = D_w(i,1)/S_wt(i,1)*60;
        t_tanker_e(i,1) = t_tanker_l(i,1);
    end
  % Time to Load and Dump Water Truck (min)
   % Assume 5 - 20 min each
    t_tanker_load = lhsu(10,20,size(x,1));
    t_tanker_dump = lhsu(10,20,size(x,1));
  % Total Cycle Time of Water Truck
   % (Eqn 27 Chee et al., 2018)
    t_tanker_cycle = zeros(size(x,1),1);
    for i = 1:size(x)
        t_tanker_cycle(i,1) = t_tanker_load(i,1) + t_tanker_l(i,1) + t_tanker_dump(i,1) + t_tanker_e(i,1);
    end
  % Daily Production Rate per Truck (L/day)
   % (Eqn 25 Chee et al., 2018)
    P_tanker = zeros(size(x,1),1);
    for i = 1:size(x)
        P_tanker(i,1) = V_wt/t_tanker_cycle(i,1)*60*T_day;
    end
  % Daily Amount of Construction Water Required (L/day)
   % (Eqn 26 Chee et al., 2018)
    V_wat_d = zeros(size(x,1),1);
    for i = 1:size(x)
        V_wat_d(i,1) = V_wat(i,1)/T_job(i,1);
    end
  % Number of Trucks Needed
   % (Eqn 24 Chee et al., 2018)
    N_tanker = zeros(size(x,1),1);
    for i = 1:size(x)
    %%%% Formula Alterd From Original Found in Chee et al., 2018 (Eqn 24)
        N_tanker(i,1) = ceil(V_wat_d(i,1)/P_tanker(i,1));
    end
%% Material Costs
  % Pipe Cost
    C_pipe = zeros(size(x,1),1);
  % Pipe Cost Uncertainty
    C_pipe_uncert = lhsu(0.9,1.1,size(x,1));
    for i = 1:size(x)
        row(i,1) = find(Pipe_Install_Data(:,1) == D_Name_in(i,1));
        C_pipe(i,1) = Pipe_Install_Data(row(i,1),3)*x(i,1)*C_pipe_uncert(i,1);
    end
  % Embedment Material
   % Assume native material is used for embedment
    C_emb_r = 0;
  % Water Cost
   % Assume water price per Litre is 0.00001
    C_wat = zeros(size(x,1),1);
    for i = 1:size(x)
        C_wat(i,1) = V_wat(i,1) * 0.00001;
    end
%% Excavating Cost
  % Labor and Equipment (Consumables) Cost for Excavating
   % RSMeans Data for (3/8), (1/2), and (3/4) cubic yd excavators
```

```
% Round CATPIL 315 capacity up to nearest cost data
% Value Accounts for 10% margins
% (RSMeans 2020 31 23 16.13)
% Assume Treches do not exceed 4 ft in Depth
% Cost is per BCY of common earth removed
  C_exc_unit = zeros(size(x,1),1);
% Excavating Cost Uncertainty
  C_exc_unit_uncert = lhsu(0.9,1.1,size(x,1));
  for i = 1:size(x)
     if V_m_w(i,1) > 0 && V_m_w(i,1) <= (0.375*0.7645)
        C_exc_unit(i,1) = 9.45*C_exc_unit_uncert(i,1);
     elseif V_m_w(i,1) > (0.375*0.7645) && V_m_w(i,1) <= (0.5*0.7645)
        C_exc_unit(i,1) = 7.20*C_exc_unit_uncert(i,1);
     elseif V_m_w(i,1) > (0.5*0.7645) && V_m_w(i,1) <= (0.75*0.7645)
        C_exc_unit(i,1) = 7.35*C_exc_unit_uncert(i,1);
     else
        break
     end
  end
%% Daily Equipment Rental Cost
 % Excavator
 % Based off CAT 315 Model
  % (Table S6 Chee et al., 2018)
  C_equip_exc = zeros(size(x,1),1);
  % Daily Excavator Rental Cost
  C_rental_exc = lhsu(676*0.9,676*1.1,size(x,1));
  for i = 1:size(x)
     C_equip_exc(i,1) = C_rental_exc(i,1)*x(i,1)/R_pipe(i,1);
  end
 % Loader
 % (RSMeans 2020 Line 01 54 33 4610-4870)
  C_equip_load = zeros(size(x,1),1);
 % Loader Cost Uncertainty
  C_equip_load_uncert = lhsu(0.9,1.1,size(x,1));
  for i = 1:size(x)
     if C_lb(i,1) <= 1.1475
        C_equip_load(i,1) = 282*C_equip_load_uncert(i,1)*T_job(i,1);
     elseif C_lb(i,1) > 1.1475 && C_lb(i,1) <= 1.33875
        C_equip_load(i,1) = 440*C_equip_load_uncert(i,1)*T_job(i,1);
     elseif C_lb(i,1) > 1.33875 && C_lb(i,1) <= 1.53
        C_equip_load(i,1) = 395*C_equip_load_uncert(i,1)*T_job(i,1);
     elseif C_lb(i,1) > 1.53 && C_lb(i,1) <= 2.6775
        C_equip_load(i,1) = 780*C_equip_load_uncert(i,1)*T_job(i,1);
     elseif C_lb(i,1) > 2.6775 && C_lb(i,1) <= 3.4425
        C_equip_load(i,1) = 890*C_equip_load_uncert(i,1)*T_job(i,1);
     elseif C_lb(i,1) > 3.4425 && C_lb(i,1) <= 4.39875
        C_equip_load(i,1) = 890*C_equip_load_uncert(i,1)*T_job(i,1);
     elseif C_lb(i,1) > 4.39875 && C_lb(i,1) <= 6.885
        C_equip_load(i,1) = 2550*C_equip_load_uncert(i,1)*T_job(i,1);
     elseif C_lb(i,1) > 6.885 && C_lb(i,1) <= 8.415
        C_equip_load(i,1) = 2700*C_equip_load_uncert(i,1)*T_job(i,1);
     else
        C_equip_load(i,1) = 'Error';
        break
     end
  end
```

```
 % Water Truck
  % Assume 12870 L (3400 gal) truck is used
  % Labor  Included
  % (Table S5 Chee et al, 2018)
    C_equip_tanker = zeros(size(x,1),1);
  % Water Truck Cost Uncertainty
    C_equip_tanker_uncert = lhsu(0.9,1.1,size(x,1));
    for i = 1:size(x)
        C_equip_tanker(i,1) = 509*C_equip_tanker_uncert(i,1)*N_tanker(i,1)*T_job(i,1);
    end
%% Mobilization and Demobilization of Equipment
 % Assume Equipment Depot is between 10 and 100 miles from project site
    Dist_mob = lhsu(10,100,size(x,1));
 % Excavator
  % Assume Equipment is less than 20 US tons
  % Assume Demobilization = Mobilization
  % (RSMeans 2020 Line 01 54 36.50)
  % Cost Represents Total Labor + Equipment and 10% profit margin
    C_mob_exc = zeros(size(x,1),1);
    C_demob_exc = zeros(size(x,1),1);
  % Mobilization Cost Uncertainty
    C_mob_exc_uncert = lhsu(0.9,1.1,size(x,1));
    for i = 1:size(x)
        if Dist_mob(i,1) <= 25
            C_mob_exc(i,1) = 855*C_mob_exc_uncert(i,1);
            C_demob_exc(i,1) = C_mob_exc(i,1);
        else
            C_mob_exc(i,1) = 855*C_mob_exc_uncert(i,1) + (Dist_mob(i,1)-25)/5*(855*0.1);
            C_demob_exc(i,1) = C_mob_exc(i,1);
        end
    end
 % Loader
  % CAT Loader Model Number
    Loader_Properties(:,1) = [926;930;938;950;962;966;972;980;982;986];
  % Loader Capacity(m^3)
    Loader_Properties(:,2) = [2.29;2.52;2.91;3.1;3.4;4.01;4.78;5.4;6.1;6.88];
  % Loader Weight (US ton)
    Loader_Properties(:,3) =
[10.24927838;13.98170004;17.06486111;19.60127642;20.47871518;19.17688707;28.89374972;32.81907563;33.1
685079;49.40332958];
    Loader_wt = zeros(size(x,1),1);
    C_mob_load = zeros(size(x,1),1);
    C_demob_load = zeros(size(x,1),1);
  % Loader Mobilization Uncertainty
    C_mob_load_uncert = lhsu(0.9,1.1,size(x,1));
    for i = 1:size(x)
        row(i,1) = find(Loader_Properties(:,2) == C_lb(i,1));
        Loader_wt(i,1) = Loader_Properties(row(i,1),3);
        if Loader_wt(i,1) <= 20
            C_mob_load(i,1) = 855*C_mob_load_uncert(i,1);
        elseif Loader_wt(i,1) <= 40
            C_mob_load(i,1) = 1000*C_mob_load_uncert(i,1);
        elseif Loader_wt(i,1) <=50
            C_mob_load(i,1) = 3000*C_mob_load_uncert(i,1);
        else
            'Error';
```

```
            break
        end
        if Dist_mob(i,1) > 25
            C_mob_load(i,1) = C_mob_load(i,1) +(Dist_mob(i,1)-25)/5*(C_mob_load(i,1)*0.1);
            C_demob_load(i,1) = C_mob_load(i,1);
        else
            C_demob_load(i,1) = C_mob_load(i,1);
        end
    end
 % Water Truck
  % Assume 12870 L (3400 gal) truck is used
  % (Table S5 Chee et al, 2018)
    C_mob_tanker = zeros(size(x,1),1);
    C_demob_tanker = zeros(size(x,1),1);
  % Tanker Mobilization Cost Uncertainty
    C_mob_tanker_uncert = lhsu(0.9,1.1,size(x,1));
    for i = 1:size(x,1)
        C_mob_tanker(i,1) = 400*C_mob_tanker_uncert(i,1)*N_tanker(i,1);
        C_demob_tanker(i,1) = C_mob_tanker(i,1);
    end
%% Total Equipment Cost ($)
 % (Eqn 35 Chee et al., 2018)
    C_equip = zeros(size(i,1),1);
    for i = 1:size(x)
        C_equip(i,1) = C_equip_exc(i,1)+C_equip_load(i,1)+...
            C_equip_tanker(i,1)+C_mob_exc(i,1)+C_demob_exc(i,1)+...
            C_mob_load(i,1)+C_demob_load(i,1)+C_mob_tanker(i,1)+...
            C_demob_tanker(i,1);
    end
%% Labor Costs
 % Excavotor
  % Included with Material and Equipment in Previous Section
 % Pipe Installation ($)
  % Assume RSMeans 2020 Crew B-20
  % Includes 10% profit margin
    C_lab_pipe = zeros(size(x,1),1);
  % Pipe Labor Cost Uncertainty
    C_lab_pipe_uncert = lhsu(0.9,1.1,size(x,1));
    for i = 1:size(x)
        C_lab_pipe(i,1) = 1699.60*C_lab_pipe_uncert(i,1) *T_job(i,1);
    end
 % Loader Operation ($)
  % Assume RSMeans 2020 Medium Equipment Operator
  % Includes 10% Profit Margin
    C_lab_load = zeros(size(x,1),1);
  % Loader Labor Cost Uncertainty
    C_lab_load_uncert = lhsu(0.9,1.1,size(x,1));
    for i = 1:size(x)
        C_lab_load(i,1) = 678*C_lab_load_uncert(i,1)*T_job(i,1);
    end
  % Water Truck Drivers ($/day)
   % Assume RSMeans 2020 Truck Driver (Heavy)
   % Includes 10% Profit Margin
    C_lab_tanker = zeros(size(x,1),1);
  % Water Truck Labor Uncertainty
    C_lab_tanker_uncert = lhsu(0.9,1.1,size(x,1));
```

```
    for i = 1:size(x)
        C_lab_tanker(i,1) = N_tanker(i,1)*586.80*C_lab_tanker_uncert(i,1)*T_job(i,1);
    end
  % Embedment Material Truck Driver
   % Indluded in Previous Calculations
%% Total Labor Costs ($)
 % (Eqn 33 Chee et al., 2018)
    C_lab = zeros(size(x,1),1);
    for i = 1:size(x)
        C_lab(i,1) = C_lab_pipe(i,1)+C_lab_load(i,1)+C_lab_tanker(i,1);
    end
 %% Total Pipe Construction Cost
  % (Eqn 29 Chee et al., 2018)
    C_construction_pipe = zeros(size(x,1),1);
    for i = 1:size(x)
        C_construction_pipe(i,1) = C_pipe(i,1)+C_wat(i,1)+C_lab(i,1)+C_equip(i,1);
    end
%% Pressure Drop
 %Conditions
  % Assume 20% safety factor
    P_o = zeros(size(x,1),1);
    for i = 1:size(x)
        row(i,1) = find(Pipe_Nom_Array(:,3) == D_Name_in(i,1));
        P_o(i,1) = Pipe_Nom_Array(row(i,1),4);
    end
 % Reynold Numer Calculation
  % Density of Arbuckle Brine is 1.015 g/mL (1015 kg/m^3)
    SG_Arbuckle = 1.015;
  % Pipe Velocity Calculation (m/s)
    v_fluid_pipe_m = zeros(size(x));
    for i = 1:size(x)
        v_fluid_pipe_m(i,1) = (Q_start(i,1)*5.615/(24*60*60)/(((D_id_in(i,1)/12/2)^2)*pi))/3.28;
    end
  % Assume Dynamic Viscosity of Brine is 1e-3 Ns/m^2
    Re = zeros(size(x,1),1);
    for i = 1:size(x)
        Re(i,1) = SG_Arbuckle*1000*v_fluid_pipe_m(i,1)*(D_id_mm(i,1)/1000)/(1e-3);
    end
 % Friction Factor
  % Determine Laminar or Turbulet Flow
    f_friction = zeros(size(x,1),1);
    for i = 1:size(x,1)
            options = optimoptions('fsolve','Display','off');
            f_friction(i,1) = fsolve(@(f) 2*log10(Re(i,1)*sqrt(f))-0.8-(1/sqrt(f)),0.001,options); % Eqution 3-2 from
AWWA M23 Manual
    end
 % Pressure Drop (ft H2O per 100 ft)
  % Darcy-Weisbach Equation
    d_P_100ft = zeros(size(x));
    d_P_100m = zeros(size(x));
    for i = 1:size(x)
       d_P_100ft(i,1) = f_friction(i,1)*100*((v_fluid_pipe_m(i,1)*3.28)^2)/(D_id_in(i,1)/12)/2/32.2;
       d_P_100m(i,1) = d_P_100ft(i,1)*3.2;
    end
%% Booster Pump Quantity and Cost
 % Assume maximum pressure drop of 20% before booster pumps needed
```

```
    N_bp = zeros(size(x,1),1);
    for i = 1:size(x)
        N_bp(i,1) = floor(x(i,1)/100*d_P_100m(i,1)/(P_o(i,1)*2.31*0.2));
    end
  % Material Cost
   % Values obtained from fitting data from Loh et al., 2002)
    C_equip_booster = zeros(size(x,1),1);
   % Booster Pump Cost Uncertainty
    C_equip_booster_uncert = lhsu(0.9,1.1,size(x,1));
    for i = 1:size(x)
        if Q_start(i,1) <= 68571.4
            C_equip_booster(i,1) = N_bp(i,1)*3855*C_equip_booster_uncert(i,1)*exp(1.635e-5*Q_start(i,1));
        else
            C_equip_booster(i,1) = N_bp(i,1)*0.1492*C_equip_booster_uncert(i,1)*Q_start(i,1);
        end
    end
 %% Electricity Cost
  % Data from EIA,2020[53]
  % Cost in $/kWh for commercial rates
  % Cost adjusted to 2020$
  % Empiracle Distribution from 2001-2020 data
    C_electricity = lhs_empir([0.1033;0.10476249;0.111177404;0.112800444;0.112927326;
        0.10906687;0.111163581;0.1077868;0.10501722;0.102941988;0.0979803;
        0.093786003;0.091761984;0.086639233;0.091148856;0.08936466;0.08967435;
        0.091283412;0.090712088;0.09209108],size(x,1));
 %% Pumping Cost Analysis
  % Does not account for pumping water out of well (needed regardless of
   % brine exchange)
  % Does not account for pumping needed for reinjection
  % Head Loss (m)
   % Convert Pressure drop per 100m to total pressure loss (ft h2O)
    d_P_total_ft_H2O = zeros(size(x,1),1);
    for i = 1:size(x)
        d_P_total_ft_H2O(i,1) = d_P_100m(i,1)*(x(i,1)/100);
    end
   % Pump Efficiency
    % Assume Centrifugal Pump Used
    % Values obtained from Loh et al., 2002[54]
    % Flow converted from bbl/day to gpm
    % Assume lowest efficiency applies when overlap in data occurs
    Eff_pump = zeros(size(x,1),1);
   % Pump Efficiency Uncertainty
    Eff_pump_uncert = lhsu(0.9,1.1,size(x,1));
    for i = 1:size(x)
        if (Q_start(i,1)*0.0292) < 50
            Eff_pump(i,1) = 0.6*Eff_pump_uncert(i,1);
        elseif 50 <= (Q_start(i,1)*0.0292) && (Q_start(i,1)*0.0292) < 200
            Eff_pump(i,1) = 0.65*Eff_pump_uncert(i,1);
        elseif 200 <= (Q_start(i,1)*0.0292) && (Q_start(i,1)*0.0292) < 500
            Eff_pump(i,1) = 0.75*Eff_pump_uncert(i,1);
        else
            Eff_pump(i,1) = 0.82*Eff_pump_uncert(i,1);
        end
    end
   % Motor Efficiency
    % Assume Efficiency Ranges from 60% - 90%
```

```
  Eff_motor = lhsu(.6,0.9,size(x,1));
 % Brake Horse Power (BHP) per pump
  BHP = zeros(size(x,1),1);
 % Q in units of gpm
 % Head loss in units of feet
  for i = 1:size(x)
     BHP(i,1) = Q_start(i,1)*0.0292*d_P_total_ft_H2O(i,1)*SG_Arbuckle/(3960*Eff_pump(i,1));
  end
 % Energy Requirements (kW)
 E_pump = zeros(size(x,1),1);
  for i = 1:size(x)
     E_pump(i,1) = 0.746 *BHP(i,1)/Eff_motor(i,1);
  end
%% Pumping Cost per Day
  C_pumping_day = zeros(size(x,1),1);
  for i = 1:size(x)
     C_pumping_day(i,1) = E_pump(i,1)*C_electricity(i,1)*24;
  end
%% Daily Injection Rate (bbl/day)
 % Assume all oil wells produce 22-barrel PW for every 1-barrel oil
 % Assume injection volume equals volume removed plus 10% to maintain pressure
 % Assume all transported water will be used for injection
 % Daily Production of Oil Well
 % Assume value of 0.5 to 50 bopd with most producing 5 bopd
  Q_oilwell_daily = lhsu(0.5,10,size(x,1)); % bbl/day
 % Assume EOR from brine exchange is 4% - 12%
  Percent_EOR = lhsu(0.04,0.12,size(x,1));
 % EOR Calculation
  Oil_EOR = zeros(size(x,1),1);
  for i = 1:size(x)
    Oil_EOR(i,1) = Q_start(i,1)/(23*1.1)*Percent_EOR(i,1);
  end
%% Monetary Benefit of EOR
 % Historic Crude Oil Prices (2001-2020) (2020$/bbl) (EIA,2021)[55]
  C_oil_bbl = lhs_empir([43.241088;34.9946104;34.1037006;40.7789448;
     54.471954;72.3176741;79.5457114;84.7998935;113.5677888;64.6194924;
     86.3141067;103.7861592;99.8459175;102.274975;95.251716;46.6071892;
     40.8458246;48.944102;63.045723;53.531698;36.29],size(x,1));
 % Cost Benefit
  C_EOR = zeros(size(x,1),1);
  for i = 1:size(x)
     C_EOR(i,1) = Oil_EOR(i,1)*C_oil_bbl(i,1);
  end
%% Disposal Cost Savings
 % Assume all PW will be piped to disposal well
 % Assume Average disposal cost is $0.12 per barrel
  C_disp_pipe = lhsu(0.10,0.14,size(x,1));
 % Savings Calculation
  C_disposal = zeros(size(x,1),1);
  for i = 1:size(x,1)
    C_disposal(i,1) = Q_start(i,1)*C_disp_pipe(i,1);
  end
%% Net Benefit
 % Income from EOR minus Daily Costs
  Net_benefit = zeros(size(x,1),1);
  for i = 1:size(x)
```

```
        Net_benefit(i,1) = C_EOR(i,1)+2*C_disposal(i,1)-2*C_pumping_day(i,1)-
2*((C_lab(i,1)+C_construction_pipe(i,1)+C_equip_booster(i,1))/10/365);
    end
%% Heatmap Creation
 % x-axis =x (Length of pipe in meters)
 % y-axis = Q_actual (bbl/day)
 % z-axis = Net Benefit
figure
scatter(x,Q_start,10,Net_benefit);
colormap(bluewhitered);
clbr = colorbar;
xlabel('Distance(m)')
ylabel('PW Flowrate (bbl/day)')
clbr = ylabel(clbr,'Net Benefit (2020$/day)');
set(clbr,'Rotation',90);
%% Functions
 % Uniform Distribution
 function s=lhsu(xmin,xmax,nsample)
% s=lhsu(xmin,xmax,nsample)
% LHS from uniform distribution
% Input:
%   xmin    : min of data (1,nvar)
%   xmax    : max of data (1,nvar)
%   nsample : no. of samples
% Output:
%   s       : random sample (nsample,nvar)
%   Budiman (2003)[56]
nvar=length(xmin);
ran=rand(nsample,nvar);
s=zeros(nsample,nvar);
for j=1: nvar
   idx=randperm(nsample);
   P =(idx'-ran(:,j))/nsample;
   s(:,j) = xmin(j) + P.* (xmax(j)-xmin(j));
end
 end
 % Budiman Minasny (2021). Latin Hypercube Sampling
(https://www.mathworks.com/matlabcentral/fileexchange/4352-latin-hypercube-sampling), MATLAB Central File
Exchange. Retrieved October 20, 2021.
function s=lhs_empir(data,nsample)
% s=lhs_empir(data,nsample)
% perform lhs on multivariate empirical distribution
%   assume no correlation
% Input:
%   data    : data matrix (ndata,nvar)
%   nsample : no. of samples
% Output:
%   s       : random sample (nsample,nvar)
%   Budiman (2003)
[m,nvar]=size(data);
ran=rand(nsample,nvar);
s=zeros(nsample,nvar);
for j=1: nvar
   idx=randperm(nsample);
   P=((idx'-ran(:,j))/nsample).*100;
   s(:,j)=prctile(data(:,j),P);
```

```
end
end
function X=roundtowardvec(X,roundvec,type)
%function newnums=roundtowardvec(X,[roundvec],[type])
% (Tom R, 2022)[57]
% This function rounds number(s) toward given values. If more than one
% number is given to round, it will return the matrix with each rounded
% value, otherwise it will return the single rounded value. It will ignore
% NaNs and return them back with NaNs.
%
% Inputs: X: the number(s) that you want rounded
%
%       roundvec:(opt) the values to round X to. If none given, it will
%         default to -inf:1:inf (and use the built in functions).
%
%       type:(opt) specifies which kind of rounding you want
%         the function to use.
%
%         Choices are: 'round' - round to nearest value
%                      'floor' - round toward -Inf
%                       'ceil'  - round toward Inf

%                      'fix'   - round toward 0
%                      'away'  - round away from 0 (ceil if positive and floor if negative)
%                    (see help files for more clarity)
%
%         If no type is given, the function will default to rounding to
%         the nearest value.
%
% Outputs: newnums: rounded values, in same shape as X input matrix
%         indices: indices of rounded values in roundvec
if nargin==0
        help roundtowardvec; %if nothing given, tell what to give
        return
elseif isempty(X)
        %if given empty, return empty without going through whole script
        return
end
if nargout>1
        error('Too many output variables are given');
end
if ~exist('type','var') || isempty(type)
        type='round';  %%round to nearest value if not specified
end
if ~exist('roundvec','var') || isempty(roundvec) || all(isnan(roundvec))
        if strcmpi(type,'round')
                %to nearest integer
                X=round(X);
        elseif strcmpi(type,'away')
                %nearest integer away from 0
                X=ceil(abs(X)).*sign(X);
        elseif strcmpi(type,'fix')
                %nearest integer toward 0
                X=fix(X);
        elseif strcmpi(type,'floor')
                %nearest integer toward -inf
```

```
                X=floor(X);
        elseif strcmpi(type,'ceil')
                %nearest integer toward inf
                X=ceil(X);
        else
                error('%sRound type not recognized. Options are:\n"round" - round to nearest value\n"floor" -
round toward -Inf\n"ceil"  - round toward Inf\n"fix"   - round toward 0\n"away"  - round away from 0',')
        end
else
        %Ignore nan in roundvec
        roundvec(isnan(roundvec))=[];

        %Record which values are nan to ignore
        Xnan=isnan(X);

        %Hold onto size for returning value
        sz=size(X);

        %Calculate differences
        X=X(:);
        roundvec=roundvec(:)';
        diffs=bsxfun(@minus,X,roundvec);

        if strcmpi(type,'round') %to nearest value
                [~,inds]=min(abs(diffs),[],2);
                X=roundvec(inds);
        elseif strcmpi(type,'fix') %to nearest value toward 0

                iless=X<0;
                X(iless)=roundtowardvec(X(iless),roundvec,'ceil');
                X(~iless)=roundtowardvec(X(~iless),roundvec,'floor');
        elseif strcmpi(type,'ceil') %nearest value toward inf
                diffs(diffs>0)=nan;
                [~,inds]=min(abs(diffs),[],2);

                i_inf=X>max(roundvec);
                X=roundvec(inds);
                X(i_inf)=inf;
        elseif strcmpi(type,'floor') %nearest value toward -inf
                diffs(diffs<0)=nan;
                [~,inds]=min(abs(diffs),[],2);

                i_inf=X<min(roundvec);
                X=roundvec(inds);
                X(i_inf)=-inf;
        elseif strcmpi(type,'away') %nearest value away from 0

                iless=X<0;
                X(~iless)=roundtowardvec(X(~iless),roundvec,'ceil');
                X(iless)=roundtowardvec(X(iless),roundvec,'floor');
        else
                error('%sRound type not recognized. Options are:\n"round" - round to nearest value\n"floor" -
round toward -Inf\n"ceil"  - round toward Inf\n"fix"   - round toward 0\n"away"  - round away from 0',')
        end

        %Return to output side
```

```
            X=reshape(X(:),sz);

            %Ignore nan in input dataset
            X(Xnan)=nan;
end
end
function newmap = bluewhitered(m)
% Nathan Childress (2021). bluewhitered[58]
% (https://www.mathworks.com/matlabcentral/fileexchange/4058-bluewhitered),
% MATLAB Central File Exchange. Retrieved October 26, 2021.

%BLUEWHITERED   Blue, white, and red color map.
%   BLUEWHITERED(M) returns an M-by-3 matrix containing a blue to white
%   to red colormap, with white corresponding to the CAXIS value closest
%   to zero.  This colormap is most useful for images and surface plots
%   with positive and negative values.  BLUEWHITERED, by itself, is the
%   same length as the current colormap.
%
%   Examples:
%   ---------------------------------
%   figure
%   imagesc(peaks(250));
%   colormap(bluewhitered(256)), colorbar
%
%   figure
%   imagesc(peaks(250), [0 8])
%   colormap(bluewhitered), colorbar
%
%   figure
%   imagesc(peaks(250), [-6 0])
%   colormap(bluewhitered), colorbar
%
%   figure
%   surf(peaks)
%   colormap(bluewhitered)
%   axis tight
%
%   See also HSV, HOT, COOL, BONE, COPPER, PINK, FLAG,
%   COLORMAP, RGBPLOT.
if nargin < 1
  m = size(get(gcf,'colormap'),1);
end
bottom = [0 0 0.5];
botmiddle = [0 0.5 1];
middle = [1 1 1];
topmiddle = [1 0 0];
top = [0.5 0 0];
% Find middle
lims = get(gca, 'CLim');
% Find ratio of negative to positive
if (lims(1) < 0) & (lims(2) > 0)
    % It has both negative and positive
    % Find ratio of negative to positive
    ratio = abs(lims(1)) / (abs(lims(1)) + lims(2));
    neglen = round(m*ratio);
    poslen = m - neglen;
```

```
    % Just negative
    new = [bottom; botmiddle; middle];
    len = length(new);
    oldsteps = linspace(0, 1, len);
    newsteps = linspace(0, 1, neglen);
    newmap1 = zeros(neglen, 3);

    for i=1:3
        % Interpolate over RGB spaces of colormap
        newmap1(:,i) = min(max(interp1(oldsteps, new(:,i), newsteps)', 0), 1);
    end

    % Just positive
    new = [middle; topmiddle; top];
    len = length(new);
    oldsteps = linspace(0, 1, len);
    newsteps = linspace(0, 1, poslen);
    newmap = zeros(poslen, 3);

    for i=1:3
        % Interpolate over RGB spaces of colormap
        newmap(:,i) = min(max(interp1(oldsteps, new(:,i), newsteps)', 0), 1);
    end

    % And put 'em together
    newmap = [newmap1; newmap];

elseif lims(1) >= 0
    % Just positive
    new = [middle; topmiddle; top];
    len = length(new);
    oldsteps = linspace(0, 1, len);
    newsteps = linspace(0, 1, m);
    newmap = zeros(m, 3);

    for i=1:3
        % Interpolate over RGB spaces of colormap
        newmap(:,i) = min(max(interp1(oldsteps, new(:,i), newsteps)', 0), 1);
    end

else
    % Just negative
    new = [bottom; botmiddle; middle];
    len = length(new);
    oldsteps = linspace(0, 1, len);
    newsteps = linspace(0, 1, m);
    newmap = zeros(m, 3);

    for i=1:3
        % Interpolate over RGB spaces of colormap
        newmap(:,i) = min(max(interp1(oldsteps, new(:,i), newsteps)', 0), 1);
    end

end
end
```

The following section contains the MATLAB code used to conduct the techno-economic simulation. The code utilizes information from an industry contact to estimate infrastructure cost.

```
%% Input Constants
x = lhsu(1,10000,10000); % distance in meters
   x = round(x);
Q_start = lhsu(1,1000,size(x,1)); % hypothetical starting volumetric flow of PW in barrels/day
%% Pipe Size
D_od_in=zeros(size(x,1),1);
D_id_in = zeros(size(x,1),1);
D_id_ft = zeros(size(x,1),1);
for i = 1:size(x,1)
   if Q_start(i,1) <= 2000
      % Schedule 40 3in pipe
      D_od_in(i,1) = 3.5;
      D_id_in(i,1) = 3.068;
      D_id_ft(i,1) = D_id_in(i,1)/12;
   else
     D_od_in(i,1) = 4.5;
     D_id_in(i,1) = 4.026;
     D_id_ft(i,1) = D_id_in(i,1)/12;
   end
end
%% Pipe Material Cost
C_pipe = zeros(size(x));
C_pipe_uncertainty = lhsu(0.9,1.1,size(x,1));
for i = 1:size(x)
   if D_od_in(i,1) == 3.5
      C_pipe(i,1) = 3.7*C_pipe_uncertainty(i,1)*x(i,1)*3.28;
   else
      C_pipe(i,1) = 4.65*C_pipe_uncertainty(i,1)*x(i,1)*3.28;
   end
end
%% Trenching and Pipe Installation
C_install_ft = lhsu(1.17,1.43,size(x,1)); % Third Party rate of $1.30/ft to trench and install
C_install_total = zeros(size(x,1),1);
for i = 1:size(x,1)
   C_install_total(i,1) = C_install_ft(i,1)*x(i,1)*3.28;
end
%% Pressure Drop
 % Pipe Velocity Calculation (m/s)
   v_fluid_pipe_m = zeros(size(x));
   v_fluid_pipe_ft = zeros(size(x));
   for i = 1:size(x)
      v_fluid_pipe_ft(i,1) = (Q_start(i,1)*5.615/(24*60*60)/(((D_id_ft(i,1)/2)^2)*pi));
      v_fluid_pipe_m(i,1) = v_fluid_pipe_ft(i,1)/3.28;
   end
 %Conditions
  % Assume all PVC Pipes have maximum pressure of 100 psi
  % Assume 20% safety factor
   P_o = 100*0.8;
 % Reynold Numer Calculation
  % Density of Arbuckle Brine is 1.015 g/mL (1015 kg/m^3)
```

```
    SG_Arbuckle = 1.015;
  % Assume velocity of 10 ft/s (3.048 m/s) before 20% safety factor
  % Assume Dynamic Viscosity of Brine is 1e-3 Ns/m^2
    Re = zeros(size(x,1),1);
    for i = 1:size(x)
        Re(i,1) = SG_Arbuckle*1000*(v_fluid_pipe_m(i,1))*D_id_ft(i,1)/(1e-3);
    end
 % Friction Factor
  % Determine Laminar or Turbulet Flow
    f_friction = zeros(size(x,1),1);
    for i = 1:size(x,1)
            options = optimoptions('fsolve','Display','off');
            f_friction(i,1) = fsolve(@(f) 2*log10(Re(i,1)*sqrt(f))-0.8-(1/sqrt(f)),0.001,options); % Eqution 3-2 from
AWWA M23 Manual
    end
 % Pressure Drop (ft H2O per 100 ft)
  % Equation 2.2 of API 14E Design Manual (Modificed Darcy Equation)
  % Q = flow in barrels per day
    d_P_100ft = zeros(size(x,1),1);
    d_P_100m = zeros(size(x,1),1);
    for i = 1:size(x)
      d_P_100ft(i,1) = f_friction(i,1)*100*(v_fluid_pipe_ft(i,1))^2/D_id_ft(i,1)/2/32.2;
      d_P_100m(i,1) = d_P_100ft(i,1)* 3.2;
    end
%% Booster Pump Quantity and Cost
 % Assume maximum pressure drop of 20% before booster pumps needed
    N_bp = zeros(size(x,1),1);
    for i = 1:size(x)
        N_bp(i,1) = floor(x(i,1)/100*d_P_100m(i,1)/(P_o*2.31*0.2));
    end
 % Material Cost
  % Values obtained from Loh et al., 2002)
    C_equip_booster = zeros(size(x,1),1);
    for i = 1:size(x)
        if Q_start(i,1) <= 68571.4
            C_equip_booster(i,1) = N_bp(i,1)*3855*exp(1.635e-5*Q_start(i,1));
        else
            C_equip_booster(i,1) = N_bp(i,1)*0.1492*Q_start(i,1);
        end
    end
%% Electricity Cost
 % Data from EIA,2020
 % Cost in $/kWh for commercial rates
 % Cost adjusted to 2020$
 % Empiracle Distribution from 2001-2020 data
    Electricity_Cost = lhs_empir([0.1033;0.10476249;0.111177404;0.112800444;0.112927326;
        0.10906687;0.111163581;0.1077868;0.10501722;0.102941988;0.0979803;
        0.093786003;0.091761984;0.086639233;0.091148856;0.08936466;0.08967435;
        0.091283412;0.090712088;0.09209108],size(x,1));
%% Pumping Cost Analysis
 % Does not account for pumping water out of well (needed regardless of
  % brine exchange)
 % Does not account for pumping needed for reinjection
 % Head Loss (m)
  % Convert Pressure drop per 100m to total pressure loss (ft h2O)
    d_P_total_ft_H2O = zeros(size(x,1),1);
```

```
 for i = 1:size(x)
    d_P_total_ft_H2O(i,1) = d_P_100m(i,1)*(x(i,1)/100);
 end
% Pump Efficiency
 % Assume Centrifugal Pump Used
 % Values obtained from Loh et al., 2002
 % Flow converted from bbl/day to gpm
 % Assume lowest efficiency applies when overlap in data occurs
 Eff_pump = zeros(size(x,1),1);
 % Pump Efficiency Uncertainty
 Eff_pump_uncert = lhsu(0.9,1.1,size(x,1));
 for i = 1:size(x)
    if (Q_start(i,1)*0.0292) < 50
       Eff_pump(i,1) = 0.6*Eff_pump_uncert(i,1);
    elseif 50 <= (Q_start(i,1)*0.0292) && (Q_start(i,1)*0.0292) < 200
       Eff_pump(i,1) = 0.65*Eff_pump_uncert(i,1);
    elseif 200 <= (Q_start(i,1)*0.0292) && (Q_start(i,1)*0.0292) < 500
       Eff_pump(i,1) = 0.75*Eff_pump_uncert(i,1);
    else
       Eff_pump(i,1) = 0.82*Eff_pump_uncert(i,1);
    end
 end
% Motor Efficiency
 % Assume Efficiency Ranges from 60% - 90%
 Eff_motor = lhsu(.6,0.9,size(x,1));
% Brake Horse Power (BHP) per pump
 BHP = zeros(size(x,1),1);
 % Q in units of gpm
 % Head loss in units of feet
 for i = 1:size(x)
    BHP(i,1) = Q_start(i,1)*0.0292*d_P_total_ft_H2O(i,1)*SG_Arbuckle/(3960*Eff_pump(i,1));
 end
% Energy Requirements (kW)
E_pump = zeros(size(x,1),1);
 for i = 1:size(x)
    E_pump(i,1) = 0.746 *BHP(i,1)/Eff_motor(i,1);
 end
%% Pumping Cost per Day
 C_pumping_day = zeros(size(x,1),1);
 for i = 1:size(x)
    C_pumping_day(i,1) = E_pump(i,1)*Electricity_Cost(i,1)*24;
 end
%% Daily Injection Rate (bbl/day)
 % Assume all oil wells produce 22 barrel PW for every 1 barrel oil
 % Assume injection volume equals volume removed plus 10% to maintain pressure
 % Assume all transported water will be used for injection
 % Daily Production of Oil Well
 % Assume value of 0.5 to 50 bopd with most producing 5 bopd
 Q_oilwell_daily = lhsu(0.5,10,size(x,1)); % bbl/day
 % Assume EOR from brine exchange is 4% - 12%
 Percent_EOR = lhsu(0.04,0.12,size(x,1));
% EOR Calculation
 Oil_EOR = zeros(size(x,1),1);
 for i = 1:size(x)
    Oil_EOR(i,1) = Q_start(i,1)/(23*1.1)*Percent_EOR(i,1);
 end
```

```
%% Monetary Benefit of EOR
 % Historic Crude Oil Prices (2001-2020) (2020$/bbl)
   C_oil_bbl = lhs_empir([43.241088;34.9946104;34.1037006;40.7789448;
       54.471954;72.3176741;79.5457114;84.7998935;113.5677888;64.6194924;
       86.3141067;103.7861592;99.8459175;102.274975;95.251716;46.6071892;
       40.8458246;48.944102;63.045723;53.531698;36.29],size(x,1));
 % Cost Benefit
   C_EOR = zeros(size(x,1),1);
   for i = 1:size(x)
      C_EOR(i,1) = Oil_EOR(i,1)*C_oil_bbl(i,1);
   end
%% Disposal Cost Savings
 % Assume all PW will be piped to disposal well
 % Assume Average disposal cost is $0.12 per barrel
  C_disp_pipe = lhsu(0.10,0.14,size(x,1));
 % Savings Calculation
  C_disposal = zeros(size(x,1),1);
  for i = 1:size(x,1)
    C_disposal(i,1) = Q_start(i,1)*C_disp_pipe(i,1);
  end
%% Net Benefit Calculation
 % Assume Project Life of 10 years
   C_Net_Benefit = zeros(size(x,1),1);
   for i = 1:size(x)
      C_Net_Benefit(i,1) = (C_EOR(i,1)+2*C_disposal(i,1)-2*C_pumping_day(i,1))-
2*((C_install_total(i,1)+C_pipe(i,1)+C_equip_booster(i,1))/10/365);
   end
%% Heatmap Creation
 % x-axis =x (Length of pipe in meters)
 % y-axis = Q_actual (bbl/day)
 % z-axis = Net Benefit
figure
scatter(x,Q_start,10,C_Net_Benefit);
old_cmap = colormap(bluewhitered);
clbr = colorbar;
xlabel('Distance(m)')
ylabel('PW Flowrate (bbl/day)')
clbr = ylabel(clbr,'Net Benefit (2020$/day)');
set(clbr,'Rotation',90);
%% Functions
 % Uniform Distribution
 function s=lhsu(xmin,xmax,nsample)
% s=lhsu(xmin,xmax,nsample)
% LHS from uniform distribution
% Input:
%   xmin    : min of data (1,nvar)
%   xmax    : max of data (1,nvar)
%   nsample : no. of samples
% Output:
%   s       : random sample (nsample,nvar)
%   Budiman (2003)
nvar=length(xmin);
ran=rand(nsample,nvar);
s=zeros(nsample,nvar);
for j=1: nvar
   idx=randperm(nsample);
```

```
   P =(idx'-ran(:,j))/nsample;
   s(:,j) = xmin(j) + P.* (xmax(j)-xmin(j));
end
 end
 % Budiman Minasny (2021). Latin Hypercube Sampling
(https://www.mathworks.com/matlabcentral/fileexchange/4352-latin-hypercube-sampling), MATLAB Central File
Exchange. Retrieved October 20, 2021.
function s=lhs_empir(data,nsample)
% s=lhs_empir(data,nsample)
% perform lhs on multivariate empirical distribution
%   assume no correlation
% Input:
%   data    : data matrix (ndata,nvar)
%   nsample : no. of samples
% Output:
%   s       : random sample (nsample,nvar)
%   Budiman (2003)
[m,nvar]=size(data);
ran=rand(nsample,nvar);
s=zeros(nsample,nvar);
for j=1: nvar
   idx=randperm(nsample);
   P=((idx'-ran(:,j))/nsample).*100;
   s(:,j)=prctile(data(:,j),P);
end
end
function z = ltqnorm(p)
%LTQNORM Lower tail quantile for standard normal distribution.
%
%   Z = LTQNORM(P) returns the lower tail quantile for the standard normal
%   distribution function.  I.e., it returns the Z satisfying Pr{X < Z} = P,
%   where X has a standard normal distribution.
%
%   LTQNORM(P) is the same as SQRT(2) * ERFINV(2*P-1), but the former returns a
%   more accurate value when P is close to zero.
%   The algorithm uses a minimax approximation by rational functions and the
%   result has a relative error less than 1.15e-9.  A last refinement by
%   Halley's rational method is applied to achieve full machine precision.
%   Author:      Peter J. Acklam
%   Time-stamp:  2003-04-23 08:26:51 +0200
%   E-mail:      pjacklam@online.no
%   URL:         http://home.online.no/~pjacklam
   % Coefficients in rational approximations.
   a = [ -3.969683028665376e+01  2.209460984245205e+02 ...
         -2.759285104469687e+02  1.383577518672690e+02 ...
         -3.066479806614716e+01  2.506628277459239e+00 ];
   b = [ -5.447609879822406e+01  1.615858368580409e+02 ...
         -1.556989798598866e+02  6.680131188771972e+01 ...
         -1.328068155288572e+01 ];
   c = [ -7.784894002430293e-03 -3.223964580411365e-01 ...
         -2.400758277161838e+00 -2.549732539343734e+00 ...
          4.374664141464968e+00  2.938163982698783e+00 ];
   d = [  7.784695709041462e-03  3.224671290700398e-01 ...
          2.445134137142996e+00  3.754408661907416e+00 ];
   % Define break-points.
   plow  = 0.02425;
```

```
  phigh = 1 - plow;
  % Initialize output array.
  z = zeros(size(p));
  % Rational approximation for central region:
  k = plow <= p & p <= phigh;
  if any(k(:))
    q = p(k) - 0.5;
    r = q.*q;
    z(k) = (((((a(1)*r+a(2)).*r+a(3)).*r+a(4)).*r+a(5)).*r+a(6)).*q ./ ...
           ((((b(1)*r+b(2)).*r+b(3)).*r+b(4)).*r+b(5)).*r+1);
  end
  % Rational approximation for lower region:
  k = 0 < p & p < plow;
  if any(k(:))
    q  = sqrt(-2*log(p(k)));
    z(k) = ((((c(1)*q+c(2)).*q+c(3)).*q+c(4)).*q+c(5)).*q+c(6)) ./ ...
           ((((d(1)*q+d(2)).*q+d(3)).*q+d(4)).*q+1);
  end
  % Rational approximation for upper region:
  k = phigh < p & p < 1;
  if any(k(:))
    q  = sqrt(-2*log(1-p(k)));
    z(k) = -((((c(1)*q+c(2)).*q+c(3)).*q+c(4)).*q+c(5)).*q+c(6)) ./ ...
           ((((d(1)*q+d(2)).*q+d(3)).*q+d(4)).*q+1);
  end
  % Case when P = 0:
  z(p == 0) = -Inf;
  % Case when P = 1:
  z(p == 1) = Inf;
  % Cases when output will be NaN:
  k = p < 0 | p > 1 | isnan(p);
  if any(k(:))
    z(k) = NaN;
  end
  % The relative error of the approximation has absolute value less
  % than 1.15e-9.  One iteration of Halley's rational method (third
  % order) gives full machine precision.
  k = 0 < p & p < 1;
  if any(k(:))
    e = 0.5*erfc(-z(k)/sqrt(2)) - p(k);          % error
    u = e * sqrt(2*pi) .* exp(z(k).^2/2);        % f(z)/df(z)
    %z(k) = z(k) - u;                            % Newton's method
    z(k) = z(k) - u./( 1 + z(k).*u/2 );          % Halley's method
  end
end
function newmap = bluewhitered(m)
% Nathan Childress (2021). bluewhitered
% (https://www.mathworks.com/matlabcentral/fileexchange/4058-bluewhitered),
% MATLAB Central File Exchange. Retrieved October 26, 2021.

%BLUEWHITERED   Blue, white, and red color map.
%   BLUEWHITERED(M) returns an M-by-3 matrix containing a blue to white
%   to red colormap, with white corresponding to the CAXIS value closest
%   to zero.  This colormap is most useful for images and surface plots
%   with positive and negative values.  BLUEWHITERED, by itself, is the
%   same length as the current colormap.
```

```
%
%   Examples:
%   -----------------------------
%   figure
%   imagesc(peaks(250));
%   colormap(bluewhitered(256)), colorbar
%
%   figure
%   imagesc(peaks(250), [0 8])
%   colormap(bluewhitered), colorbar
%
%   figure
%   imagesc(peaks(250), [-6 0])
%   colormap(bluewhitered), colorbar
%
%   figure
%   surf(peaks)
%   colormap(bluewhitered)
%   axis tight
%
%   See also HSV, HOT, COOL, BONE, COPPER, PINK, FLAG,
%   COLORMAP, RGBPLOT.
if nargin < 1
  m = size(get(gcf,'colormap'),1);
end
bottom = [0 0 0.5];
botmiddle = [0 0.5 1];
middle = [1 1 1];
topmiddle = [1 0 0];
top = [0.5 0 0];
% Find middle
lims = get(gca, 'CLim');
% Find ratio of negative to positive
if (lims(1) < 0) & (lims(2) > 0)
   % It has both negative and positive
   % Find ratio of negative to positive
   ratio = abs(lims(1)) / (abs(lims(1)) + lims(2));
   neglen = round(m*ratio);
   poslen = m - neglen;

   % Just negative
   new = [bottom; botmiddle; middle];
   len = length(new);
   oldsteps = linspace(0, 1, len);
   newsteps = linspace(0, 1, neglen);
   newmap1 = zeros(neglen, 3);

   for i=1:3
      % Interpolate over RGB spaces of colormap
      newmap1(:,i) = min(max(interp1(oldsteps, new(:,i), newsteps)', 0), 1);
   end

   % Just positive
   new = [middle; topmiddle; top];
   len = length(new);
   oldsteps = linspace(0, 1, len);
```

```
    newsteps = linspace(0, 1, poslen);
    newmap = zeros(poslen, 3);

    for i=1:3
        % Interpolate over RGB spaces of colormap
        newmap(:,i) = min(max(interp1(oldsteps, new(:,i), newsteps)', 0), 1);
    end

    % And put 'em together
    newmap = [newmap1; newmap];

elseif lims(1) >= 0
    % Just positive
    new = [middle; topmiddle; top];
    len = length(new);
    oldsteps = linspace(0, 1, len);
    newsteps = linspace(0, 1, m);
    newmap = zeros(m, 3);

    for i=1:3
        % Interpolate over RGB spaces of colormap
        newmap(:,i) = min(max(interp1(oldsteps, new(:,i), newsteps)', 0), 1);
    end

else
    % Just negative
    new = [bottom; botmiddle; middle];
    len = length(new);
    oldsteps = linspace(0, 1, len);
    newsteps = linspace(0, 1, m);
    newmap = zeros(m, 3);

    for i=1:3
        % Interpolate over RGB spaces of colormap
        newmap(:,i) = min(max(interp1(oldsteps, new(:,i), newsteps)', 0), 1);
    end

end
end
```